Fall 1998

Computer Simulations of Electromigration Based on a Molecular Dynamics Approach

John Stephen Peake
Old Dominion University

COMPUTER SIMULATIONS OF ELECTROMIGRATION BASED ON A MOLECULAR DYNAMICS APPROACH

By

John Stephen Peake
B.S. December 1994, Old Dominion University

A Thesis Submitted to the Faculty of
Old Dominion University in Partial Fulfillment of the
Requirement for the Degree of

MASTER OF SCIENCE

ELECTRICAL ENGINEERING

with an emphasis on Physical Electronics

OLD DOMINION UNIVERSITY
December 1998

Approved by:

_____
Dr. Ravindra P. Joshi (Director)

_____
Dr. Glenn Gerdin (Member)

_____
Dr. James Leathrum (Member)

ABSTRACT

COMPUTER SIMULATIONS OF ELECTROMIGRATION BASED ON A MOLECULAR DYNAMICS APPROACH.

John Stephen Peake
Old Dominion University, 1998
Director: Dr. Ravindra P. Joshi

Most research on electromigration has centered around macroscopic simulations of electromigration where a value for the diffusion coefficient was assumed to be spatially uniform throughout the material. The research in this thesis goes a step further and, through microscopic molecular dynamics computer simulations, calculates and updates the atomic drift velocity and atomic position as a function of time to analyze how various defects within the conductor affect these quantities. The simulations are carried out with defects in the form of dislocation half-planes placed in different locations within the simulation space. The atomic drift velocity and position changes derived from these simulations can then be used to carry out further research involving both microscopic as well as macroscopic computer simulations. In addition, the simulations proposed in this thesis can be extended to include other materials in different environments by changing the parameters. All simulations presented here are bound by 2-D simulation spaces containing only a few atoms in order to determine if a molecular dynamics simulation approach is appropriate for simulating electromigration.

Co-Directors of Advisory Committee: Dr. Glenn Gerdin
Dr. James Leathrum

ACKNOWLEDGMENTS

I wold like to thank Dr. Joshi who generously gave of his time to work with me while developing this Master's Thesis. His enthusiasm and unique way of explaining technically difficult concepts and his unwavering encouragement made this work possible. I also wish to express appreciation to Dr. Glenn Gerdin and Dr. James Leathrum for their comments on this research work and for being on the committee.

TABLE OF CONTENTS

Page

Chapter Page

LIST OF TABLES

LIST OF FIGURES

CHAPTER I

INTRODUCTION

1.1 Electromigration

Electromigration in semiconductors can be described as the mass transport of conductor material due to high current density stressing. For electromigration to take place, current densities within the conductor should be on the order of $1x10^6$ A/cm^2 **[1]**. Today's integrated circuits are manufactured on an ever-decreasing die size, with more narrow conductor line widths, allowing current densities within these integrated circuits to approach $1x10^6$ A/cm^2. Because of this, electromigration takes on an even more important role in chip reliability assessment.

Reduction in device dimension and the subsequent increase in current density are the main effects of device scaling that have taken place over the years. In addition to an increase in j, the current density, the increase in $j^2\rho$, the Joule heating, can raise the conductor temperature, giving rise to higher atomic diffusivity and mass transport. The increase in power density as well as current density necessitates improved heat rejection of the device during normal operation. With the projected high current density in sub-micron metal lines, there will be increasing concern over reliability caused by electromigration-induced failures. In fact, it is the current-carrying capability of sub-micron thin-film IC interconnects that will constitute one of the factors limiting the scaling of VLSI devices **[1]**. The values for j and $j^2\rho$ predicted for FET and bipolar devices for different periods of technology development are listed in Table 1.1 **[2]**.

The references in this document conform to the Journal of Applied Physics standard.

Table 1.1

Trends in device electromigration parameters

		Current Density (10^5 A/cm^2)		Joule Heating $J^2\rho$ (W/cm)	
Period	Linewidth (um)	FET	Bipolar	FET	Bipolar
1970s	3-6	0.2-0.5	0.5-1.0	1.0	4.0
1980-1985	1.5-3.0	0.5	1.0	2.0-4.0	4.0-15.0
Late 1980s	0.5-1.5	1.0-2.0	8.0-15.0	15.0	200

It is useful to consider three general aspects when characterizing the electromigration behavior in fine metal lines. These are geometry, process, and material related **[3]**. These geometry-related problems arise basically from the changes in grain size and structure as a result of the reduction in line dimension to the sub-micron range. The grain size is about the same as the film thickness for metal films. The thickness usually used in IC's for conductor lines is on the order of 1um. When the line width is reduced to the micron range, the grain size begins to approach that of the line width and takes on a bamboo-like morphology. This is a significant change in the microstructure of the conducting line and hence a corresponding change in the electromigration behavior can also be expected. As the grain boundary area reduces, the surface and interface become increasingly important for transporting atoms in the metal line. This introduces additional structural defects in the formation of electromigration-induced damage.

The process-related problems originate from process induced imperfection in the metal line, on the substrate, or in the passivation layer. The substrate and/or passivation layer are what is largely responsible for the removal of Joule heating that arises from current densities exceeding $1x10^6$ A/cm^2. An isolated metal line can only carry about $1x10^5$ A/cm^2 before melting. The substrate and/or passivation layer allow the conducting lines in IC's to carry current densities on the order of $1x10^6 - 1x10^7$ A/cm^2. Processing

defects can cause current crowding because they cause shrinkage of the current-carrying cross-sectional area. As this happens, the local temperature will be increased. Other local heating problems can be caused by other defects, such as a poor adhesion spot in the substrate and/or passivation layer. This will increase the atomic diffusivity and lead to accelerated electromigration-induced failures or thermal runaway, which can destroy the metal line. The third aspect involves material-related problems that come about because other materials such as silicides, polysilicon, and the diffusion barrier, are employed together with the metallic thin film to form the multilayered structure. These materials usually have a higher resistivity and a finer grain size than those of the metal lines due to the different functional and stability requirements. These material combinations can give rise to flux divergence and a peculiar mode of electromigration-induced damage, depending on the specific layered structure and device geometry.

In addition to the increasingly smaller manufacturing process playing a role in increasing the likelihood of electromigration, there are also electromigration concerns for high power devices such as GaAs power MESFETs. The large gate bias voltage and drain voltage for FETs result in a high current density at microwave frequencies in the gate metallizations. In these devices, electromigration damage can be seen in the gate fingers **[4]**. This can be seen in Fig. 1.1.

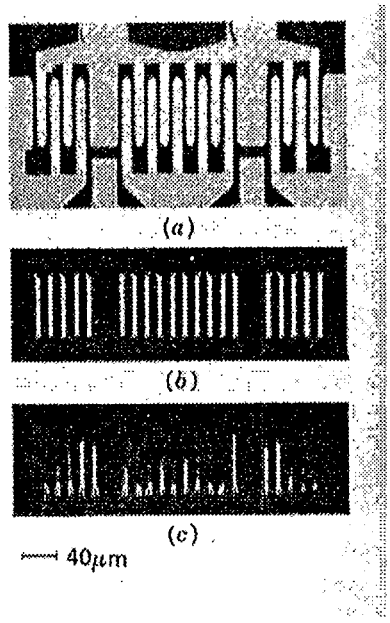

Fig. 1.1 (a) SEM micrograph of the gate area of an Al multigate GaAs power MESFET; (b) EBIC image at the same magnification of an untested sample; (c) EBIC image of a degraded sample after 2000 test hours with a gate current density of $5x10^5 A/cm^2$ at 200°C. Interruption of most of the gate fingers is evident **[4]**.

This results in a loss of control of device drain current and an increase in series resistance in the ohmic contacts. The increased series resistance leads to two potential problems: (a) Enhanced RC time constants which reduce the frequency response, and the cut-off frequency limit f_T. (b) Larger internal heating which could degrade device performance due to mobility deterioration **[4]**.

Since electromigration plays an important role in integrated circuit reliability, especially as manufacturing processes become smaller in the quest for more processor speed for example, an accurate method of simulating electromigration in integrated circuits is needed. With a computer simulation of electromigration applied to an

integrated circuit prototype, integrated circuit designers would be in a better position to predict the projected reliability of the device.

Electromigration is a diffusion based/controlled process and as such, much of the research performed thus far has assumed that the diffusion coefficient is spatially uniform throughout the conductor material. This has given reasonable results in many studies in the past. However these studies were performed on relatively large, micron-sized interconnect lines. In such structures, many of the microscopic details and inhomogeneities become inconsequential and do not play a significant role. In smaller sub-micron and nanolength structures, details of the internal spatial inhomogeneities and connectivity between the various electromigration paths become very important. This thesis suggests the idea that the diffusion coefficient may not always be the same throughout the material and may in fact, depend on what impurities are present in the material as well as various grain boundary structures.

Grain boundaries are the result of atomic misalignments and arise during the metalization process. Physically, their origin is linked to the requirement of simultaneously minimizing the internal energy and maximizing the system entropy. This thesis will attempt to probe the validity of spatially uniform diffusion coefficients through computer simulations of electromigration, which will be based on a molecular dynamics approach. This computer simulation will, among other things, continuously calculate and update the atomic position and atomic drift velocities along the entire length of the material under test. It is believed that this microscopic determination of these variables will be far more accurate than the macroscopic approach usually taken in other

experiments, particularly in the context of conductors having widths in the nanoscale range.

Several damage characteristics have been observed in electromigration research and these damage characteristics seem to take on different morphologies as the width of the conducting line decreases. For example, hillocks formed in micron-sized lines or sub-micron-sized lines take on a distinctive angular shape resembling an actual hill or triangle on one side of the conductor. In nano-sized lines, a hillock can be seen as a bulge or balloon across the conductor having a much more smooth and symmetric shape than its angular micron-sized counterpart, see Fig. 1.2. Perhaps this distinct change in electromigration morphology can be explained best by looking at the changes in variables, such as the drift velocity and atomic position on a microscopic scale.

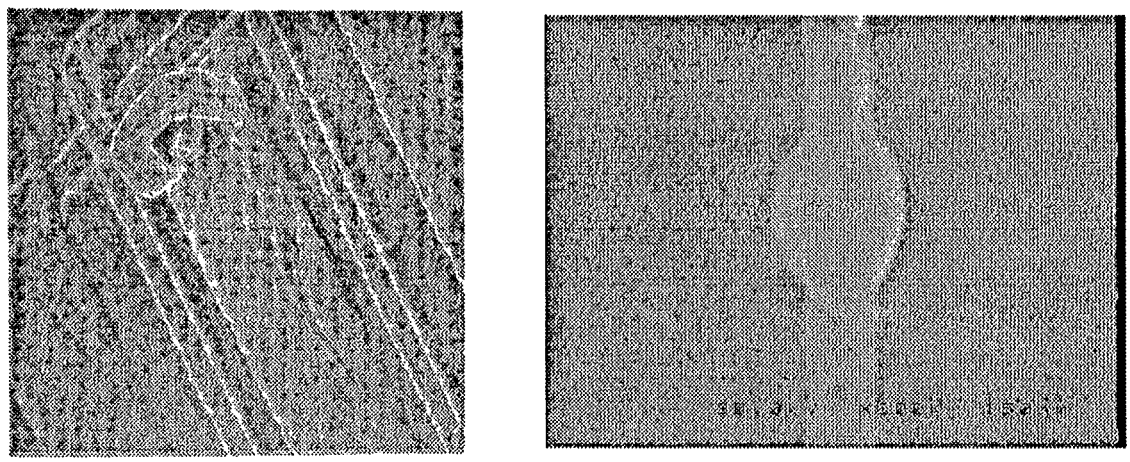

(a) (b)

Fig. 1.2 (a) An example of sharp, angular defect in the form of a hillock or whisker along the conducting line; (b) Example of a nano-sized (60nm) conductor line with a hillock formation. Note the smooth, balloon-shaped feature **[4]**, **[5]**.

Chapter II of this thesis provides a literature survey on different types of electromigration as well as various ways researchers have simulated electromigration. Some of the ideas described here are the effects of void shape in relation to critical and non-critical voids, macroscopic and microscopic molecular dynamics simulation techniques of electromigration and their results, and computer modeling techniques of integrated circuit conductor lines used in these computer simulations.

Chapter III details the numerical simulation procedures. This chapter describes the model of the conductor line under consideration and its relevance to electromigration. Next, the rationale and outline of a computer program that performs molecular dynamics simulations is described. Simple 1-D and 2-D test cases will be presented along with the simulation results in an effort to demonstrate the validity of the simulation technique proposed in this thesis. These simulations will emphasize different electromigration forces to examine their contribution to electromigration. These simulations will not contain any defects in the simulation space. This facilitates study into how each of the three forces of electromigration considered here (electric field, electron wind, and Lennard-Jones potential) interact with each other.

Chapter IV then discusses and compares the results of the molecular dynamics simulation with the results found by other researchers, namely the atomic drift velocity. Like chapter III, several cases will be presented, each emphasizing a different electromigration force. These cases will be simulated in the presence of microscopic defects such as dislocation boundaries to examine how microscopic defects influence atomic position and drift velocity. In doing so, this chapter also serves to prove the validity of the program and its relevance and contribution to electromigration simulation.

Chapter V provides a conclusion to the research outlined is this thesis with some comments on further directions that research in the field of electromigration study can take. Several ways to extend these simulation programs to take into account a wider variety of conductor types, defect types, and grain boundary types are also introduced.

CHAPTER II

LITERATURE REVIEW AND BACKGROUND

2.1 Introduction

Electromigration is the process of transport of material within a conductor at high current densities. These current densities should be on the order of $1x10^6$ A/cm^2 in order for electromigration to begin to occur. In a bulk material alone, current densities can approach $1x10^5$ A/cm^2. For integrated circuit interconnects, the thin-film conductors are in much more intimate contact with the surrounding substrate. Substrates are usually made from silicon, silicon oxide, and nitride, which have good heat conductivities. This facilitates dissipation of the Joule heat generated by an electric current passing through the conductor. The small dimensions of the cross section of the thin-film conductor which are usually not more than 5 *u*m thick and 10 *u*m wide are small compared to the thermal diffusion length which is on the order of several tens of microns. This allows for, and facilitates fast heat removal in the thin-film conductor. The thin-film conductors can therefore carry currents in the range of $1x10^6 - 1x10^7$ A/cm^2 and still allow the device to operate at temperatures at or below one half the melting point of the materials. This is one of the reasons why current densities of this magnitude can exist in today's IC's without rapid destruction of the device.

An increasing amount of research is being done on this destructive process since integrated circuits today are being manufactured on an increasingly smaller process. The smaller dimensions are becoming necessary to increase the on-chip density, reduce costs, and enhance the device operating speeds. The electromigration process has actually been

known for some time, but it did not play a major role in chip reliability since integrated circuits during the 60's and 70's were manufactured on a process that was characterized by feature size on the order of several microns. This automatically mitigated the occurrence of extremely high current densities. Today however, since integrated circuits manufactured on a .35 micron process or smaller are common place, and since circuit densities within these chips have increased at an exponential rate, current densities approaching or exceeding $1x10^6$ A/cm^2 are also common place. This fact tends to put the concept of electromigration in the forefront when studying integrated circuit reliability.

2.2 Overview of the Electromigration Process

There are three main forces to be concerned with when discussing the electromigration process and its physics. These are the electron wind force, the electrostatic Coulombic force, and the Lennard-Jones inter-atomic potential. In any conductor that is carrying a current, there will be an electron wind force associated with that current. Physically, this wind force arises from the continuous, stochastic collisions of the moving electrons with the lattice atoms. Hence, this force only exists in the presence of an applied electric field which provides net electron drift. The magnitude of this force is directly proportional to the applied electric field. An expression for the total average force on the atoms can thus be written as

$$\langle F_{atom} \rangle = qE - \langle m_e dv/dt \rangle + \langle F_{LJ} \rangle \quad , \qquad (2.1)$$

where q is the electronic charge, E is the applied electric field, m_e is the effective electron mass, and $\langle F_{LJ} \rangle$ is the time averaged Lennard-Jones potential. Assuming each atom is

symmetrically surrounded by a cluster of similar atoms the time averaged net Lennard-Jones force, $\langle F_{LJ} \rangle$, is zero and equation 2.1 becomes

$$\langle F_{atom} \rangle = qE - m_e v_{dr}/\tau_c + 0 \quad . \qquad (2.2)$$

The collision time, τ_c, can be related to the mobility, u_e, as

$$u_e = q\tau_c/m_e \quad . \qquad (2.3)$$

Hence, $$\langle F_{atom} \rangle = qE - q(v_{dr}/u_e) \quad . \qquad (2.4)$$

In the linear regime, $v_{dr}/u_e = E$. Hence,

$$\langle F_{atom} \rangle = qE - qE = 0 \quad . \qquad (2.5)$$

Thus, the average force on an atom in the presence of an applied electric field is zero.

The electron wind force is random in nature and can therefore be described in terms of a statistical distribution function. Due to the large number of electrons involved in the collisions, a Gaussian distribution function can perhaps be deemed to be a good characterization, as follows from the Law of Large Numbers. The average value of this force can be used in describing its role in the electromigration process. Thus, a curve representing the Gaussian distribution of forces associated with the electron wind would be centered about -qE in a perfect conductor. If the applied electric field were increased, the distribution curve for the electron wind would move more toward the negative direction in order to maintain equilibrium for the system, and provide a higher average value |qE|. The applied electric field is a constant and the Coulomb force it creates on the ions is equal to qE. In a perfect conductor with no defects such as voids, hillocks, or impurities, the average value of the electron wind force exactly cancels the Coulomb force due to the applied electric field, and hence relatively little electromigration takes place. However, since the electron wind force is random, it is possible for some of the

electrons to have unusually large velocities, which may have enough kinetic energy to break atomic bonds and knock a lattice atom loose from its neighbors. In a perfect conductor, such an event does not provide for electromigration due to the restoring Lennard-Jones potential. This force tends to counteract the forces of the electron wind and tends to keep all of the lattice atoms in place and undisturbed.

Electromigration can also be characterized by an atomic flux (J_A) related to the ion flux (j_k) through the equation **[4]**

$$J_A = (ND/kT)Z^*q\rho j_k \quad , \qquad (2.6)$$

where N is the number of atoms, k is Boltzmann's constant, T is temperature, q is the electronic charge, ρ is the resistivity, D is the atomic diffusivity, and Z* is the effective charge density **[4]**. For electromigration to occur, there must be a non-vanishing divergence of atomic flux. This divergence may be due to a temperature gradient or to microstructural inhomogeneities. Since electromigration is cumulative, it affects the failure rate. The median time to failure (MTF) in the presence of electromigration is given by the equation **[4]**

$$MTF = AJ^{-n}\exp(Q/kT) \quad , \qquad (2.7)$$

where A is a constant, J is the current density, and Q is the activation energy which is 0.6eV for Al and 0.9eV for Au. T is the temperature and k is the Boltzmann's constant. The electromigration exponent, n, ranges from 1 to 6 **[4]**.

In a real conductor, due to the manufacturing process and atomic misalignment during the growth process, grain boundaries are formed. These grain boundaries break the perfect periodicity of the crystalline lattice. This symmetry-breaking then creates a

non-vanishing divergence of the atomic flux and contributes to net electromigration. The conductor material is usually aluminum for several reasons **[4]**:

1) Ease of deposition: it can be sputtered or evaporated at fairly low temperatures.
2) Ease of patterning: phosphoric acid is usually used as the removal agent.
3) Aluminum forms ohmic/non-rectifying contact with silicon.
4) Schottky barrier contacts can be formed through careful process control.
5) Aluminum adheres to the die because it reacts slightly with SiO_2.
6) Aluminum will slightly reduce SiO_2 in thin layers and can deplete the very thin skin of native oxide that forms contact windows.
7) Glass deposited onto an aluminum surface sticks easily.
8) Aluminum is a good electrical conductor.

There are several drawbacks to the use of aluminum however:

1) Aluminum migrates easily at low current densities and temperatures. Gold is at least 10 times better in resisting electromigration; however its costs are higher.
2) Aluminum can absorb up to about 3% silicon. This creates alloying and aluminum spikes.
3) Aluminum corrodes easily in ionic solutions.
4) Addition of silicon is risky because silicon can precipitate out as nodules in an aluminum film.

In today's integrated circuits (IC's) which are manufactured on an extremely small process (0.35 micron and less), the conductors are very narrow, and so the grain

boundaries take on a bamboo-like structure. These grain boundaries can be nearly perpendicular to the axis of the conducting line **[6]**. The grain boundaries generally do not impede the flow of current or block the motion of electrons. However, they do allow for regions within the conductor between which the lattice spacing is not constant and spatially uniform. In this situation, some lattice atoms at the boundaries may be located further apart from each other, creating a localized void. In the void region, the Lennard-Jones potential is extremely small since its value is inversely proportional to $1/r^{13}$ with r being the lattice spacing. These voids are largely responsible for the beginnings of electromigration. In a void region, if an electron from the electron wind has sufficient energy, it can break a lattice atom loose from its bond. Once freed from its bond, the atom having acquired kinetic energy from the electronic collision, will tend to move towards the region containing a void. The perfect lattice sub-regions, on the other hand, present locally symmetric Lennard-Jones potential distributions, which prevent the moving atoms from coming to rest in these regions.

Voids are not only formed during the manufacturing process, but they can also be created due to thermal excitation. Under the influence of high temperature, perhaps caused by the presence of large current densities, the lattice atoms gain energy from the large number of collisions with the in-flowing, high-density, and high-energy stream of electrons **[1]**. Under a high enough temperature, it is possible that some lattice atoms may have enough kinetic energy to break loose from their bonds. This breakage significantly alters the spatial distribution of the Lennard-Jones potential in such regions. It then becomes possible for a subsequent incoming atom broken loose from its bond in a prior electron wind collision, to occupy that empty space. Such a distorted region of the

lattice can then begin to provide a nucleation point for a hillock to form some time later in the process.

2.3 Flux Divergence and Electromigration

For the case of an ideal conductor with no temperature gradient, there is no flux divergence, and so electromigration damage will not occur. However, most conductors are really polycrystalline thin films that contain structural defects. In these conductors, the temperature gradient cannot be completely eliminated. Whenever there is a spatial variation in the atomic density, the diffusivity, the current density, or the effective charge, divergence in the atomic or vacancy flux will be present and can give rise to local vacancy supersaturation or depletion.

Electromigration-induced damage begins by first nucleating voids under a sufficiently high local vacancy supersaturation. Further void growth requires a sustained vacancy flux divergence. After the void reaches a certain size, the current density and temperature distributions near the void will increase, accelerating the rate of damage formation. Damage formation in the form of hillocks occurs in a similar manner with local accumulation of atoms. Growth and linkage of voids and hillocks causes permanent damage in the conductor line by a void-induced open or an extrusion-induced short, known as a hillock. In this last stage, the time and the location for the permanent damage to appear are basically the result of a statistical process, depending largely on the spatial distribution of flux divergent sites. In general, the processes of damage formation starting from the electromigration-induced atomic flux, flux divergence, vacancy supersaturation or depletion, void nucleation and hillock formation, and finally growth

and linkage of voids and hillocks are very complex in nature. Computer modeling would have to be applied for simulating these processes **[1]**.

2.4 Types of Integrated Circuit Interconnects

Electromigration research is based on two separate methods and types of analyses:

1) Experimental observation of conductor samples subjected to high current density stressing. Quantities such as mean time to failure and void shape change are studied.

2) Simulations of electromigration based either on a molecular dynamics model employing a microscopic approach or macroscopic flux approaches.

These analyses are highly dependent on the microstructure of the conductor lines within the integrated circuit. Therefore, a brief description of integrated circuit interconnects is in order.

Electrical connections within IC devices mainly consist of segments that are oriented horizontally and vertically to the wafer surface, as shown in Fig. 2.1. The horizontal sections are referred to as runners, stripes, or lines, and the vertical sections are referred to as posts, studs, or plugs and are formed within openings in the dielectric called vias. Interconnects in IC's consist of some combination of layers of polycrystalline metals, most commonly Al alloys and refractory metals. Within the IC, multilevel interconnects are separated by insulating inter-level dielectrics (ILD's). It is possible that

as many as nine interconnect levels, linked by vias, will be employed in IC manufacture by the year 2012. The layers that comprise these levels are thin metallic films intimately laminated on each other. For Al alloys, each level is composed of some three to five layers of different metallic components. *Nearly every characteristic of metal lines has a measurable effect on electromigration lifetime* **[5]**.

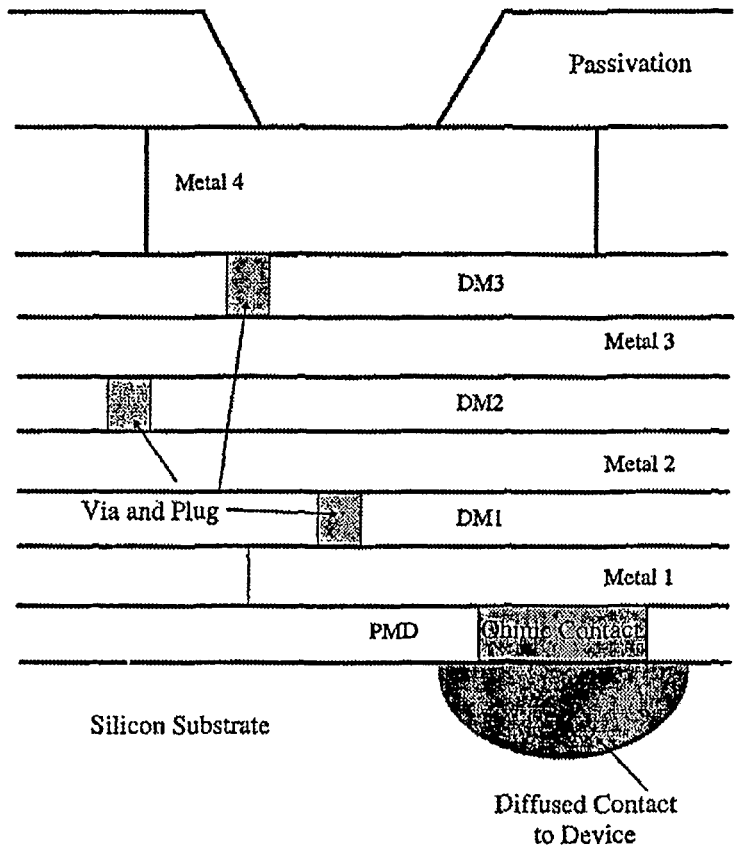

Fig. 2.1 Side view of a typical integrated circuit showing three layers or levels of metal interconnects. This illustration depicts many of the features that are common to today's IC's including vias, and plugs, and how they are used to construct a complete circuit **[5]**.

Most of today's integrated circuits have conductors with very narrow widths, only a few microns. The type of conductor material (usually aluminum) and the deposition process sets up a grain-like structure for the conductor. The grain patterns are more pronounced in a thin and narrow conductor since the size and spacing of the grains approach the width of the conductor. If the conductor is narrow enough, it could take on a bamboo-like structure, having nearly vertical lines across the conductor. These bamboo-like structures are really the result of atomic mismatch between different sections of the conductor during the deposition process **[4]**. Instead of the conductor having a smooth symmetric arrangement, some of the atoms making up the conductor are not in atomic alignment with each other, setting up an imbalance of forces even when the conductor is in an equilibrium state, i.e. no current flow and room temperature. This creates an environment that is perfect for electromigration; that being built in internal stress. Since lines with bamboo-like structures are becoming more common place in the integrated circuit due to the extreme miniaturization within these devices, this section focuses on such bamboo-like structures.

Bamboo-like grain structures exist where linewidths are smaller than the median grain size of the parent film. These lines are characterized by polycrystalline regions, or polygranular clusters, separated by one or more grains that span the width of the line, as shown in Fig. 2.2. This gives rise to two distinct diffusion paths that are available for atomic migration in this mixed microstructural regime. Atoms in the polygranular clusters may diffuse along the high diffusivity grain boundaries, while atoms in the bamboo segments must diffuse at much lower rates along the metal/oxide interface or

through the metal lattice. A large change in the diffusivity will occur at the beginning and end of a polygranular cluster and will lead to a large atomic flux divergence **[6]**.

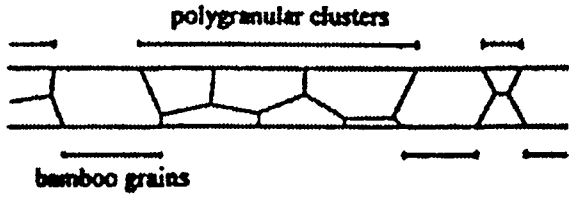

Fig. 2.2. This figure illustrates the concept of bamboo-like grain boundaries. The polygranular clusters are separated by nearly vertical (bamboo) grain boundaries. The dominant diffusion pathway is fundamentally different in each region **[6]**.

Electromigration in structures containing bamboo-like grains is less likely to occur, and in fact designers preferentially choose integrated circuit line widths such that if there is any grain boundary at all, it will be a bamboo-like grain boundary. This is because other grain boundaries which are not bamboo-like tend to form what are called triple points. This is where three grain boundaries intersect. The particle current flowing into the triple point junction is usually not the same as the particle current coming out; hence a flux divergence exists making conditions favorable for electromigration **[1]**. Therefore, it is a good rule to make the grains grow much larger than the line width, minimizing the number of triple point junctions.

Electromigration will still occur along grain boundaries because it is not possible to have all grain boundaries exactly perpendicular to the conductor line. Therefore, there will always exist some component of electromigration force in the direction along the line which can lead to void or hillock formation. However, the electromigration rate

along bamboo-like grain boundaries is usually much less than the electromigration rate for grain boundaries containing triple junctions, accounting for the relative longevity of bamboo-like interconnects. Therefore, most integrated circuit interconnects found today will contain mainly bamboo-like grain boundaries.

2.5 Effects of Grain Structure and Conductor Geometry

Electromigration lifetime is strongly correlated to the geometry and microstructure of the metal lines. Several studies have been carried out to investigate the effect of microstructure on electromigration lifetime. The increase of electromigration lifetime with increasing grain size has been reported in Al conductors with a width exceeding several microns **[7], [8], [9]**. This improvement in lifetime was found to increase approximately linearly with grain size. However, another study showed that such an improvement is limited by the ultimate grain size that can be reached by means of primary grain growth **[10]**. The electromigration lifetime of Al-Cu stripes was also found to depend on the grain size distribution **[11]** and film orientation **[12]**. Results of these studies indicated that when the variation of the grain size distribution is large, the standard deviation in the fail time of the lines increases while the electromigration lifetime decreases **[1]**.

The effects of grain size and grain morphology on the electromigration lifetime in Al-Cu fine lines has been investigated **[13]**. It was found that the electromigration lifetime depends on the grain size as well as the grain morphology in metal lines that are less than 2 um wide. The electromigration lifetime was found to increase until grain growth was constrained by the metal line thickness by annealing 2.0 um wide Al-Cu lines

at elevated temperatures to induce grain growth. The effect of grain structure on lifetime is no longer independent of the linewidth at this point. The dependence of the electromigration lifetime on grain size in 2.0 *u*m wide Al-Cu lines is shown in Fig. 2.3 (7 of Ho & Kwok) [1].

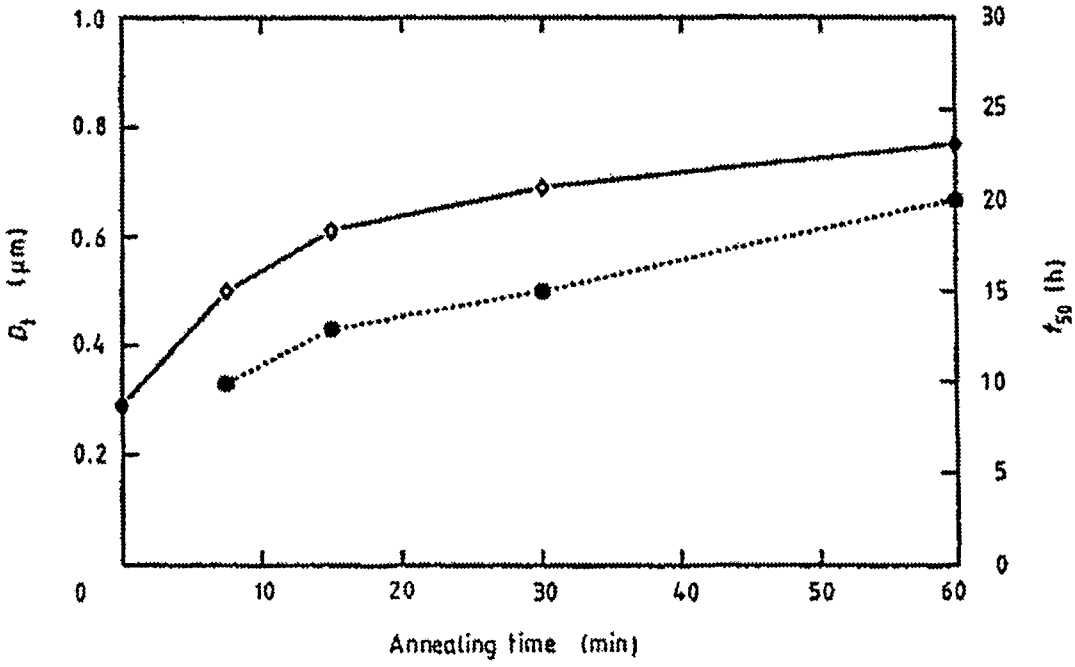

Fig. 2.3. Grain size (◊) and electromigration lifetime (•) of a 2.0 *u*m wide Al-Cu line annealed at 400°C for various periods. The test conditions were, T = 127°C, J = $5x10^6$ A/cm^2 [1], [13].

Studies have been performed that investigate the effect of geometry, including the linewidth, line length, and the film thickness. The results of these studies indicate that the effect is primarily in changing the statistical nature of the damage formation process. Several studies have been carried out on relatively wide lines that are several microns wide and about 1 *u*m thick. These conductor lines have several grains spanning across

the line, with an average grain size of about 1 um or less. With such a grain structure, the electromigration lifetime is expected to increase with the linewidth. This is because it becomes increasingly difficult for a crack to form across a wider line, either by statistical link-up of several damage sites or by the propagation of a single crack. A linear relationship between lifetime and linewidth of Al lines, with linewidth down to 5.0 um has been observed. The results are shown in Fig. 2.4 **[1], [14]**.

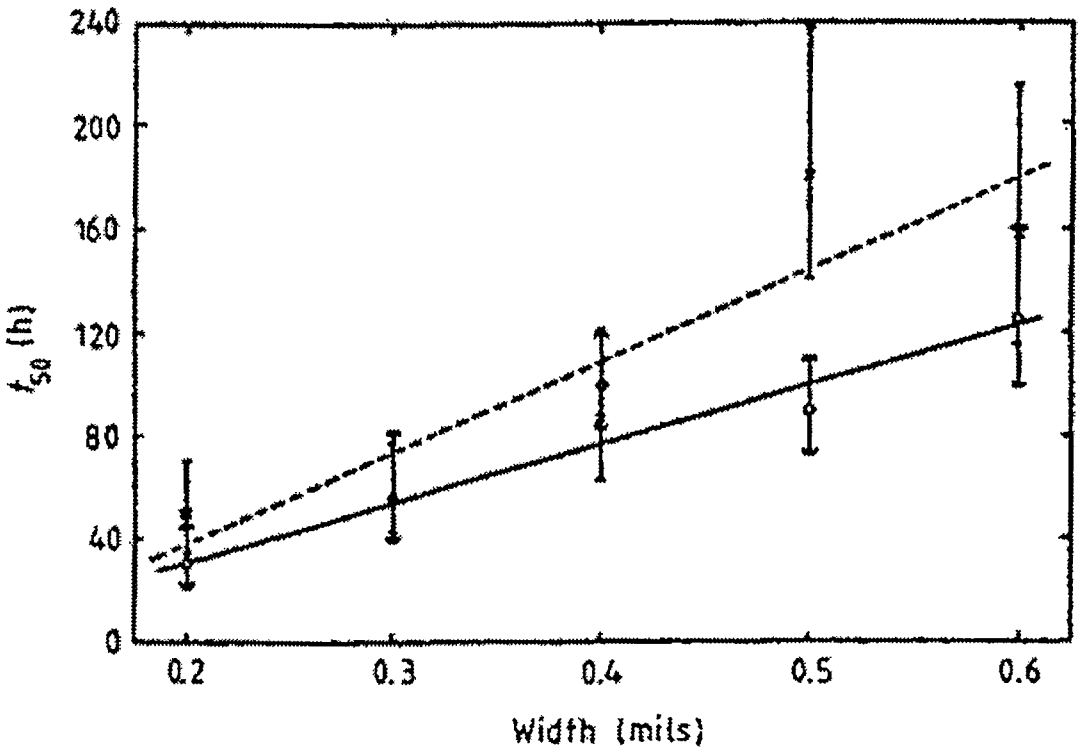

Fig. 2.4. T_{50} vs. width of the (x) 20 and (o) 45-mil-long conductors. Test conditions were, T = 130°C, J = 0.75x10^6 A/cm^2 (1mil = 25.4 um) **[1], [14]**.

The geometry effect can be significantly different as a result of changes in the grain structure when the linewidth decreases to about 1-2 um. This is because the development of the grain structure (the grain size) is controlled by grain growth. For a fine line, this can be constrained by the line dimension. For example, this point can be

reached for Al lines with 1 *u*m thickness within a width range of 1-2 *u*m. This effect was observed in Al alloy lines where the electromigration lifetime was found to increase or level off as the linewidth decreases below a critical value, reversing the trend in wide lines. The critical linewidth for Al-Cu lines has been found to be 3.5 *u*m **[15]** and 2.0 *u*m **[16]**. In a separate study involving Al-Ti fine lines, the lifetime was found to be essentially constant within a range of 1.8 to 1.2 *u*m linewidth and only increased sharply when the linewidth decreased to the range of 0.45 to 1.2 *u*m **[1], [17]**.

In a recent study **[18]**, the onset of the critical linewidth for Al and Al-Cu fine lines was investigated by varying the thickness of metal lines. As shown in Fig. 2.5, the critical linewidth was found to vary between 0.625 *u*m and 2.0 *u*m when the film thickness changes from 0.35 to 0.9 *u*m. Transmission electron microscopy (TEM) was used to observe the change in the grain structure with the onset of the critical linewidth. The study revealed that the grain size becomes comparable to the width. The microstructure of the line converges toward a bamboo-like structure with most of the grain boundaries perpendicular to the length of the line as the width of the Al-Cu lines decrease to values below 2 *u*m. An example of the microstructure of a series of Al-Cu lines with a width ranging from 0.5 to 2.0 *u*m is shown in Fig. 2.6 **[1]**.

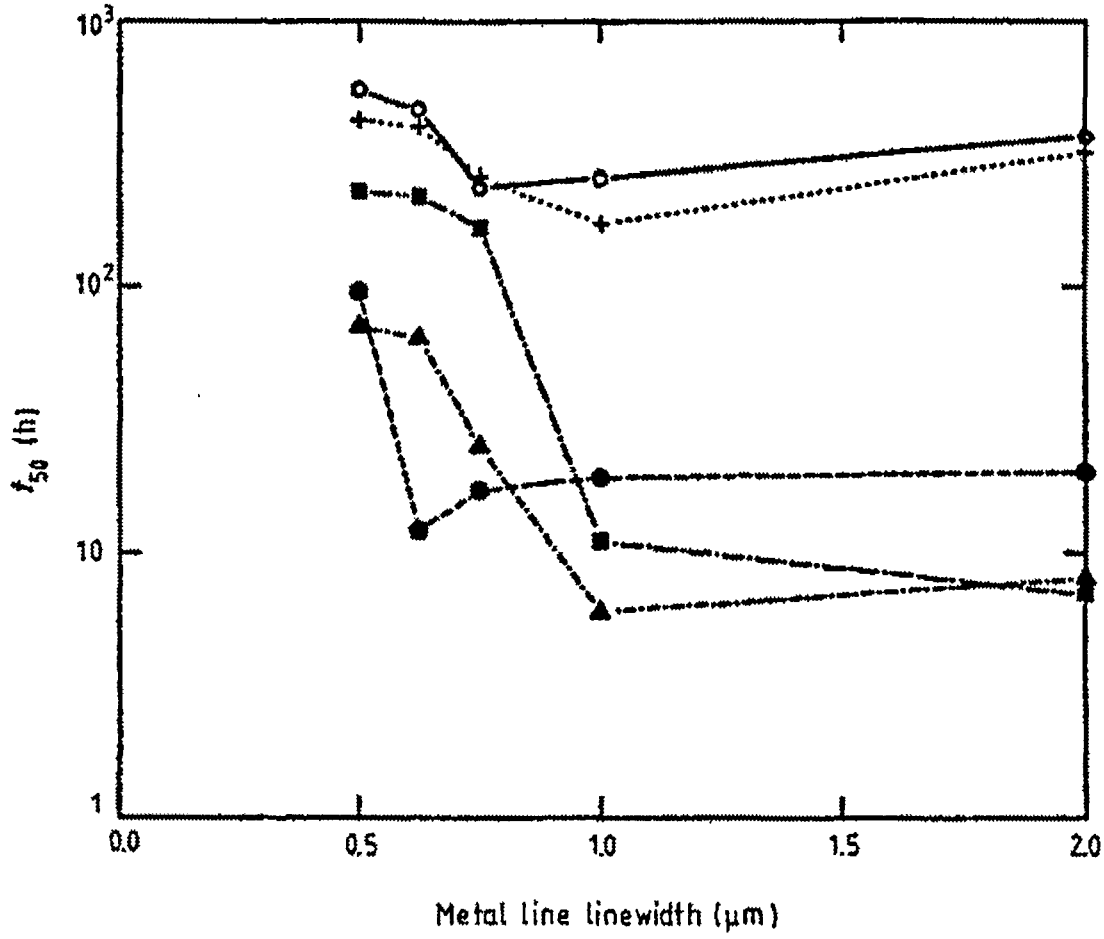

Fig. 2.5. This figure shows the effects of linewidth and film thickness on electromigration lifetime in fine metal lines. Test conditions were, T = 182°C, J = $1x10^6$ A/cm^2. Metal line thickness': •, 0.35 *u*m Al; ▲, 0.75 *u*m Al; ■, 0.90 *u*m Al; O, 0.5 *u*m Al-Cu; +, 0.86 *u*m Al-Cu. **[1], [18]**.

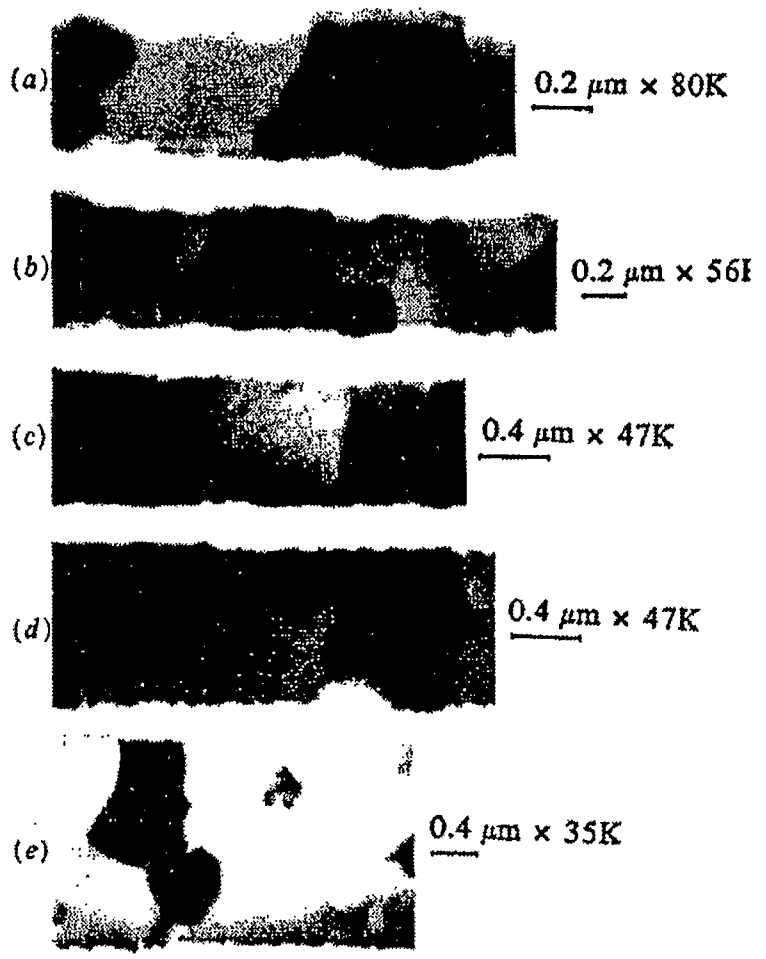

Fig. 2.6 Transmission electron micrographs of Al-Cu fine lines with 0.5 *u*m film thickness after annealing at 400°C for 1 hour. (a) Linewidth 0.5 *u*m, (b) linewidth 0.625 *u*m, (c) linewidth 0.75 *u*m, (d) linewidth 1.0 *u*m, (e) linewidth 2.0 *u*m. **[1], [37]**.

The linelength dependence of electromigration lifetime has been studied by several groups. Its extent depends on the nature and the distribution of the defects since the effect due to length changes reflects mainly the probability of finding a damage site. If there were an abundance of damage-forming defects in the metal line, there would be no linelength dependence of the lifetime. Conversely, if there were damage formed by the most severe defects, which are distributed randomly in the line, the lifetime would be

expected to decrease with increasing linelength. A combination of these characteristics was observed in an early study of Al lines by *Agarwala* **[14]**.

These authors found the electromigration lifetime decreasing rapidly with increasing linelength until the length reached a threshold value, as shown in Fig. 2.7. The saturation length changed from 62.5 *u*m to 125 *u*m when the Al linewidth increased from 10 to 15 *u*m. The extent of the length dependence was found to be much smaller in a recent study of Al-Si lines of 3 *u*m in width, where the lifetime decreased by only 16% and 5% with length increasing from 400 to 800 *u*m and from 800 to 1200 *u*m, respectively **[19]**. The lifetime in Al-Cu sub-micron lines was also found to decrease slightly with increasing linelength from 10 to 50 *u*m and then levels off to 500 *u*m as shown in Fig. 2.8. The length dependence of lifetime is not as systematic as the width dependence, varying in addition according to the film deposition condition and the type of metallurgy **[1]**, **[9]**.

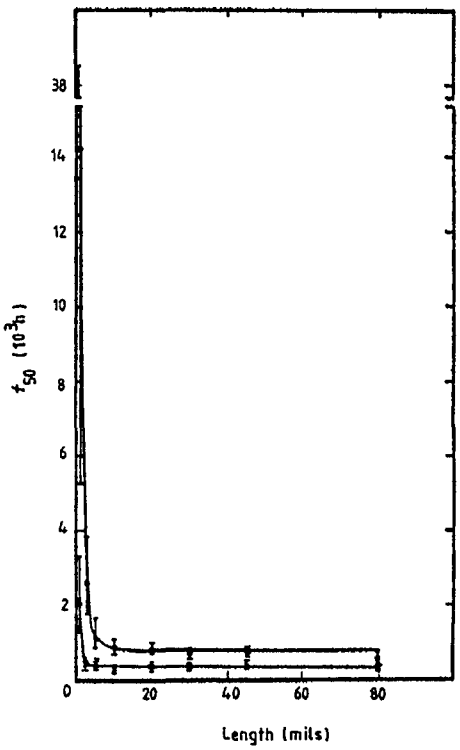

Fig. 2.7 t_{50} versus length of the conductors of width 0.4 (x) and 0.6 (o) mil. Test conditions were, T = 130°C, J = 0.75x10^6 A/cm^2 (1 mil = 25.4 um) **[1], [14]**.

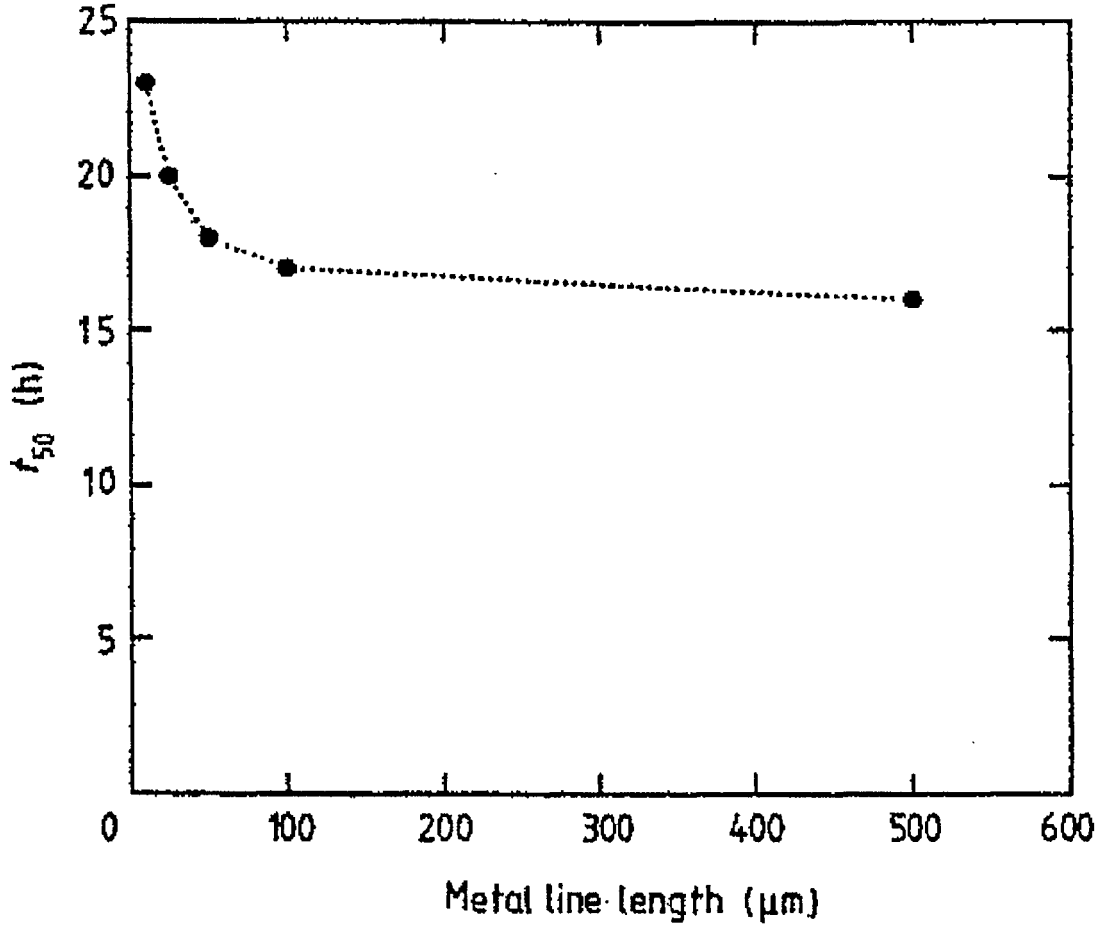

Fig. 2.8 Effect of metal line length on the median time-to-failure in Al-Cu sub-micron lines. Test conditions were, T = 227°C, J = 2.5x10^6 A/cm^2 **[1], [20]**.

The results from studies of conductor geometry indicate that the grain morphology becomes an important parameter in controlling the electromigration lifetime, as the linewidth and film thickness decrease to the sub-micron range. The extent of microstructural modification in fine lines may be a function of patterning techniques, deposition conditions, and metallurgy **[1]**.

In general, the effect that conductor line geometry has on lifetime due to electromigration in aluminum-copper sub-micron lines can be summarized as follows:

1) Lifetime decreases slightly with increasing line length and then levels off after a critical value.
2) As linewidth decreases, lifetime decreases, goes through a minimum, and then increases for less than a critical width.
3) Lifetime increases with decreasing film thickness.
4) Critical length and width decrease with decreasing linewidth and film thickness, respectively.
5) Grain morphology is an important parameter to control the electromigration lifetime.

For VLSI circuits, the increase in circuit complexity demands an increase in wiring density, which required multilevel interconnections. With these structures, there are many contacts connecting the metal lines from one level to an adjacent level or to a semiconductor junction. The electromigration characteristics of these contacts are usually different from those for flat metal lines. At a contact, material interactions can occur at the interface of two dissimilar materials, even when there is no current present. The addition of a current does however, disturb the temperature distribution as well as the driving force for mass transport. The resulting flux divergence at the interface can be very different from that of a flat line. In VLSI, the device scaling trend required significant increases in the current density at the contacts. This, coupled with the decrease in the contact dimension, has made contact electromigration a greater concern now than in the past, especially since for bipolar devices high driving current is needed for speed performance **[2]**.

Most of the studies on contact electromigration have been carried out on ohmic contacts in silicon with Al or Al alloy metal lines. A typical test structure used to study contact electromigration [21] is shown in Fig. 2.9. In this structure, two metal/silicon contacts are fabricated in a n^+ diffused resistor, so contact electromigration with opposite current flow directions can be observed simultaneously. A metal line is fabricated to link two diffused resistor contacts, a design which allows a comparative study of electromigration in metal lines and contacts.

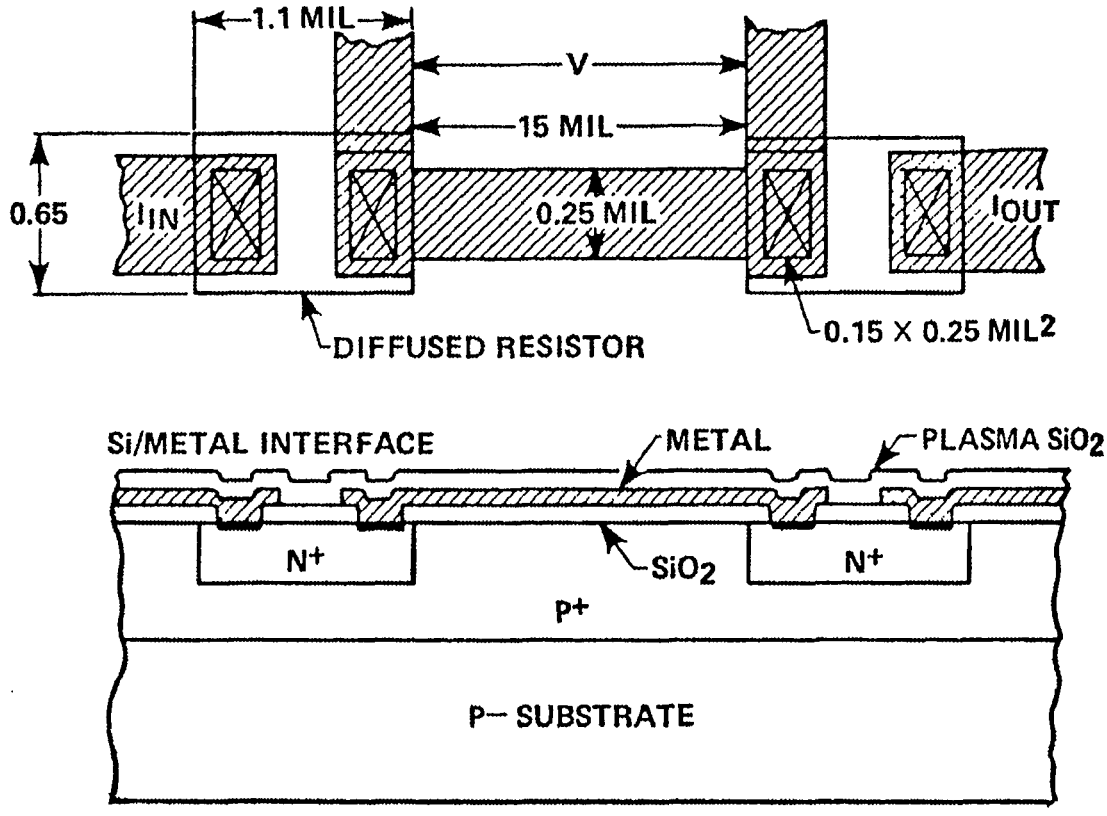

Fig. 2.9 Test structure HCS01-high current stress Si/metal interface [1], [21].

Based on the results of studies on line geometry and grain structure, several factors can contribute to the improvement of electromigration resistance. First, the

number of grain-boundary paths for diffusion along the metal line is small, so the amount of mass transport is reduced. Second, as the number of grain-boundary triple points per unit length is reduced, so is the number of divergent sites for damage formation. And third, the electromigration flux is reduced since most of the grain boundaries are perpendicular to the direction of current flow **[1]**.

Another force to consider when studying electromigration effects are the mechanical forces within the IC during and after the manufacturing process. For example, many IC's are manufactured at an elevated temperature. This temperature is well outside the normal operating range for the finished IC. As the newly manufactured IC cools from this temperature, mechanical tensile and compressive forces are set up due to differing thermal coefficients of expansion between the adjacent metal and semiconductor layers. Different coefficients of expansion exist, for example, at the metal/substrate boundary. The only way that this type of tensile straining can be relieved is by the formation of voids, as it tends to minimize the internal energy. The void formation over time leads to eventual conductor failure. The problem is made more severe by the fact that the line is surrounded on all sides by some dielectric material within the IC. In the worst cases, this type of voiding, which is strongly process related, can occur without the other two driving forces, the electron wind and the electric field. In some cases, IC's have been known to fail during storage with no current passing through the interconnects **[5]**.

2.6 Techniques for Lifetime Measurement

The lifetime measurement of conductor lines is the most commonly used method for evaluating electromigration resistance. The results of these techniques usually follow a lognormal distribution and are provided in terms of a median time-to-failure (MTF). This quantity can also be represented by the term t_{50}, which is the time needed to reach a failure of 50% of a group of identical conductor lines. The electromigration lifetime test is usually carried out under a set of accelerated test conditions at elevated temperatures and with high current density stressing in order to obtain the results of lifetime measurements in a reasonable time frame. The data are usually then extrapolated to the device operating conditions, which are typically at room temperature and with current density stressing below $5x10^5$ A/cm^2. This extrapolation assumes that the mechanisms leading to electromigration-induced failures under the accelerated lifetime test conditions are the same as those under device operating conditions.

Recently, four faster techniques for electromigration lifetime measurement have been proposed. The temperature-ramp resistance analysis to characterize electromigration (TRACE) method **[22]** is based on resistance measurements in the early stages of electromigration-induced damage. The Standard Wafer-level Electromigration Acceleration Test (SWEAT) method **[23]** monitors electromigration susceptibility of the wafer level. The breakdown energy of metal (BEM) method **[24]** measures the median-energy-to-fail of properly designed structures during a ramp current stress. The 1/f **[25]** and $1/f^2$ **[26]** noise methods are basically electrical noise measurements. At this time, these four new techniques are all in the exploratory stage. The validity of these tests and their correlation to electromigration has yet to be established.

2.7 Conductor Characteristics

A conductor with a bamboo-like grain boundary structure exhibits very different characteristics than a conductor with a perfectly symmetric lattice structure when exposed to an electric field and corresponding electron wind. A perfect conductor would have a completely symmetric and repetitive arrangement for all the atoms that make up the conductor. Along with this perfect arrangement of the lattice atoms would be a balance of forces that bind these atoms to the lattice. One of the main forces of interest here is the Lennard-Jones potential. This force takes on the following form:

$$F_{lj} = 12\varepsilon[d^{12}/r^{13} - d^{6}/r^{7}] \quad , \quad (2.8)$$

where F_{lj} is the force between the l^{th} and j^{th} atoms, r is their separation distance, ε is a restoring force constant equal to 1.656×10^{-21} for copper lines, and d is the equilibrium lattice spacing or atomic radius. A plot of this equation is shown in Fig. 2.10.

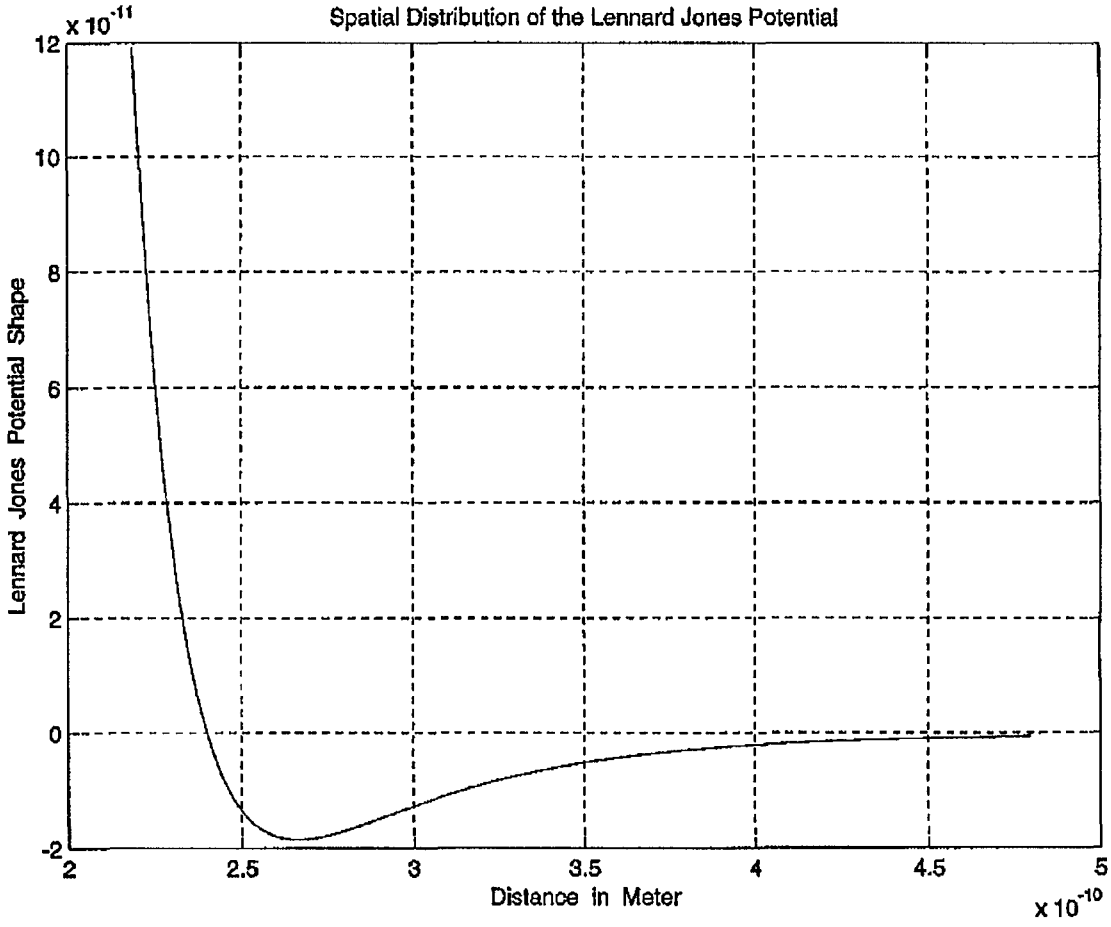

Fig. 2.10 Plot of the Lennard-Jones potential. The Lennard-Jones potential falls off very rapidly as the atomic distance, r, is increased. For small r however, the Lennard-Jones Potential can become quite large.

As the equation indicates, this force is highly dependent on the separation distance, r, between the atom of interest and its nearest neighbor. The Lennard-Jones potential is an effective pair potential that describes the interaction between two uncharged particles. In an uncharged particle, a symmetrically distributed (round) electron cloud exists around its nucleus. As a result, the particle has no dipole moment because no charges are concentrated in any one direction. An atom conducting current within a conductor is constantly in motion, undergoing collisions and near-collisions with

other atoms. When two uncharged particles approach one another, the charge clouds remain undistorted and have no net dipole moment. During an interaction between charged particles, each undergoes deformation and the particles no longer have a symmetrical electron cloud distribution. As a result, particles leaving the interaction acquire a net dipole moment. This is called an induced dipole moment. It lasts for only a short time, but during this time particles with dipoles are attracted to each other. This potential is called the Lennard-Jones (L-J) potential **[27]**. If all of the atoms were perfectly arranged symmetrically within the conductor, it would be very difficult for these atoms to break loose from their bonds since the L-J potential provides a restoring force. The effect of the electron wind force is therefore minimal. In this situation, a balance of L-J forces (from the atoms' nearest neighbors) would tend to resist any change in direction from the electron wind.

Unlike the perfect conductor, a real conductor (and in particular, a conductor with a bamboo-like grain structure or grain boundaries) does not have a complete balance of forces. Within the vicinity of the grain boundaries of the conductor, there exists a stress gradient. This stress gradient (and hence the internal strain with spatial non-uniformity) sets the stage for some of the lattice atoms to break loose from their bonds. This is because some of the atoms are left without a binding force in a particular direction and will preferentially tend to move in the direction where there is the weakest restoring force to counter the electron wind. This direction is typically along the grain boundaries of the grain-like structure. When the lattice atoms that make up the conductor begin to move under the force of the electron wind, we have the beginning of electromigration.

2.8 Stress Characteristics of a Conductor under Electromigration

Under the effects of electromigration, mass will tend to accumulate at the downwind end of the cluster and deplete at the upwind end, leading to a compressive and tensile stress and the development of a non-uniform stress gradient along the length of the cluster. This stress gradient will create a diffusive driving force for atomic motion, which opposes the electromigration driving force. As the stress profile evolves, equilibrium will eventually be established where the driving force due to the stress gradient exactly counterbalances the electromigration driving force. The maximum stress achieved at steady state is therefore dependent on cluster length. Continuing this line of reasoning, there should exist a critical cluster length, Lc, such that the critical length will be able to support a stress large enough to cause line failure. Grain boundary diffusion should therefore be the diffusion mechanism that determines the time to failure of the line. Lines in this category could be said to fail due to polygranular failure mechanisms. On the other hand, a failure in a line that contains only short clusters ($L < Lc$) requires significant diffusion through the bamboo segments. Therefore interfacial or lattice diffusion will control the failure time. These lines will be said to fail due to transgranular failure mechanisms. Hence, the distribution of cluster lengths should determine which failure mechanism would be observed in a population of lines **[6]**.

This gives rise to the idea of bimodal failure mechanisms. If the magnitude of the critical stress is small, the conductor lines will tend to fail due to polygranular mechanisms since those clusters can easily support a stress large enough for failure. If the magnitude of the critical stress is large, the opposite is true, and significant diffusion

in bamboo segments would be required before failure can occur. Bimodal failure distributions are a common problem and are expected whenever feature sizes such as linewidths (or via diameter) and grain sizes are comparable **[6]**.

This bimodal behavior has been responsible for a large deviation in failure times in experiments. The reason seems to come from the fact that the maximum line steady-state stress achieved is sensitive to the spatial distribution of polygranular clusters along the line. A line in which the clusters are distributed relatively evenly along its length will survive longer than a line in which the clusters are distributed unevenly along its length. An extreme example is shown in Fig. 2.11. In this representation of a line, the number and lengths of clusters in each line are identical. Since the clusters are evenly spaced along the first line, the stress coupling between clusters will be small and the steady-state stress will be low. For the second line, the clusters are spaced very close to one another and will interact strongly and generate a much larger steady-state stress. Therefore, the distribution of clusters within a conductor also dictates how much stress the conductor can take, and hence the time-to-failure of the conductor under electromigration stress **[6]**.

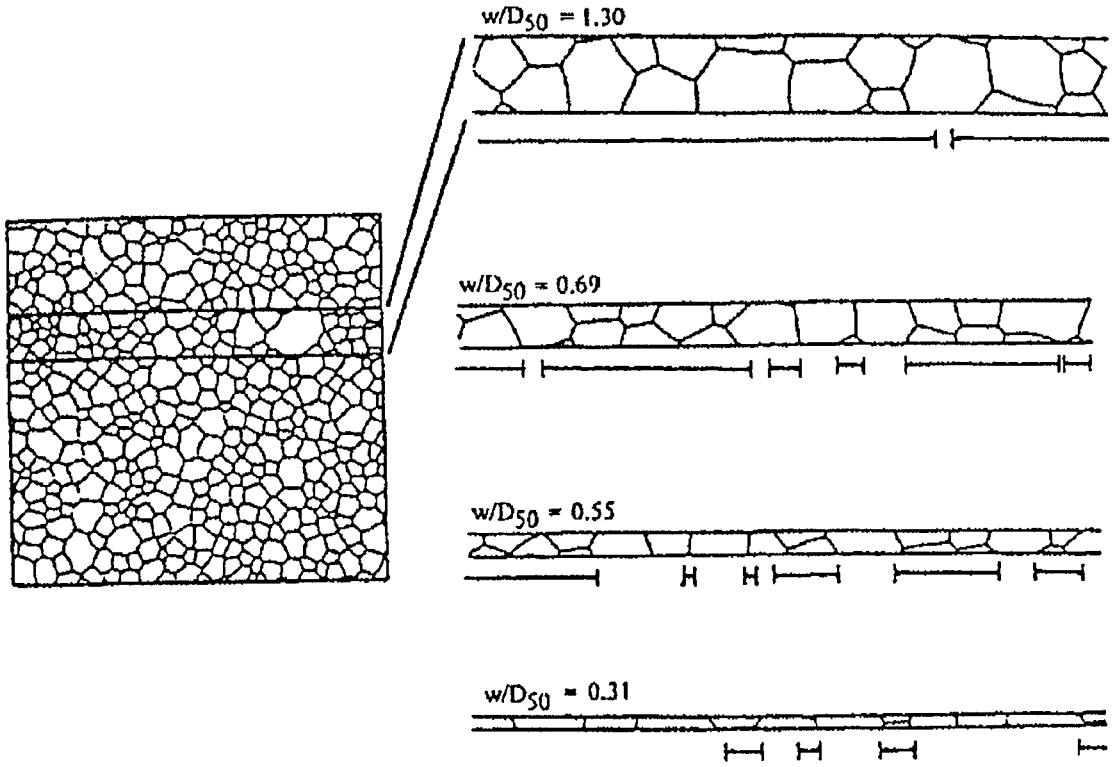

Fig. 2.11 A lognormal grain size distribution and lines of varying widths patterned from the conducting film. As the linewidth decreases below the median grain size of the continuous film, the average length of the polygranular clusters decreases **[6]**.

Polygranular clusters can also interact. If two clusters are located very close to each other, their stress profiles will overlap. This stress coupling leads to larger stresses than those expected assuming that the clusters act independently. The degree of coupling depends on the length of the intervening bamboo segment and on the ratio of grain boundary to bamboo diffusivity. If two clusters close to the critical length are separated by a very short bamboo grain or segment, they will interact with each other and may still cause relatively rapid failure.

It is possible for grain boundary diffusion to be the dominant diffusion mechanism in a line containing no clusters longer than Lc, the critical cluster length. The existence of two different failure mechanisms greatly complicates reliability assessment. Therefore, in order to accurately predict interconnect reliability, knowledge of the dominant diffusion mechanism is required. This diffusion process or more accurately, the diffusion coefficient thus becomes one of the critical parameters that can provide insight into the unique behavior of electromigration **[6]**.

2.9 Void Shape Change

Research on electromigration in the area of void shape change has also been carried out. It has been discovered through experimental observation that the shape of the void, as well as other parameters such as diffusivity and grain boundary structures can be used to describe and predict electromigration behavior. A typical void shape has been identified which appears to be necessary for the development of a failure site **[28]**. This "fatal void" usually takes on a slit-like morphology, which gives the appearance of a crack perpendicular to the conducting line as shown in Fig. 2.12 **[28]**.

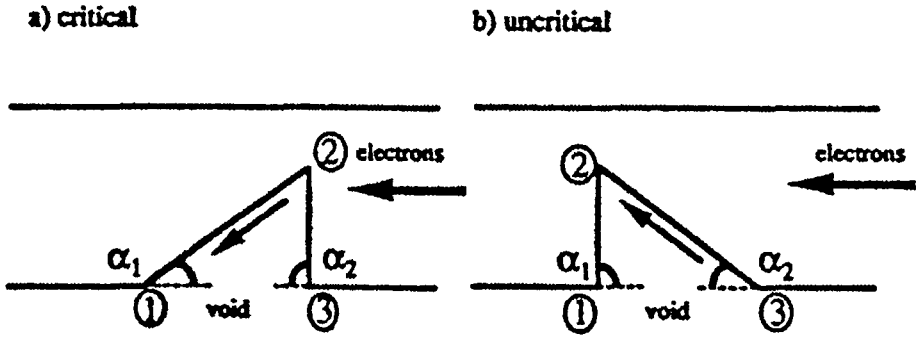

Fig. 2.12 This is a schematic representation of the interaction between the void shape and the electron wind: (a) Since $\alpha_2 = 90^\circ$, no electromigration-induced mass flux exists from 3 to 2 but there is flux from 2 to 1 as a function of α_1. Consequently, mass is removed at 2 and the void tends to become fatal with a critical void shape. (b) No electromigration-induced mass flux on the void surface from 2 to 1 ($\alpha_1=90^\circ$), but from 3 to 2, as a result mass is removed at 3 and the void grows along the line with an uncritical void shape **[28]**.

In this figure, there are two angles, α_1 and α_2, that describe the void shape. If $\alpha_2 = 90^\circ$, there is no electromigration induced mass flux from point 3 to point 2, but there is from point 2 to point 1 as a function of α_1. Mass is gradually removed at 2 and the void becomes fatal. In the process, the "neck" at point 2 keeps getting narrower, until eventually an open circuit condition occurs. If $\alpha_1 = 90^\circ$, there is no electromigration induced mass flux on the void surface from point 2 to point 1, but there is from point 3 to point 2. So mass is removed at point 3 and the void grows along the line, making it uncritical.

Research using scanning electron microscopes (SEM) and focused ion beam techniques and by transmission electron microscopes (TEM), shows that these slits frequently do not follow grain boundaries, as might be expected, but are actually transgranular. This is not to say that grain boundaries are not important. They can trap voids until they reach a critical size. In general, small voids migrate more rapidly. In fact, a critical void size exists for which void motion is a minimum; the consequence could be that larger voids catch up with smaller ones, as they move more rapidly. The result can be a catastrophic mechanism of void growth and failure **[28]**.

Fig. 2.13 shows a damage site that illustrates this concept. Here, the void is observed for the first time after 65.8 hours, then it grows linearly with time along the edge of the line [Figs. 2.13(a) – 2.13(e)]. The big white spot on the line, probably alumina on the surface, can serve as a stationary marker; it is invisible in the SEM if the Al beneath it has been removed by electromigration. In this example, the void breaks into two [Fig. 2.13(f)], with the total void volume remaining nearly constant. Although the void on the left of Fig. 2.13(f) grows to over about 80% of the line width, failure does not occur at this site. Contrary to this, the void on the right moves several microns and grows at the expense of the other void. Void nucleation takes up only a small fraction of the total lifetime and void growth is linear in time. Looking at Fig. 2.13(g), it is striking that the void contour, which is turned against the direction of the electron flow, is more or less perpendicular to the line. During the course of their investigations, more than 500 fatal voids in lines of various widths and alloy composition were investigated and this shape asymmetry was a common observation, especially in narrower lines **[28]**.

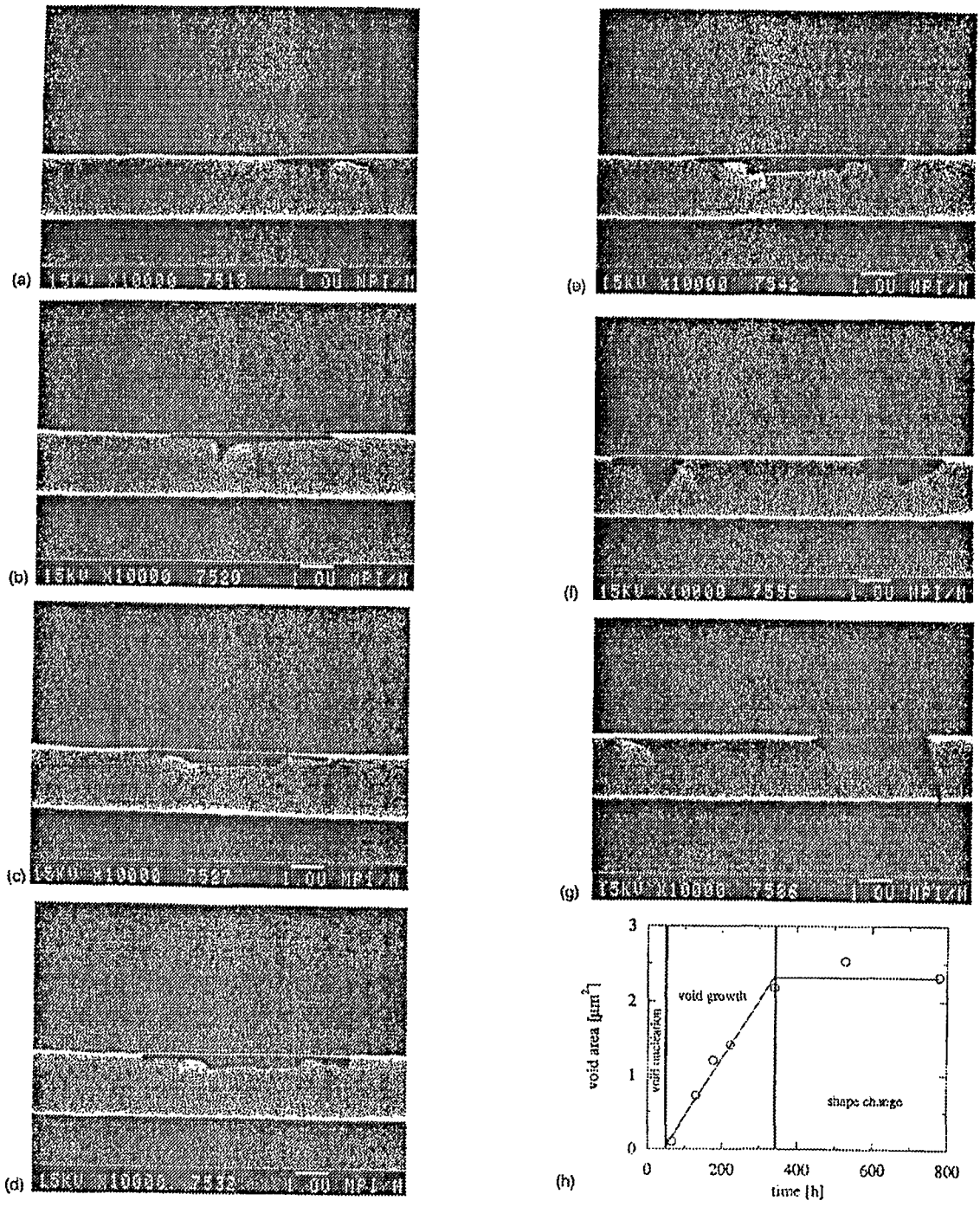

Fig. 2.13 This is a sequence of SEM micrographs. Testing time (a) 65.8 h, (b) 131.8 h, (c) 177.2 h, (d) 224.3 h, (e) 341.9 h, (f) 528.6 h, and (g) 780.6 h, (h) Void area as a function of time **[28]**.

Fig. 2.14 shows a sequence of electromigration in a line with a near bamboo structure. Fig. 2.14(a) depicts a void and the corresponding hillock after 12.2 hours, both of which had not been observed after 9.4 hours. Grain boundary grooves, which are partly visible in the SEM, are highlighted. After 16.5 hours Fig. 2.14(b) and 25.5 hours Fig. 2.14(c) the void shape has not changed significantly, only the angle between the cathode (right) boundary of the void and the line changes from 40 degrees to 10 degrees, indicating that this boundary probably does not reflect a particular crystallographic plane. Fig. 2.14(d) shows the final void shape after 42.2 hours, which is totally different from those before. The void grows linearly with time (as in the previous figure), but its shape changes simultaneously. The cathode boundary is neither straight nor perpendicular to the line all the way. The left part of the void, where the opening occurred, could be approximated as a wedge whose anode sidewall is oriented at a more acute angle to the line than the cathode one. With this sample, grain boundaries had not moved under their grooves and the opening had not occurred along any grain boundaries **[28]**.

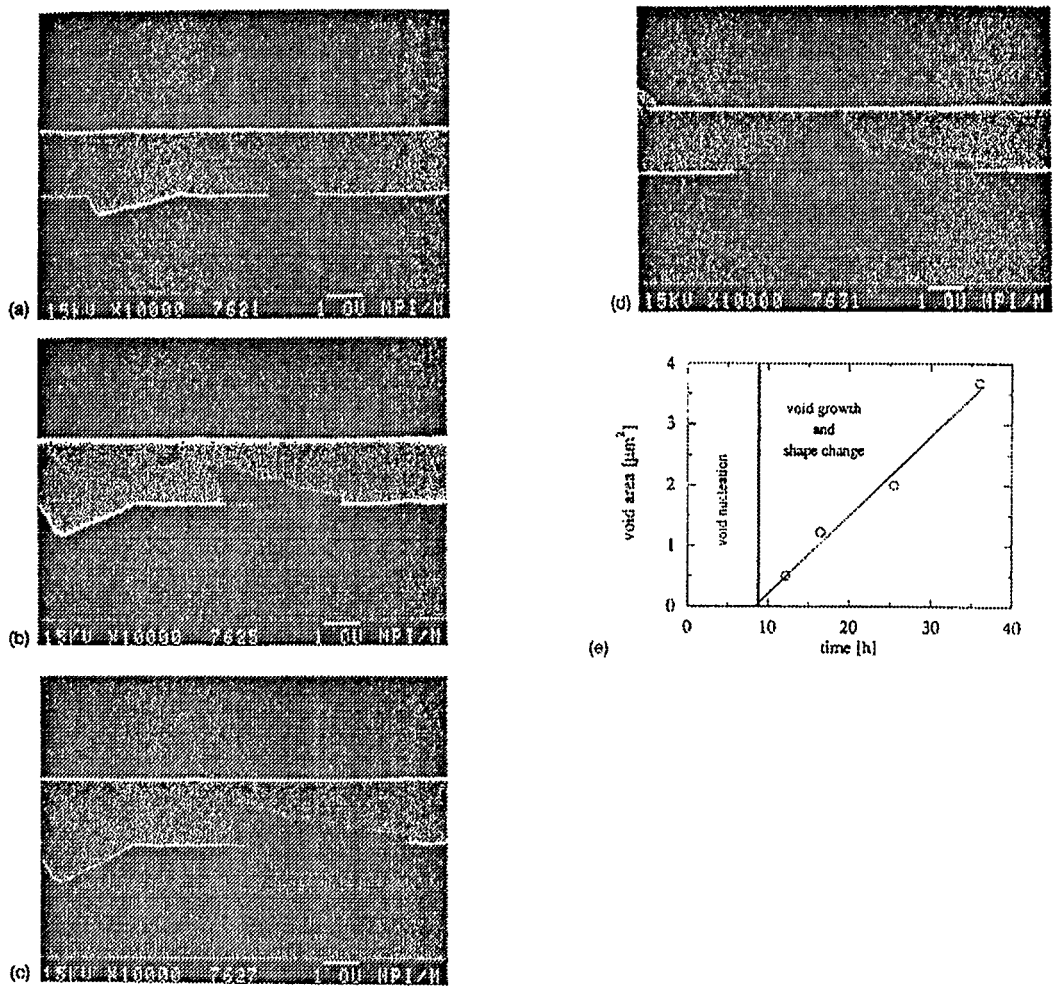

Fig. 2.14 SEM micrographs showing a time sequence on a conductor line of the re-flowed film (grain boundaries are artificially highlighted): (a) 12.2 h, (b) 16.5 h, (c) 25.5 h, and (d) 42.2 h. (e) Void area as a function of time **[28]**.

2.10 Analytical and Numerical Simulations

Computer simulations of electromigration are essential tools in the study of electromigration because the simulations allow us to evaluate and measure various aspects of electromigration that would otherwise not be possible through simple

experimental observation. The detailed physics can also be better understood and analyzed. For example, it would be difficult to track the continuously varying temperature gradient along the conductor, ascertain the local diffusivity magnitudes, or the effect of individual polycrystalline grains. Likewise, it is also difficult to keep track of all the continuously varying grain boundary misorientation angles, θ's, and the inclinations with respect to electron flow of all the grain boundaries in a conductor line. Computer simulations allow us to determine the influence of microscopic parameters on conductor material and effects of electromigration.

2.10.1 Macroscopic Simulations of Electromigration

This type of simulation often used in electromigration studies relies on the probability approach for calculations of the failure rates and mean time-to-failure (MTF) lifetimes. These models are statistical in nature, and seek to predict the average global effects arising from the various internal microscopic stressing and failure mechanisms. Such methods are appropriate in the performance predictions of large complex VLSI circuits having a large number of interconnects. Instead of probing the physics and details of electromigration along single metallic lines, the probabilistic behavior of the overall system is predicted. In this approach, the statistical aspects of lifetime to failure such as the failure time distribution, the MTF, the standard deviation, and their dependence on line geometry are the main concerns and outputs. The model uses a probability calculation to determine these values. It assumes that a conductor line is composed of a number of unit elements connected in a certain manner, and the failure

time of each unit element is an independent random variable following a lognormal distribution.

Macroscopic models and simulations usually employ bulk material characteristics in their approach. One of the more important bulk material characteristics is the diffusion coefficient. This is a coefficient that describes the rate at which atoms will diffuse into a sample material. Diffusion of atoms within a material occurs anytime when there exists an atomic concentration gradient. These atomic concentration gradients exist mainly because of slight defects in the material. Voids and hillocks are examples of extreme cases of where an atomic concentration gradient would exist. Grain boundaries are a more subtle example of where there could exist an atomic concentration gradient. Therefore, it is easy to see why most researchers have discovered that electromigration takes place mainly among these grain boundaries, voids, and hillocks. For example, the atomic flux through a region within a semiconductor is usually described using a diffusion coefficient, which traditionally is a constant in most calculations. This is shown in the following equation:

$$F = D\nabla N \qquad (2.9)$$

where F is the atomic flux, D the diffusion coefficient, and ∇N is the atomic gradient.

Other models in this category employ physically based analytical approaches based on averaged atomic flux to describe the stress related electromigration process. An example of such a model is by Borgesen et al. **[29]**. Their model goes somewhat further than the statistical model mentioned above, but still is considered a macroscopic model since it mainly deals with flux at the macroscopic level. This model states that when an electric current passes through a polycrystalline thin film interconnect, the atomic flux at

moderate temperatures comes primarily from electromigration along grain boundaries. **[29]**. In their research, they deal with a normalized diffusion coefficient that corresponds to the *entire* cross section of the line. The equation that describes this is

$$D_a = \delta D_{GB}/d \quad , \qquad (2.10)$$

where δ is the grain boundary width, D_{GB} is the grain boundary diffusion coefficient, and d is the grain size **[29], [2]**. This equation is a good example of a macroscopic approach where the entire cross section of a line is considered rather than the atomic flux among grain boundaries. The mechanism that their model uses looks at the net number of atoms, $\mathrm{div}(J_a)dt$ entering a volume element of the interconnect line in a time dt. The volume is assumed to be large enough to include vacancy sources and sinks. These atoms can be spent in changing the vacancy concentration dC_v, or be deposited on grain boundaries or lattice dislocations **[29]**. Again, their model is talking about a net number of atoms, rather than treating each atom individually or including just a small number of atoms. Though this is a very good model and has much utility, information about the true anisotropic nature of the diffusion coefficient is lost when considering the diffusion coefficient to be spatially uniform throughout the entire material. A microscopic simulation, such as the one this thesis proposes, would hopefully reveal the anisotropic nature of the true diffusion coefficient. As a result, such parameters could be fed into macroscopic scale simulators for greater accuracy.

However, such macroscopic simulations do have a number of fundamental drawbacks. First, the predictions are only as good as the input statistical data and distribution functions. This generally requires excessive a priori testing to construct accurate and reliable mathematical models. Next, the simulation results are always

statistical in nature, and hence not deterministic quantities. Also, non-linear behavior and the inter-dependencies of parameters are not modeled. As a result, predictions of the current scaling behavior are difficult. Finally, the role of grain boundaries, the breakdown physics, and local inhomogeneities cannot be explicitly analyzed.

2.10.2 Microscopic (Molecular Dynamics) Simulations of Electromigration

These types of simulations involve simulating electromigration behavior on the microscopic level. This means that inter-atomic forces, such as the Lennard-Jones potential and electron wind are taken into account. This approach has the characteristic of taking into account the local geometric properties of the conductor under consideration. Instead of focusing on average values of the current density or diffusion coefficient, this technique focuses on specific values of these variables by taking into account geometric properties like voids, hillocks, and grain boundaries. In doing so, the true anisotropic nature of the diffusion coefficient is realized. Once the diffusion coefficient is described by this microscopic approach, it can then be fed back in to a macroscopic simulation to provide more accurate results.

Advantages of a Molecular Dynamics Scheme

- Can incorporate many-body effects
- Accurate results due to microscopic calculations at the atomistic level: no macroscopic fitting parameters are required
- Automatic inclusion of space and time dependant screening
- Flexibility and ease of treating complex geometry's, corners, and bends

- Solute in solvent and many-species inclusion possible, as well as overlayers
- No diffusion parameters or measured values are required
- Automatically builds in changes in local configuration and connectivity. Hence, it can better treat electromigration in bulk material, in the presence of defects and grain boundaries, cracks and bamboo structures, or combinations thereof
- It can include temperature effects by building in kinetic energy distribution based on host lattice temperature for the initial motion of ions and atoms
- It allows for smooth ionic motion based on Newton's laws, not discontinuous hops and jumps that are unphysical in nature
- It can include the statistical nature of the electron wind
- It is easy to probe geometric and grain size effects and multi-layers

One such Molecular Dynamics (M.D.) simulation discussed recently by a Japanese group **[30]** uses a conductor formed in an "H" like structure, as shown in Fig. 2.15. This molecular dynamics (or collision based) simulation uses the Lennard-Jones potential, and Newton's equation of motion for each atom as the primary governing equations. Within this H like structure, exists a grain-like pattern that closely matches the grain-like structure found in real conductors.

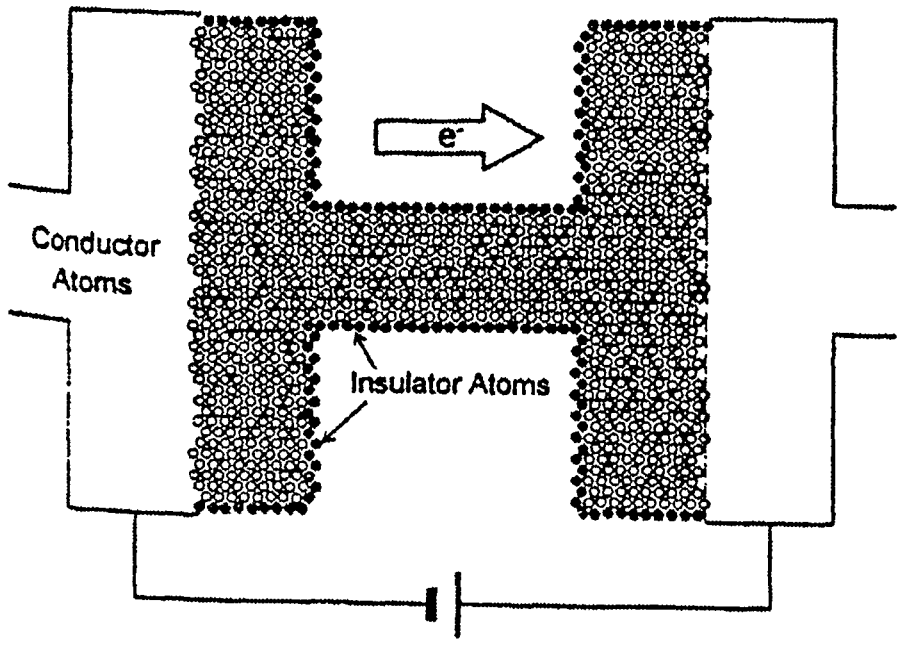

Fig. 2.15 Two-dimensional single crystal structure and electron flow. The atoms around the periphery were treated as species which keep their positions but influence inner atoms through interatomic potentials **[30]**.

The H pattern is chosen so as to concentrate the bulk of the current flow to the middle of the structure. The resulting enhanced current density/flux makes it easier for electromigration to take place in that region. For the boundary conditions, all of the atoms around the peripheries are made to be fixed in position. However, these same atoms can exert their contribution to the L-J restoring force for all the other atoms. The

force generated on the i^{th} atom is calculated by combining the electric field force and atomic pair potential forces as in the following equation:

$$F_i = \Sigma F_{LJ}(r_{ij}) + F_e(x,y) \quad , \quad (2.11)$$

where $F_e(x,y)$ is associated with the electrostatic field and the electron wind and F_{LJ} is the Lennard-Jones force **[30]**.

This method calculates the change of the position, velocity, and acceleration of the lattice atoms by solving Newton's equation of motion for each atom. The first term in equation (2.11) is the Lennard-Jones pair potential given by equation (2.8). A time step is then used to control program execution. A typical value for the time step would be 0.005ps **[30]**. The current in these types of experiments is usually considered to be time independent since the flow of the electrons is much faster than the actual movement of the atoms. As time goes on and under the influence of the electron wind, the atoms positions are updated using equations (2.8) and (2.11).

As seen in Fig. 2.15, the electron flow is from left to right. As the simulation continues, electrons from the electron wind collide with the lattice atoms within the conductor and hence, are broken loose from their bonds. This happens when the atomic pair potential and other binding forces are no longer able to counteract the force from the electron wind. Atoms that are most susceptible to being broken loose from their bonds are the atoms that are near the grain boundaries, since the forces on these atoms lack symmetry. Atoms that are located some distance away from the grain boundary remain relatively stable. Atoms that are removed from an area tend to form voids. In contrast, some of the atoms that begin to move along with the electron wind "drop out" and are usually deposited on various sites of the conductor surface. These atoms tend to form

what are known as hillocks. Excessive void formation can cause an open circuit failure condition, whereas excessive hillock formation can cause short circuit failure. The simulation keeps track of the atoms by continually updating the positions of these atoms. A three-dimensional plot is then generated that graphically depicts the eventual morphology of the void and hillock formations **[30]**.

CHAPTER III

NUMERICAL IMPLEMENTATION AND SIMULATION DETAILS

3.1 Introduction

The simulation used in this research is a molecular dynamics, microscopically based computer simulation. This simulation uses momentum exchange between nearest neighboring atoms as the primary force to describe the general movement of a grid of atoms with a given spatial arrangement. One of the characteristics that this simulation has is that it is capable of taking into account many-body contributions. This simulation, as it updates the position and velocity of each atom, is effectively implementing a many-body approach. Taking the many-body effects into account leads to a more realistic simulation. The many-body effects can be thought of as the culmination of forces induced by several thousand atoms colliding with each other randomly. Two atoms colliding together will tend to have an effect on their neighboring atoms and may, in turn, cause their neighboring atoms to collide with other atoms and so on. Some of these atoms will be lattice atoms broken loose by the electron wind and some atoms will be stationary lattice atoms.

3.2 Molecular Dynamics Schemes

Molecular dynamic simulations deal with the interaction of atoms with all of their neighboring atoms taken into account. The simulation begins by assigning initial positions and velocities to an array of atoms. The positions, velocities, accelerations, etc.

are tracked in small time steps so that many-body, inter-atomic forces are accurately updated.

In general, the movement of an atom in a solid is controlled by the collective forces from all of the target atoms in its neighborhood. The Newtonian equations for this type of situation would be **[31]**:

$$M_i d^2x_i(t)/dt^2 = \sum_{j=1}^{N} F_{ij} = F_i(x_i(t)) \qquad (3.1)$$

where N is the number of atoms in the model solid, M_i is the mass of each individual atom, $x_i(t)$ is the time-dependant atomic position, and F is the force on each atom. The magnitude of the force exerted by atom i on atom j is the same as that by atom j on atom i. The atom cannot act on itself. Therefore, we have two additional equations **[31]**:

$$F_{ij} = -F_{ji} \quad , \quad j \neq i \qquad (3.2)$$

$$F_{ii} = 0 \quad . \qquad (3.3)$$

Including all of the atoms in a given metal interconnect line for simulation purposes is an impossible task. Even a few neighbors for each atom can quickly become untractable since the force calculation for N atoms scales as N^2. In the present implementation, eight neighbors were considered for each atom.

3.2.1 Boundary Conditions

The main types of boundary conditions that are of interest here for the microscopic simulations are hard-wall boundary conditions. Hard-wall boundary conditions, in our case, assume that all of the atoms around the periphery of a simulation space are fixed in position for both the 1-D and 2-D cases. This has the advantage of

simplifying the simulation from a computational perspective. However, invoking this boundary condition means that some information about the boundary atoms is lost and hence their motion is not what it would be in a real-world case. Therefore in the strictest sense, these boundary conditions would not aid in a true real-world simulation case. However, since our simulation focuses mainly on the interior atoms where a void or hillock would likely be, the atoms around the periphery would not really play a major role in the electromigration phenomenon. Arguably then, the use of hard-wall boundary conditions would present a simple yet reasonable implementation of the bounded simulation space. If we take into account a sufficiently large number of atoms for our simulation we can still get reasonably accurate results while simplifying the simulation code and hence making the simulation time shorter.

Periodic boundary conditions, on the other hand, let the atoms around the periphery of the simulation space move, just like the atoms in the interior of the simulation space. This, if implemented, would provide very accurate simulation results at the expense of program code complexity and simulation time. With these boundary conditions, there is a chance that the atoms around the periphery could deviate too far from their positions, beyond the initial boundaries of the simulation space. This tends to make the simulation space more distorted and less well defined. However, because of the periodic nature of the boundary conditions, the simulation space is effectively translated, (in the X and Y dimensions for example, in two-dimensional simulations) thus restoring the distortions in the basic simulation region. However, this scheme is more difficult to implement. For convenience, ease of implementation, and given the nature of our

research focus, hard-wall boundary conditions will consistently be used in this work wherever possible.

3.3 Discrete Implementation Schemes

There are several methods to integrate the coupled differential equations in (3.1). The algorithm should be chosen so as to provide the maximum stability, accuracy, reliability, and efficiency. Simplicity is also a very important consideration since simple algorithms are often the fastest for computers to calculate. For maximum speed, algorithms can be chosen to allow vectorization in order to utilize the parallel architecture of modern supercomputers.

3.3.1 Central Difference Scheme

For this scheme, the position $x_i(t+\Delta t)$ of an atom at time $t+\Delta t$ can be determined by the position $x_i(t)$ at time t plus the change in position, which depends on the velocity of the atom. The velocity $dx_i(t)/dt$ is determined at half the time interval $\Delta t/2$. Thus

$$dx(t+\Delta t/2) = dx(t - \Delta t/2) + \Delta t F_i(t)/M_I , \qquad (3.4)$$

and $$x_i(t+\Delta t) = x_i(t) + \Delta t dx_i(t+\Delta t/2) \quad . \qquad (3.5)$$

The name originates from the fact that the velocity is determined at $\Delta t/2$, which is at the center of the time step **[31]**.

3.3.2 Average Force Method

This method is a modification of the central difference method and was first developed by Harrison **[32]**. It uses a mean force to determine the position and velocity of an atom. The Taylor series for $x_i(t+\Delta t)$ gives

$$x_i(t+\Delta t) = x_i(t) + \Delta t dx_i(t) + 1/2\Delta t(\Delta dx_i(t)) \quad , \qquad (3.6)$$

terminating the series after the second derivative. Then the average force is found by

$$\Delta dx_i \equiv \Delta t \langle F_i \rangle / M_I \quad , \qquad (3.7)$$

leading to the following equations for dx_i/dt and x_i:

$$dx_i(t+\Delta t) = dx_i(t) + \Delta t \langle F_i \rangle / M_I \quad , \qquad (3.8)$$

and $$x_i(t+\Delta t) = x_i(t) + \Delta t[dx_i(t) + \Delta t\langle F_i \rangle/(2M_i)] \quad . \qquad (3.9)$$

The mean force, $\langle \mathbf{F}_i \rangle$ would be given by

$$\langle \mathbf{F}_i \rangle \equiv \tfrac{1}{2}\{\mathbf{F}_i[x_i^*(t+\Delta t)] + \mathbf{F}_i[x_i(t)]\} \quad , \text{ with} \qquad (3.10)$$

$$x_i^*(t+\Delta t) = x_i(t) + \Delta t dx_i(t) + (\Delta t)^2 \mathbf{F}_i(x_i(t))/2M_i) \quad . \qquad (3.11)$$

With this method, x_i and dx_i can be determined simultaneously. The time steps Δt can be chosen to be twice as large as in the central difference method to achieve about the same accuracy **[31]**.

3.3.3 The Euler-Cauchy Scheme

This method is well established as an iteration procedure **[31]**, where the first iteration is given by

$$x^{(1)}(t+\Delta t) = x(t) + \Delta t dx(t) + \tfrac{1}{2}(\Delta t)^2 d^2x(t) \quad , \qquad (3.12)$$

$$dx^{(1)}(t+x\Delta t) = dx(t) + \Delta t d^2x(t) \quad . \quad (3.13)$$

With this method, higher order iterations are then applied until the change in x and dx becomes small enough:

$$d^2x^{(n)}(t+\Delta t) = \mathbf{F}(x^{(n-1)}(t+\Delta t))/M \quad , \quad (3.14)$$

$$dx^{(n)}(t+\Delta t) = dx(t) + (\Delta t/2)[d^2x(t) + d^2x^{(n)}(t+\Delta t)] \quad , \quad (3.15)$$

and $$x^{(n)}(t+\Delta t) = x(t) + (\Delta t/2)[dx(t) + dx^{(n)}(t+\Delta t)] \quad . \quad (3.16)$$

3.3.4 Predictor-Corrector Scheme

In the predictor-corrector scheme, a prediction is made for x and dx **[31]**:

$$x_p(t+\Delta t) = x(t-\Delta t) + 2\Delta t dx(t) \quad , \quad (3.17)$$

and $$d^2x_p{}^{(1)}(t+\Delta t) = \mathbf{F}(x_p(t+\Delta t))/M \quad . \quad (3.18)$$

The corrected values are given by

$$dxc^{(1)}(t+\Delta t) = dx(t) + (\Delta t/2)[d^2xp^{(1)}(t+\Delta t) + d^2x(t)] \quad , \quad (3.19)$$

and $$xc^{(1)}(t+\Delta t) = x(t) + (\Delta t/2)[dxc^{(1)}(t+\Delta t) + dx(t)] \quad . \quad (3.20)$$

Higher-order iterations follow the same scheme:

$$d^2x_p{}^{(n)}(t+\Delta t) = \mathbf{F}(x_c{}^{(n-1)}(t+\Delta t))/M \quad , \quad (3.21)$$

$$dx_c{}^{(n)}(t+\Delta t) = dx(t) + (\Delta t/2)[d^2x_p{}^{(n)}(t+\Delta t) + d^2x(t)] \quad , \quad (3.22)$$

and $$x_c{}^{(n)} = x(t) + (\Delta t/2)[dx_c{}^{(n)}(t+\Delta t) + dx(t)] \quad . \quad (3.23)$$

3.3.5 The Verlet Scheme

This scheme uses the following Taylor expansion **[31]**:

$$x(t+\Delta t) = x(t) + dx(t)\,\Delta t + 1/2d^2x(t)\,\Delta t^2 + 1/6d^3x(t)\,\Delta t^3 + O(d^4x(t)) \quad , (3.24)$$

and $$x(t-\Delta t) = x(t) - dx(t)\,\Delta t + 1/2d^2x(t)\,\Delta t^2 - 1/6dx^3(t)\,\Delta t^3 + O(d^4x(t)) \; . \; (3.25)$$

Adding the two equations together yields the result

$$x(t+\Delta t) = 2x(t) - x(t-\Delta t) + d^2x(t)\Delta t^2 \quad , \qquad (3.26)$$

where the first and third derivatives cancel and all terms of order Δt^4 and higher are neglected. The velocity can be determined by subtracting (3.25) from (3.24)

$$dx(t) = [x(t+\Delta t) - x(t-\Delta t)]/(2\Delta t) \quad , \qquad (3.27)$$

where second-order and higher terms are omitted. If x(t) and dx(t) are kept, $x(t+\Delta t)$ can be determined by

$$x(t+\Delta t) = x(t) + dx(t)\,\Delta t + 1/2d^2x(t)\,\Delta t^2 \quad . \qquad (3.28)$$

For the velocities, the following equation holds:

$$dx(t) = \tfrac{1}{2}[dx(t+1/2\Delta t) + dx(t-1/2\Delta t)] \quad . \qquad (3.29)$$

The velocities can be improved by

$$dx(t) = \tfrac{1}{2}\{dx(t+1/2\Delta t) + dx(t-1/2\Delta t)] + 1/12[d^2x(t-\Delta t) - d^2x(t+\Delta t)]\,\Delta t \; . \; (3.30)$$

3.3.6 The Time Step

Choosing a time step in these integrations usually involves a compromise between accuracy and computing time. As a rule, a time step is chosen such that the fastest knock-on atom does not move more than 5% of the inter-atomic distance, d, in one time step **[31]** as shown in equation (3.31),

$$\Delta t = 0.05d(M/2T_m)^{1/2} \, , \qquad (3.31)$$

where M is the mass of the moving atoms and T_m is its kinetic energy. With decreasing energy of the fastest knock-on atom in the cascade, the time step can be increased while still maintaining the above condition. This can be done in the following way **[31]**:

$$dx(t+\Delta t_2/2) = dx(t-\Delta t_1/2) + \tfrac{1}{2}(\Delta t_1 + \Delta t_2)F/M \ , \qquad (3.32)$$

$$dx(t+\Delta t_2/2) = x(t) + dx(t+\Delta t_2/2)\ \Delta t_2 \qquad . \qquad (3.33)$$

This procedure applies to the central difference scheme and is good up to the second order. Typical time steps for the integration are of the order of 1-10 fs, and a full calculation may require 100-1000 time steps.

3.3.7 Choice for Present Molecular Dynamics Simulation

Extreme caution was exercised in choosing the time step in order to ensure the accuracy of the predicted results. Hence, a very small time step of just 0.02fs was chosen based on a very conservative estimate. The integration of Newton's equations was performed based on the Verlet **[27]** scheme. This scheme has been used in the molecular dynamics literature, and so has been proven to be accurate and robust.

3.4 Validation of Molecular Dynamics Scheme

In order to demonstrate the validity of the M.D. numerical simulations, several simple test programs were written to analyze 1-D atomic chains. These test programs were much like the main program in terms of the algorithm and implementation, but much more simple in terms of the number of atoms simulated and the spatial dimensionality to test and validate the overall simulation scheme.

A particular challenge for these simulation programs and the main program is to realistically model the electron wind. In addition to this, a value is needed for the force generated by the electron wind and this force must be within reasonable ranges. As stated in chapter II, section 2.2, the electron wind is a random force and consequently, the force it imparts on surrounding atoms is also random. We would be incorrect in assigning values to this force with only a random number generator. This force must be within a certain range in relation to the applied electric field and it should have a Gaussian distribution due to the Law of Large Numbers and the Central Limit Theorem. Therefore, what is really needed is a rule or equation related to the applied electric field for calculating realistic values of the electron wind force as a function of time using a random number generator.

Since we are dealing with a significant quantity of electrons in considering the electron wind, we can use the Law of Large Numbers to describe the probability distribution to that of a Gaussian distribution. In addition, the Central Limit Theorem states that the mean of any set of variates with any distribution having a finite mean and variance tends to the Gaussian distribution **[33]**. To apply the Central Limit Theorem to this case, the electron wind force, FE, has a finite mean equal to the magnitude of the applied electric field, but in the opposite direction, and the variance is also finite since it is specified in the program. The cumulative distribution function, F(FE), is the integral of the probability density function, f(FE), and takes on the following form:

$$f(FE) = \frac{1}{\sigma\sqrt{2\pi}} e^{\frac{-(FE-\overline{FE})^2}{2\sigma^2}} \quad , \qquad (3.34)$$

$$F(FE) = \frac{1}{\sigma\sqrt{2\pi}} \int_{-\infty}^{FE} e^{\frac{-(FE-\overline{FE})^2}{2\sigma^2}} d(FE) \qquad (3.35)$$

where FE is the force due to the electron wind, $\overline{FE}$ is the average value of the electron wind force, and σ is the standard deviation. A plot of a general Gaussian distribution is shown in Fig. 3.1

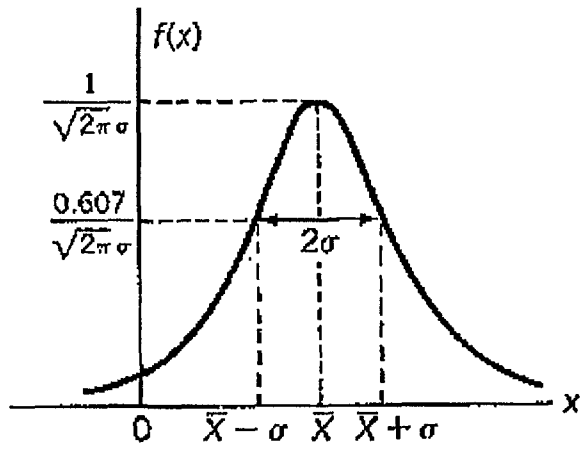

Fig. 3.1 Plot of a Gaussian distribution. This is the distribution chosen to represent the force generated by the electron wind. Using the Law of Large Numbers and the Central Limit Theorem, this is a reasonable choice for the electron wind force **[33]**.

The mean of this Gaussian distribution will be $\overline{FE}$, which will exactly equal the applied electric field, |qE| in magnitude, leaving σ to be the only variable specified for the electron wind function in the simulation program. FE, the electron wind force, is the unknown random variable. We know that $0 < FE < 1$. If we pick values for FE with a random number generator between the values of zero and one in the program, choose σ, and solve equation (3.35) for FE, then equation (3.35) will serve as our rule for

calculating the electron wind force at each time step. This way, we insure that the electron wind contribution is indeed random in nature with an average value equal to the magnitude of the applied electric field following a Gaussian distribution.

The electron wind force is opposite in direction to the applied electric field. As the electric field is increased, the Gaussian distribution curve will more towards the negative X direction. As the electric field is decreased, the Gaussian distribution curve will move more towards the positive X direction, with the X axis representing the electric field values in V/M.

1-D Simulation Case One: Lennard-Jones Potential Only

To start off with, four atoms are involved, with the two extreme atoms fixed at each end along the X-axis to implement hard-wall boundary conditions. Two atoms are laterally movable in the middle. All four atoms are equally spaced by multiples of 2.5 Angstroms, which was chosen as a typical representation of a metallic lattice constant. The simulation space is shown in Fig. 3.2.

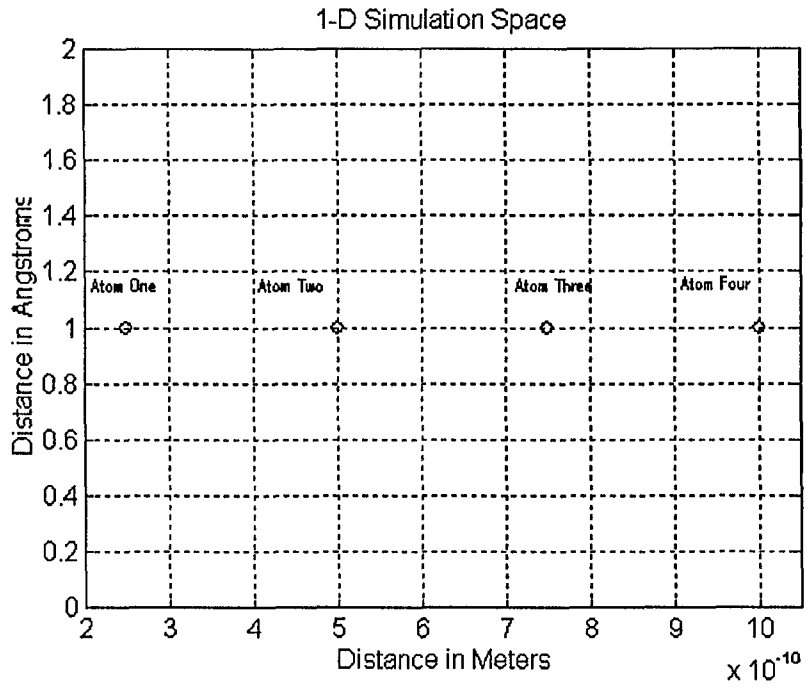

Fig. 3.2 Initial position of the four atoms in the 1-D simulation space.

The two atoms in the middle were given an initial velocity according to the following two equations:

$$1/2mv^2 = KT/2 \quad , \quad (3.36) \quad \text{or}$$

$$v = \pm (KT/m)^{1/2} \quad . \quad (3.37)$$

Thus it was implicitly assumed that the atoms are in thermal equilibrium with the ambient temperature. Thermodynamically then, their temperature is equal to T, the lattice value. The initial direction of movement for the two middle atoms alternate in this case. Atom two had an initial velocity in the positive X direction while atom three had an initial velocity in the negative X direction. This is known as *anti-parallel motion.* Using the Lennard-Jones potential and Newton's equations of motion as the only external forces acting on these atoms, the numerical simulation yielded the changes in velocity and

position as a function of time. What is found when the program is run is that each individual atom that is allowed to move does so and changes its velocity periodically with alternating direction. These directional changes occur within the confines of the "system" which basically consists of just four atoms. The two movable atoms begin to oscillate anti-symmetrically back and forth in position, but no net displacement is observed of the system as a whole; i.e. there is no electromigration taking place in this case. Indeed, this is to be expected since the only forces that are at work in this simulation are the Lennard-Jones forces. With no other external forces applied to the system, one would expect that on a macroscopic scale, there would be no net movement even though on a microscopic scale, there could be a periodic movement of the two atoms due to the Lennard-Jones potential. Figure 3.3 shows this behavior graphically. In the figure, there are two traces, each spaced 2.5 Angstroms apart on the Y-axis starting at Y=2.5 Angstroms, which is the equilibrium lattice constant used in the simulation program. The initial velocities of the two atoms had been assigned to be equal, but in opposite directions to initiate anti-parallel motion. However, the restoring force due to the Lennard-Jones potential acts on each atom. It can be seen that atoms two and three move toward each other and that their positions vary about their mean starting positions. This whole process repeats itself and the whole system of two atoms vibrates or oscillates on an atomic scale, with zero net displacement of all four atoms as a whole. As can be seen in the figure, the program correctly predicts the atomic behavior of the system when there is no electron wind force or external bias (electric field).

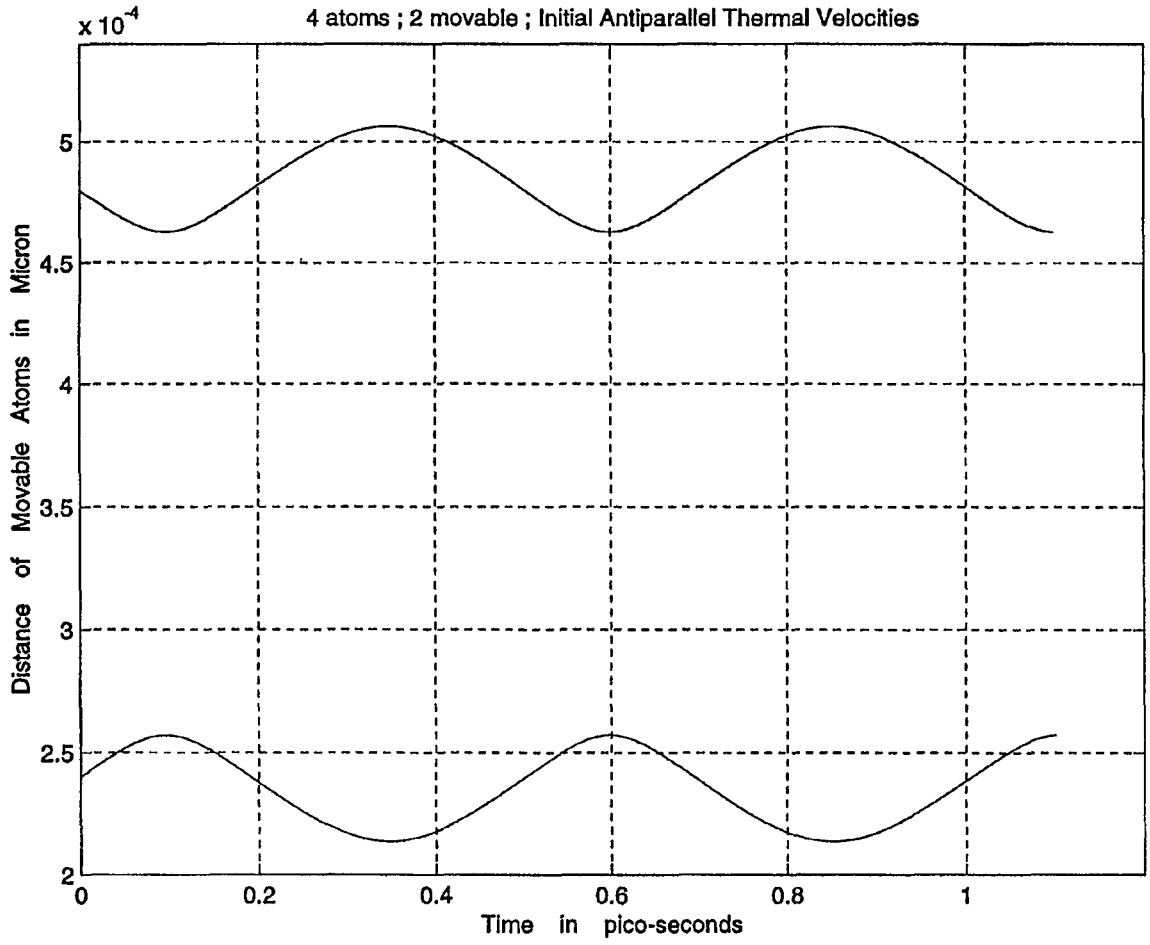

Fig. 3.3 Graphical representation of distance vs. time for four atoms in the 1-D simulation with no electron wind or electric field. The two outer atoms are made to be fixed, while the two inner atoms are given initial, but opposite velocities. This is known as *anti-parallel* motion. As the figure indicates, the two atoms gently move about sinusoidaly in opposite directions.

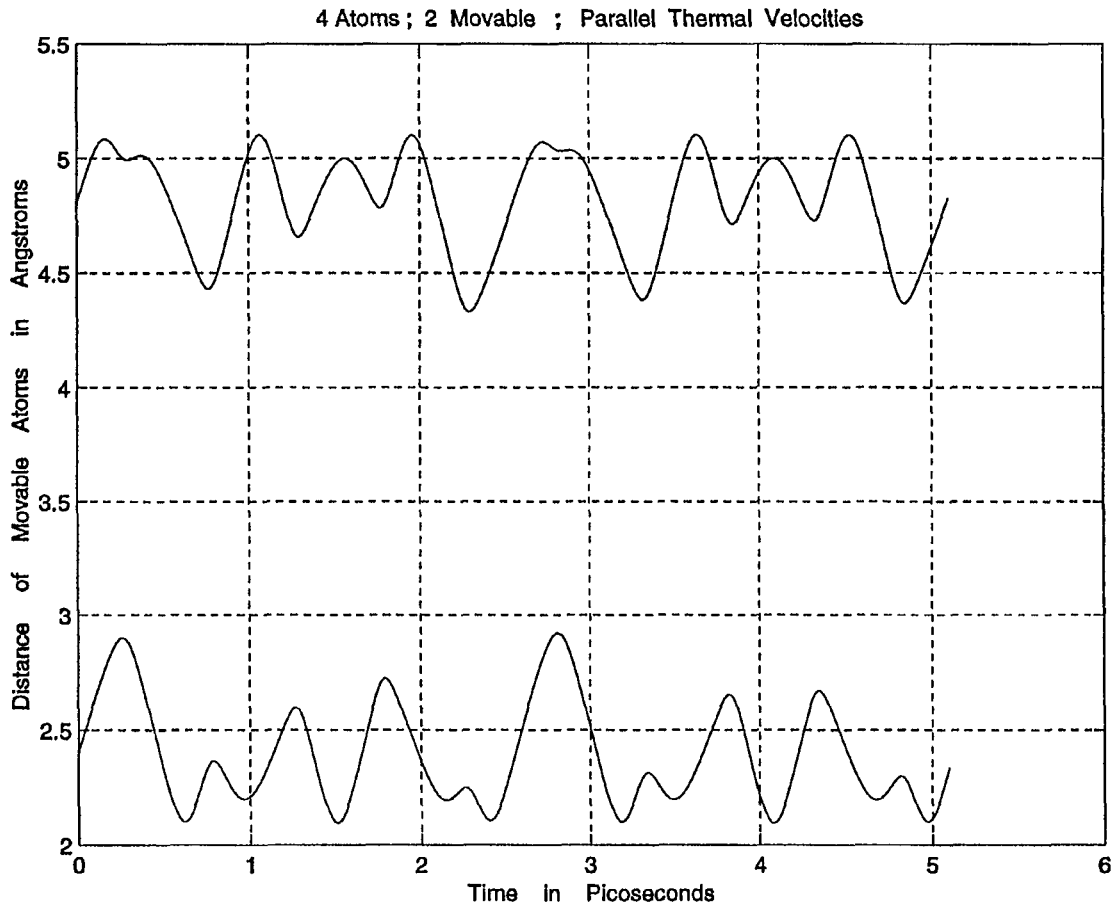

Fig. 3.4 Graphical representation of distance vs. time for four atoms in the 1-D simulation with no electron wind or electric field. The two outer atoms are made to be fixed, while the two inner atoms are given initial, but parallel velocities. This is known as *parallel* motion. As the figure indicates, the two atoms move about, but in a more jagged fashion compared to the anti-parallel case.

In Fig. 3.4, the two outer atoms being fixed while the two inner atoms are given initial, but parallel velocities changes the figure notably. The curve takes on a more jagged appearance. The atoms move about in a more jagged fashion due to interference with each other. Basically, one atom comes to rest before the other atom does. As atom

three comes to rest, atom two is still moving until it gets close enough to atom three that the force from atom three causes atom two to also come to rest. Then, the process reverses itself where atom two now comes to rest before atom three does.

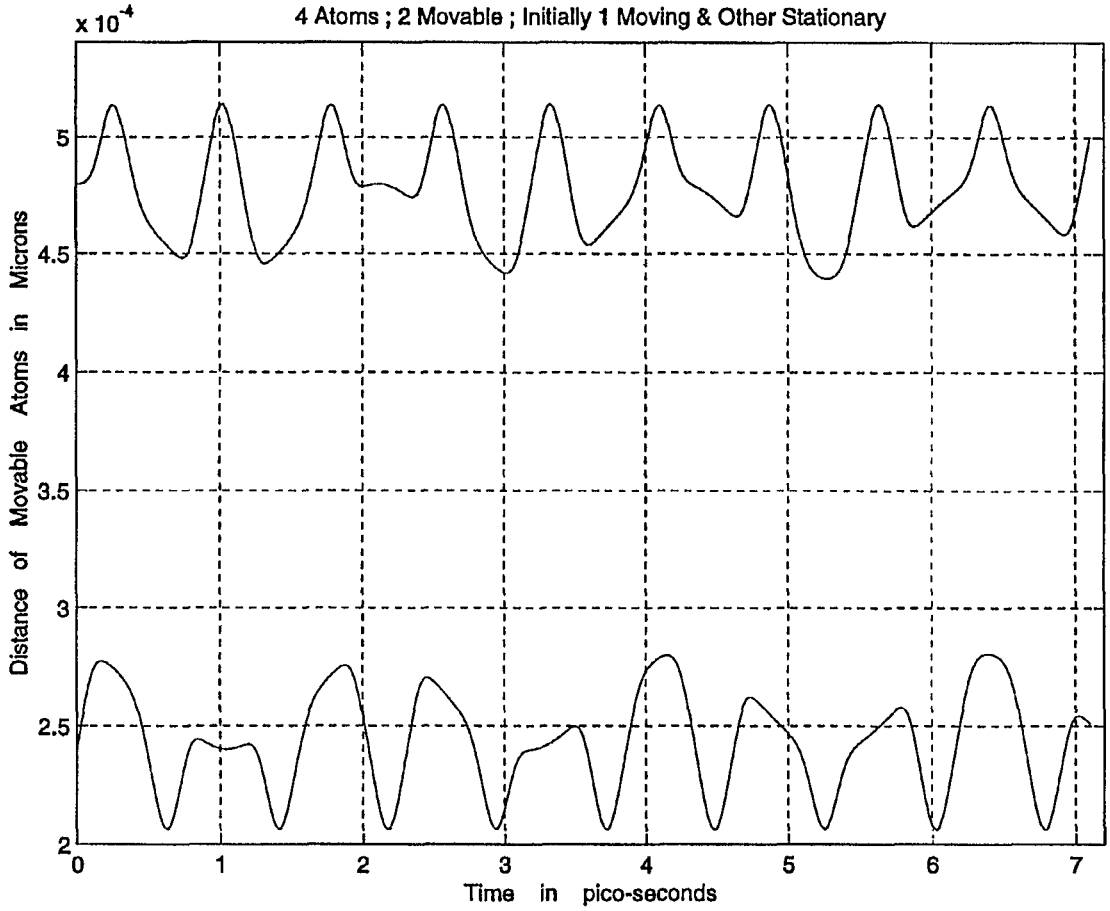

Fig. 3.5 Graphical representation of distance vs. time for four atoms in the 1-D simulation with no electron wind or electric field. The two outer atoms are made to be fixed, while atom three has an initial velocity of zero. Atom two is given an initial velocity given by equation 3.37.

In Fig. 3.5, the two outer atoms are made to be fixed, while atom three has an initial velocity of zero. Atom two has an initial velocity given by equation 3.37. As the

figure indicates, atom three does not move for the first part of the simulation (0.125ps) until atom two moves close enough to atom three that it is able to exert enough force upon atom three to start it in motion. Once the two atoms are in motion, their motion is very similar to the anti-parallel case.

What these plots show is a simplified version of the main program in an effort to determine if the main program provides results that make sense. The assumption is that if the 1-D programs generate accurate results, then the 2-D simulation with many more atoms will be merely an extension of the 1-D case and hence its results should also make sense and can be trusted. As the above figures indicate, the 1-D programs do indeed generate data that is consistent with what one would find by manually calculating and updating the Lennard-Jones forces and Newtonian forces for these four atoms.

1-D Simulation Case Two: Lennard-Jones Potential with an Electric Field

This 1-D molecular dynamics simulation is just like the first 1-D simulation in case one and also has anti-parallel motion, but now we have the inclusion of the electric field in addition to the Lennard-Jones potential with the electron wind force set to zero. It must be pointed out that an electric field will cause an electron wind force as well and these two forces cannot be decoupled in reality. If one has an electric field, then there will always be a corresponding electron wind. In actuality, the electric field has to be very large in order to create an electron wind force capable of breaking lattice atoms loose from their bonds.

We set the electron wind force to zero in our simulation based wholly on a theoretical basis so that we can break down all three forces, the Lennard-Jones potential, the electric field, and the electron wind, and threat them separately to simulate and gauge their individual contributions towards electromigration. What is expected with this additional force is that the atoms should translate in the direction of the electric field while vibrating randomly within their range of motion. There should be no net atomic displacement. The electric field simply offsets the simulation space, but since there is no electron wind (theoretically) and no lattice imperfections there should be no net displacement of the atoms. This is indeed the case as seen in Fig. 3.6.

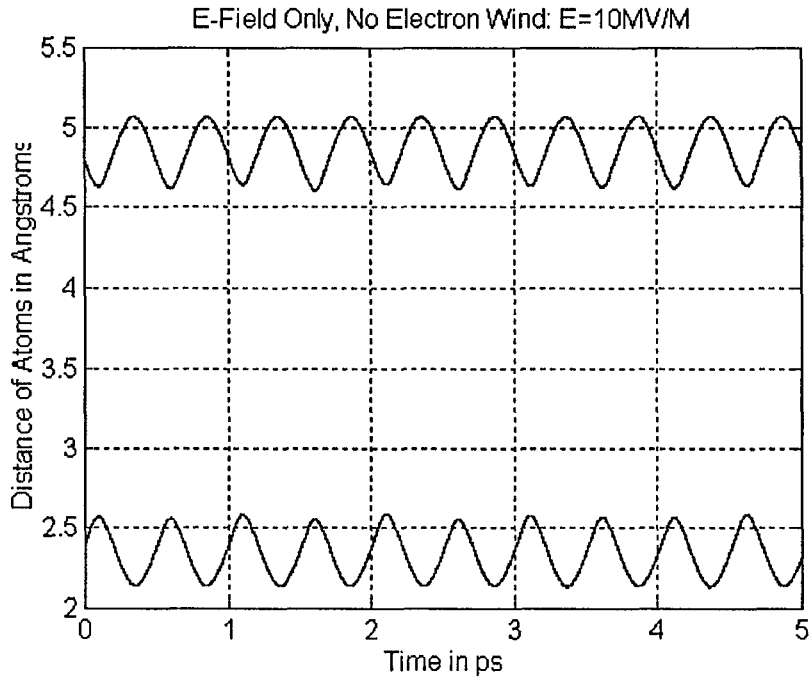

Fig. 3.6. In this figure, the electric field is 10MV/M and the atoms are given anti-parallel initial velocities. As indicated, the atomic position oscillates back and forth in a symmetric fashion.

As shown in Fig. 3.6, the atoms still continue to oscillate back and forth in a symmetric fashion, even under the influence of a very large electric field. On the surface, this behavior would not be intuitive. But on a microscopic scale, what is really at work here to, maintaining symmetry and smooth atomic motion, is the interaction of the Lennard-Jones restorative force with the force of the electric field. This figure illustrates just how strong the Lennard-Jones restorative force really is. As the electric field tries to move atom two closer to atom three, the Lennard-Jones potential pushes or repulses atom two back toward its initial position, even with E set to 10MV/M. It is not until E is set to 1GV/M that we begin to see the electric field play the dominant role in the Lennard-Jones-electric field interaction. This interaction can be seen in Fig. 3.7.

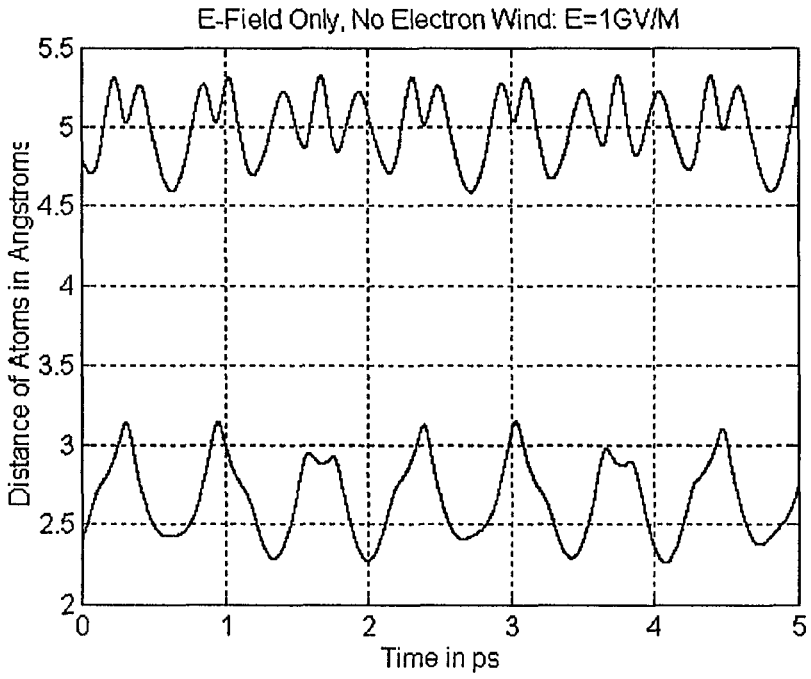

Fig. 3.7. In this figure, the electric field is 1GV/M. It can be seen that the magnitude of the electric field is large enough to overcome the Lennard-Jones potential, creating distortion in the interatomic movement.

With the electric field set to 1GV/M, distortions in the interatomic motion can be observed and we can begin to see how the electric field not only offsets the atomic motion, but also changes the nature of the motion itself. The Lennard-Jones potential plays a less dominate role compared to the electric field in this case. Atom two moves much more close to atom three and reaches almost 3.3 Angstroms of displacement compared to about 2.6 Angstroms of displacement for atom 3 in Fig. 3.6. Also, atom three moves less in the negative direction from 4.75 Angstroms to 4.7 Angstroms compared to a swing down to 4.6 Angstroms in Fig. 3.6.

1-D Simulation Case Three: Electric Field with Electron Wind

This 1-D molecular dynamics simulation is like the previous two 1-D cases, but now all three forces are involved, the Lennard-Jones potential, electric field, and the electron wind. What is expected in this case is that the individual atoms will still vibrate back and forth just as they did before, but all of the atoms as a whole still should not collectively move or migrate. This is because now we have the electron wind supplementing the Lennard-Jones potential in resisting the electric field force. The electron wind moves in a direction that is opposite to the applied electric field. Thus the electron wind serves to counteract the electric field, as can be seen in Fig. 3.8. In this figure, the electric field is set to 1GV/M and the inter-atomic motion remains undistorted. This is in contrast to Fig. 3.7 for which deviations from periodic behavior were predicted. These deviations resulted from the absence of the electron wind.

However as stated earlier, the magnitude of the electron wind force is random in nature and hence, it is possible for the electron wind force to not exactly counteract the electric field due to its variance. The electron wind force in our simulation was modeled as a Gaussian distribution with a standard deviation, σ, narrow enough ($\sigma = 1x10^4$) to cause the electron wind to counteract the electric field almost on a one-for-one atomic basis. Hence, the curves generated show that the interatomic motion is indeed maintained in a symmetric fashion. If we modify σ to even larger values, effectively injecting more randomness into the electron wind contribution, we should expect there to be more distortions in the inter-atomic motion and asymmetry, similar to case two with a very large electric field and a sigma of zero.

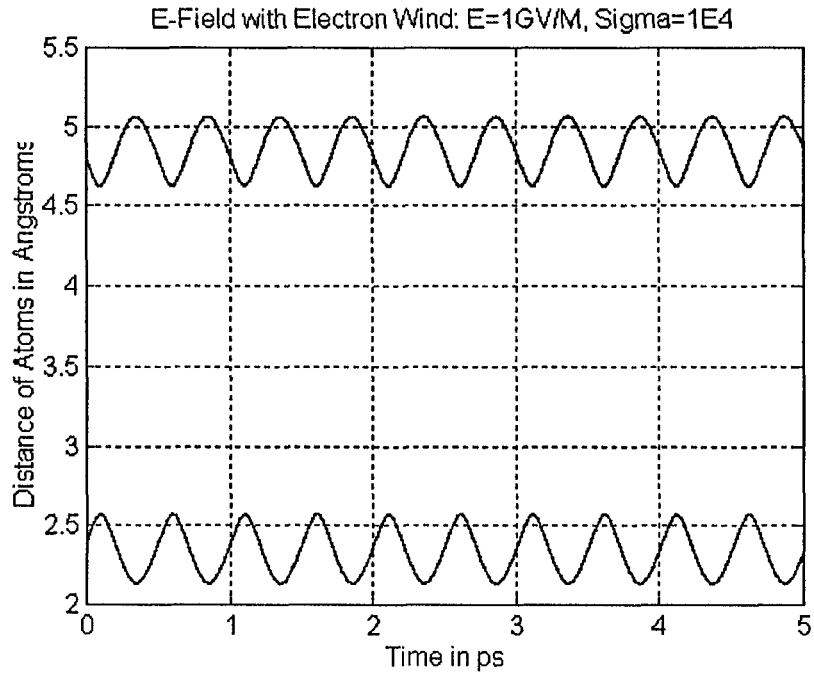

Fig. 3.8 Even at an electric field intensity of 1GV/M, the inter-atomic motion remains very symmetric due to the electron wind effectively canceling the effects of the electric field.

When we change sigma from $1x10^4$ to $1x10^8$ thereby injecting significantly more randomness into the electron wind force, the electron wind force is hampered in its ability to resist the electric field effects as seen in Fig. 3.9. Some of the electrons in the electron wind do not have sufficient energy to resist the electric field while others deliver a severe knock-on force. Hence in those cases, the electric field is able to distort the inter-atomic motion in that region.

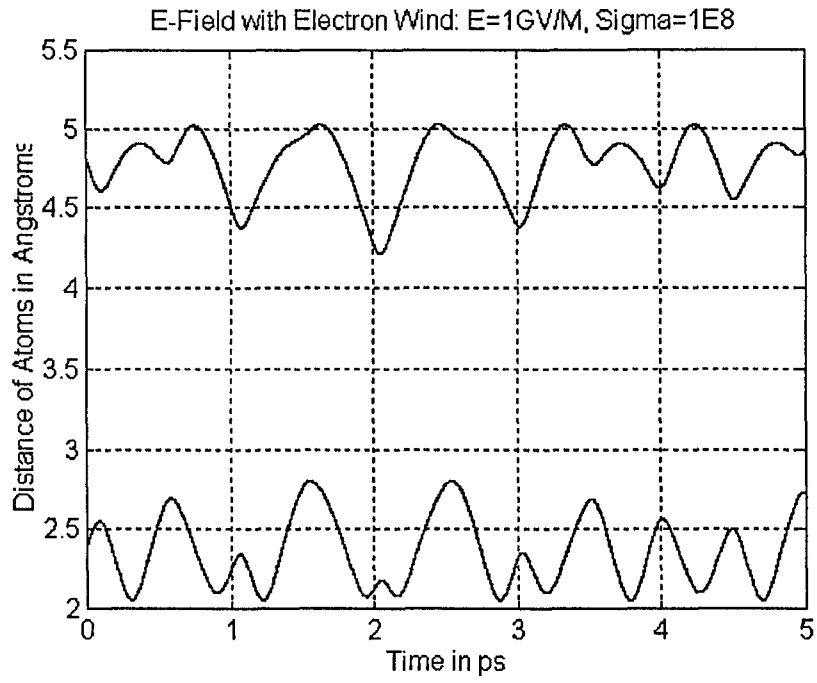

Fig. 3.9 When the electric field is held at 1GV/M just as in Fig. 3.8, but with a sigma of $1x10^8$, the electron wind force is less capable of resisting the effects of the electric field, thereby allowing the electric field to dominate the motion of the atoms.

2-D Simulation Case One: Lennard-Jones Potential Only

This molecular dynamics simulation is like case one in the 1-D simulation, but now the atoms are allowed two degrees of freedom. The only force involved here is the Lennard-Jones potential. The simulation starts off with a rectangular grid of atoms that is four atoms wide by four atoms high for a total of 16 atoms for the simulation space. The simulation space is shown in Fig. 3.10. In keeping with the chosen hard-wall boundary conditions, all of the atoms around the perimeter of the simulation space are made to be

fixed. Therefore, only the four interior atoms are allowed to move. These atoms are perfectly arranged in a regular square lattice at the start of the simulation.

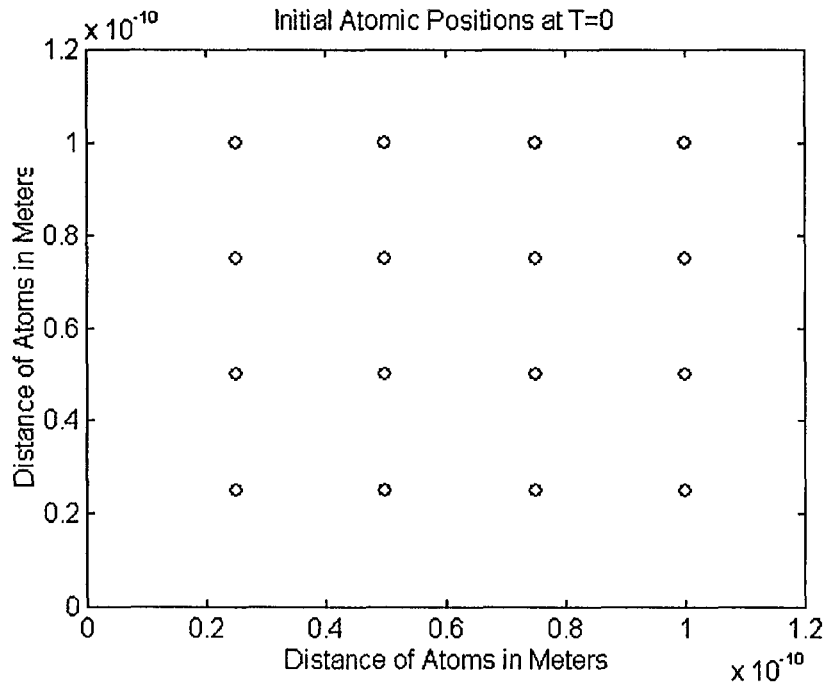

Fig. 3.10 4x4 array of atoms forming a simulation space of 16 atoms for all three 2-D simulation cases.

What is attempted in the first part of the simulation is to verify that the computer program is accurate and generates results that are in accord with those reported by other researchers. In this simple simulation no electron wind force or electric field is considered. The only force employed at this point is the Lennard-Jones restorative force. Each of the 4 atoms in the grid is assigned a random velocity that does not exceed KT. This choice simply represents the average thermal energy for a system having two degrees of freedom. The positions of the atoms are then plotted after some sufficiently long time interval. If the program is correct, there should be no net movement of the

atoms. This is to be expected in the absence of an external electric field or electron wind. Though thermal motion associated with the initial thermal velocities should occur, the net average displacement over a sufficiently long time interval should be nearly zero. Each atom may move within its own range, but the Lennard-Jones potential should restore or "pull" the atoms back to their equilibrium positions, giving a net result of near zero net displacement. For example, if there are 7 time steps, an atom may move from its rest position by some small amount, but when all of the small displacements are averaged together and divided by the number of time steps, the net displacement should be close to zero. If the numerical results demonstrate, then a validation for the program would automatically be provided. One would then have confidence in the simulation, its results, and implementation.

Fig. 3.11 is a plot of the four interior atoms in our simulation space that are allowed to move. The initial conditions of motion for the atoms are as follows: Atom one moves in a Northeast direction, atom two moves in a Northwest direction, atom three moves in a Southeast direction and atom four moves in a Southwest direction. Each atom is spaced a distance of 2.5 Angstroms apart from each other. This establishes anti-parallel motion, just as we did for all of the 1-D cases. As can be seen in the figure, in the absence of any external field or electron wind, each of the four atoms simply moves back and forth very symmetrically, re-tracing their initial directions of movement. This agrees with the theory in that there is no net atomic displacement in the absence of an external electric field or electron wind given a sufficiently long time interval.

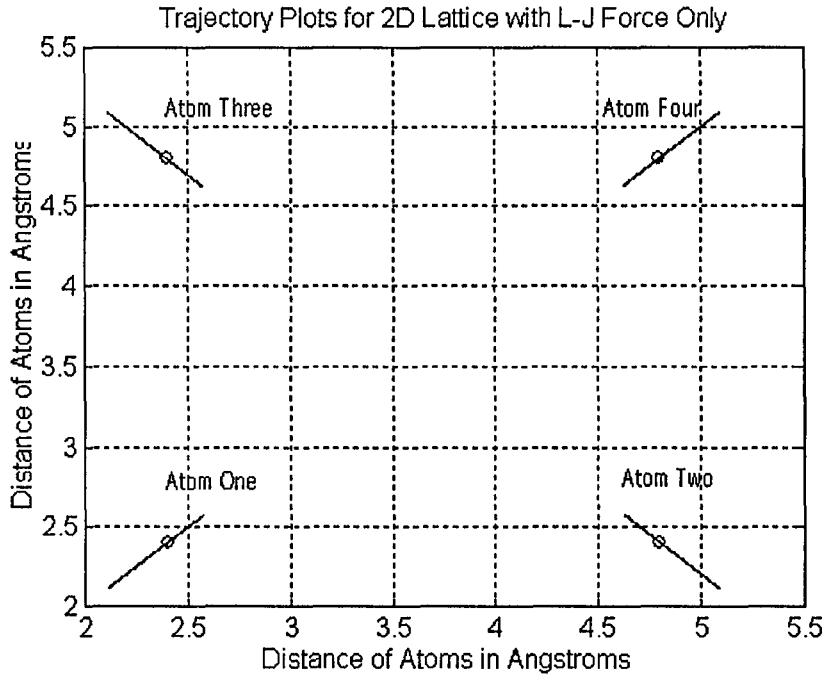

Fig. 3.11 Plot of the four interior atoms in the simulation space showing symmetric movement about their initial positions. The atoms positions after one time step are indicated by the circles over the lines. The atoms re-trace their paths and do not deviate from their initial path in the absence of an electric field or electron wind.

2-D Simulation Case Two: Lennard-Jones Potential with an Electric Field

This simulation adds the electric field in addition to the Lennard-Jones restorative force. As in the 1-D case two simulation, the electric field should offset or translate the atoms in the 2-D simulation space in the direction of the applied electric field. The atoms will vibrate randomly within their range of motion, but there should be no net displacement of the atoms and the simulation space should remain undistorted.

For this case, the electric field is set at 10MV/M. This simulation, like the others, uses anti-parallel initial velocities. Again, there are four atoms that are allowed to move

in this case. As shown in Fig. 3.12, the bottom left trace is for atom one, the bottom right trace is for atom two, the top left trace is for atom three, and the top right trace is for atom four. Each atom is again spaced 2.5 Angstroms apart on the X and Y axes respectively.

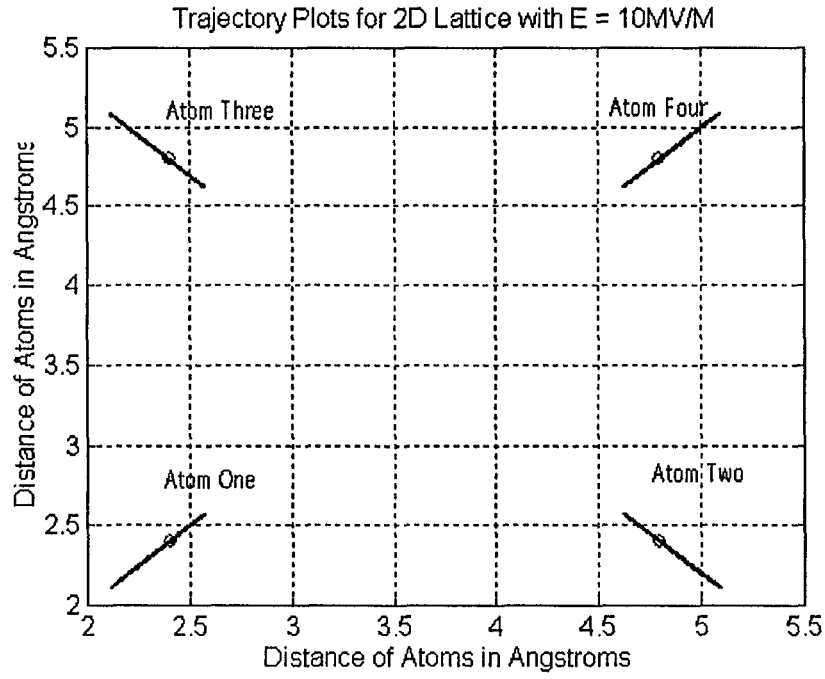

Fig. 3.12 Trace of the four center atoms in the simulation space, showing each atom retracing its defined anti-parallel path under moderate electric field conditions (E = 10MV/M). The positions of the atoms after one time step are indicated by the circles over the traces.

This figure correctly shows that the atoms gently move back and forth, retracing their path of anti-parallel motion. Also the atoms do not move towards each other as much as they move away from each other. Atom one moves towards atom three by only a small amount compared to how far atom one moves away from atom three. This type of behavior is a logical extension to the 1-D cases where the Lennard-Jones potential

becomes extremely strong near the vicinity of two approaching atoms, but falls off rapidly as the atoms move away from each other.

As the electric field is increased to 1GV/M, the motion of all four atoms becomes more erratic, but all four atoms still remain within their defined quadrants in the simulation space, as indicated in Fig. 3.13. This type of behavior is very similar to case two in the 1-D simulation where the atomic motion was more erratic, but the atoms were within their space as defined in the initial conditions.

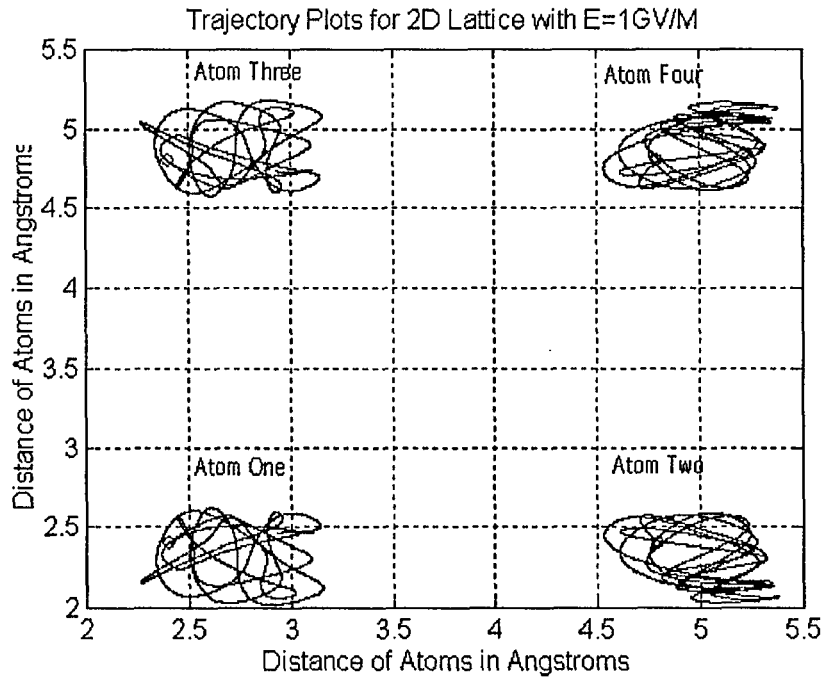

Fig. 3.13 Trace of the four center atoms in the simulation space. Each of the four atoms moves in a much more erratic fashion due to the cumulative effects of the Lennard-Jones potential and electric field. However, each atom still moves within its range defined in the initial conditions. The positions of the atoms after one time step are indicated by the circles over the traces.

2-D Simulation Case Three: Electric Field with Electron Wind

Next, the electron wind force is introduced in the simulation along with the usual Lennard-Jones restorative force and electric field. These forces are applied to the same perfect periodic arrangement of atoms in the grid used for simulation verification.

Fig. 3.14 shows the behavior graphically. When compared to Fig. 3.13, it can be seen that introducing the electron wind component into the simulation has the effect of damping or smoothing out the atomic motion as the electron wind tries to resist the effects of the electric field. The atomic motion is still very random in nature, but the movements are more localized now to the region defined in the initial conditions.

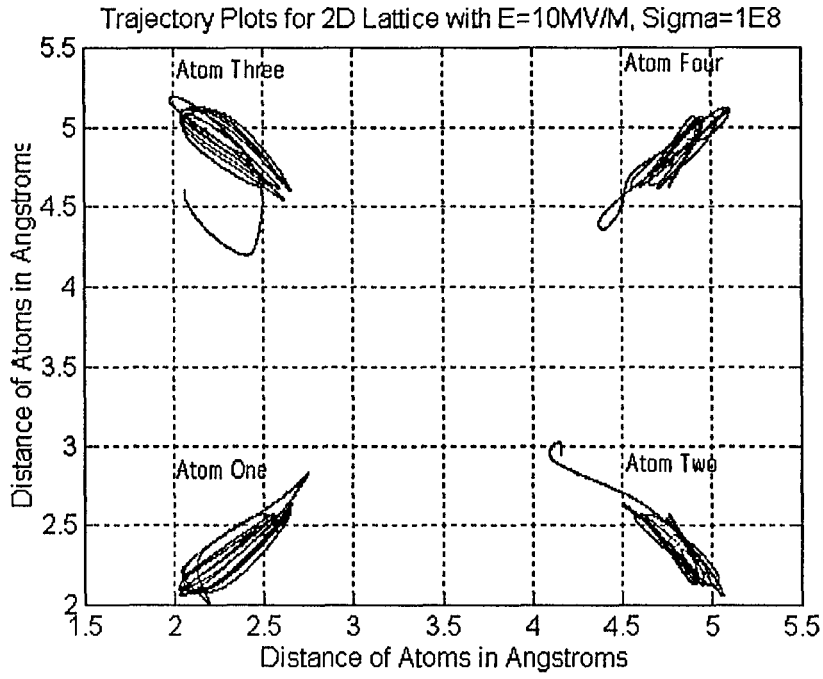

Fig. 3.14 Plot of the four atoms under the influence of a moderate electric field of 10MV/M. The electron wind counteracts the effects of the electric field somewhat and effectively acts to dampen the motion of the four atoms while at the same time injecting randomness into their motion.

If an imaginary line were drawn through the center of movement of the four atoms, that line would be very much like (but not equal to) the path taken by the four atoms in case one with only a Lennard-Jones potential. This makes it easy to see how the electron wind begins to restore the original range of movement. Much of the randomness indicated in the figure is due to a larger value for σ which is $1x10^8$. Although this value may inject more randomness into the system, the effects of the electron wind are quite profound and are still capable of resisting the effects of the electric field.

CHAPTER IV

RESULTS AND DISCUSSION

4.1 Introduction

With our theoretical model and implementation program validated in the above sections for the 1-D and 2-D cases, with no voids or hillocks or any other imperfections, we now attempt in this chapter to modify the code to include 56 atoms along with various imperfections, such as voids. A larger number of atoms are needed in order to have accurate simulations. This is because there needs to be a sufficiently large number of atoms between an imperfection and the boundary atoms. This allows the atoms near the vicinity of the void to have maximum freedom of movement, just as in a real world case while still maintaining the hard wall boundary conditions for the overall system as in the previous chapters. This freedom of movement for the atoms insures that there are no artificial forces involved that would tend to make the results less realistic. Important tasks carried out and reported in this chapter pertain to the evaluation of sigma for the theoretical model and comparisons with experimental data.

4.2 Simulation Cases

What will be presented in the following sections in this chapter are several iterations of the main program with various parameters modified such as the electron wind variance, boundary conditions, voids, and externally applied bias. As before in the previous chapters, three basic cases will be presented: Case One, Lennard-Jones potential

only; Case Two, Lennard-Jones potential and Electric field; and Case Three, Lennard-Jones potential with electric field and electron wind. The initial and final atomic positions as well as the atomic drift velocities will be obtained through simulations.

Case One: Lennard-Jones Potential Only with No Imperfections

The following figure, Fig. 4.1, depicts the simulation space at T=0. All of the sides of this space have hard wall boundary conditions except for the right hand side. As before, the inter-atomic spacing is 2.5 Angstroms. The only force that is active here is the Lennard-Jones potential. A plot of the initial atomic positions is shown in Fig. 4.1.

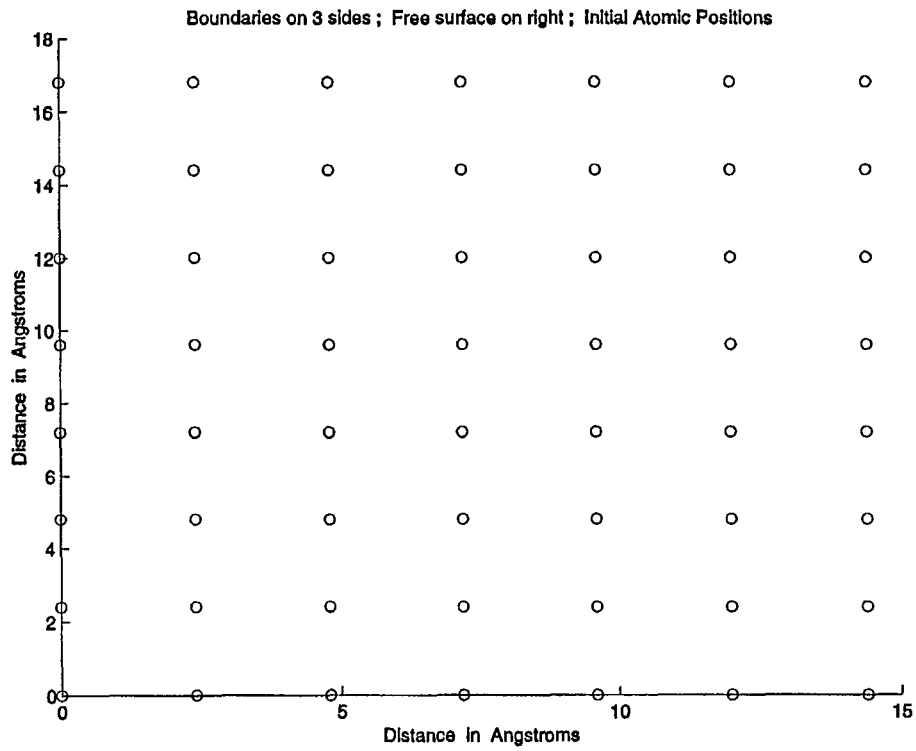

Fig. 4.1 Plot of the simulation space indicating the atoms positions at T=0, with the Lennard-Jones potential being the only force involved. Notice the symmetry that exists before any time has elapsed.

After some time T, their final positions are distorted as can be seen in Fig. 4.2. In this figure, the atoms along the right hand side, where there is no boundary, have been pulled inwards towards the adjacent column of atoms. This distortion, as can be expected, decreases as one gets closer to any boundary. This arises because of the hardwall boundary conditions used, which prevent the movement of the boundary atoms. In the absence of a boundary on the right hand side, there are no atoms there to generate a Lennard-Jones potential in the opposite direction to counteract the Lennard-Jones potential generated by the atoms to the immediate left.

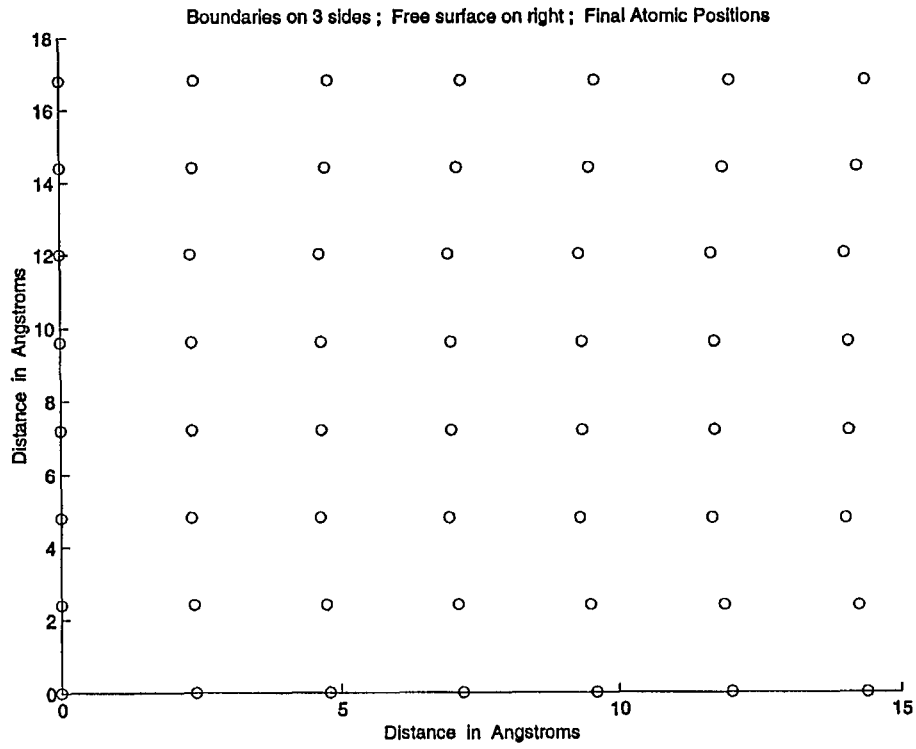

Fig. 4.2 Plot of the final positions of the atoms in the simulation space. Notice the distortion that takes place among all of the atoms, especially those atoms that are farthest away from any boundary. This space is bound on all sides, except for the right side.

As one gets very close to the left boundary, there is actually very little distortion observed, as can be seen in Fig. 4.3. These M.D. simulations thus naturally bring out a surface tension effect associated with a minimization of the total energy of the atomic system. Surface tension is a well-known phenomenon, and its prediction by the M.D. approach underscores a correct, valid, and useful implementation.

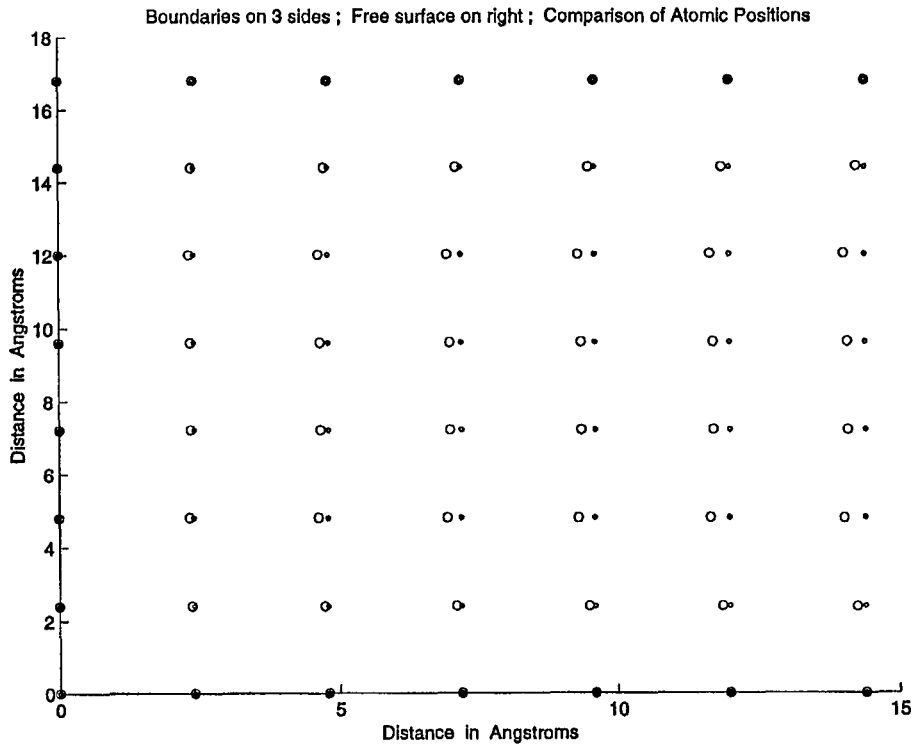

Fig. 4.3 Composite plot indicating initial and final atomic positions with the only acting force being the Lennard-Jones potential. The atomic displacement becomes less distorted as one gets closer to any boundary. As can be expected, distortion is most profound in the middle of the far right column of atoms since they are farthest away from any boundary.

Lennard-Jones Potential Only with Imperfections Added

For these simulations, we restore the boundary on the right-hand side so that all four sides of our space are bounded using hard wall boundary conditions. Doing this has the effect of concentrating all of the effects that we are interested in to the region with the defect. This new space is now a 13x13 matrix of 169 atoms as seen in Fig. 4.4. An

imperfection has been added in the form of a symmetrical void directly in the middle of the space. This void is 9 atoms square, making the simulation space 160 atoms in size.

For the first simulation for this case, the only force to consider is the Lennard-Jones potential. Since a void exists in this region, some distortion is expected around the void region with the distortion gradually tapering off away from the void region. Fig. 4.5 illustrates this behavior. As can be seen in the figure, the atoms around the perimeter of the void get pulled outwards towards their neighboring atoms since there are no atoms in the void region to generate a counteracting Lennard-Jones force. Because of the built-in Lennard-Jones potential, the void region is effectively made somewhat larger than it was initially. As will be shown later, the results are quite different in the presence of an electron wind. The Lennard-Jones potential will always serve to draw atoms away from a void region and towards other neighboring atoms. However, the void only grows to a point in this case. With the absence of any external forces, the void only grows large enough to the point where the atoms around the perimeter of the void are in equilibrium with their neighboring atoms and so on. Therefore, void growth does eventually stop, but will never self-heal.

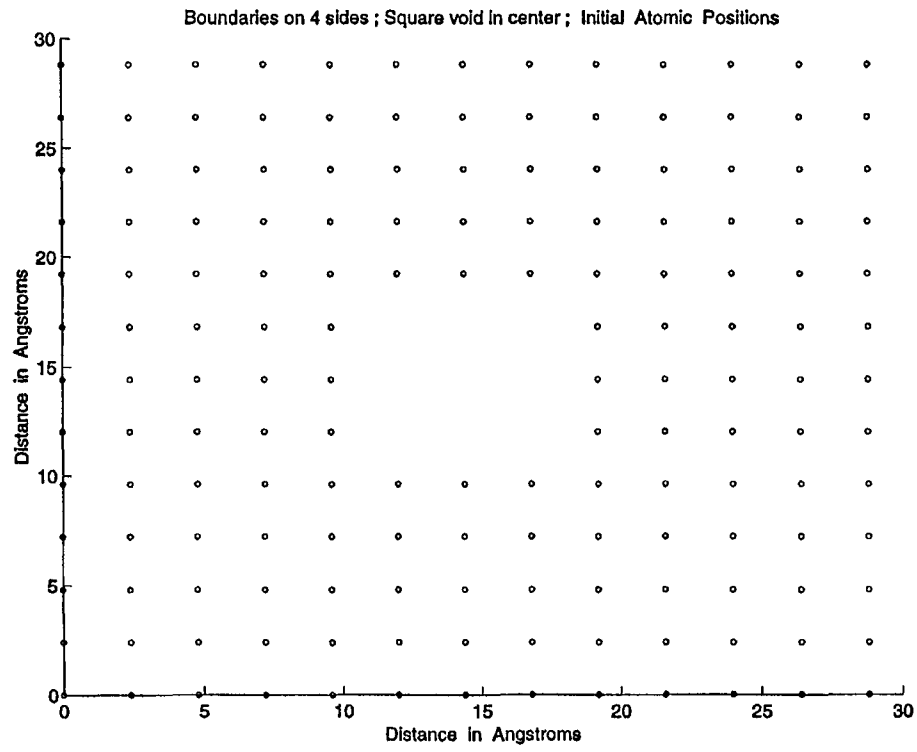

Fig. 4.4 Plot of the initial atomic positions for the 13x13 simulation space. There is a 3x3 void in the center of the space. At time T=0, there is no distortion around the void.

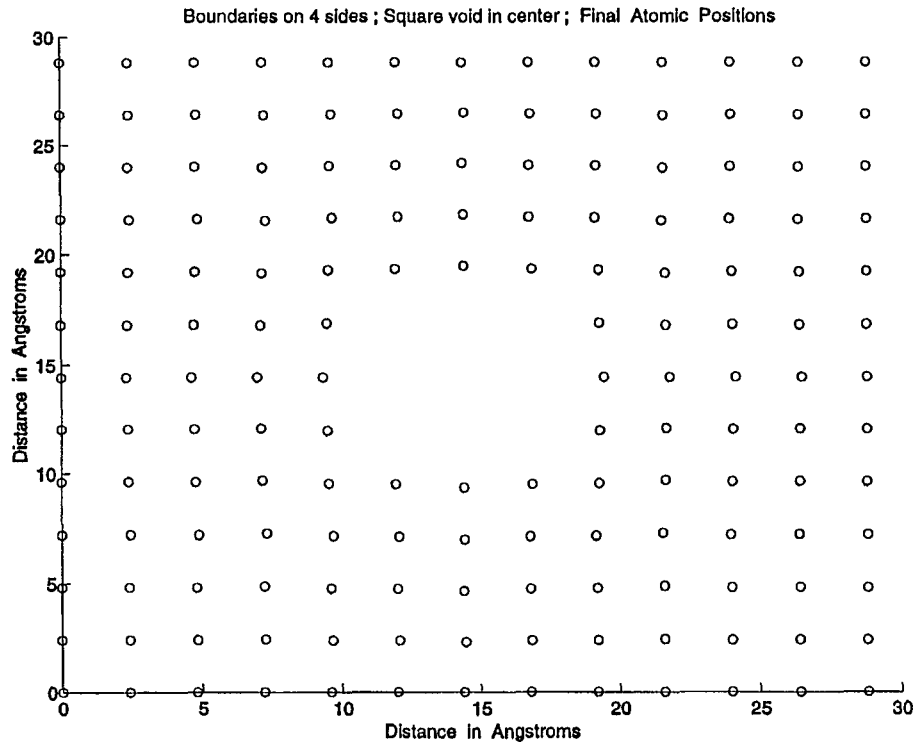

Fig. 4.5 Plot of the simulation space indicating the final position of each atom. Note the distortion around the void region. This distortion arises from the fact that there are no atoms to generate a Lennard-Jones force in the void region. Therefore, the atoms around the perimeter of the void get pulled away from the void region.

Figure 4.6 is a composite plot of the initial atomic positions and final atomic positions for the simulation space containing a void. As can be seen, void growth and atomic distortion are more profound in the vicinity of the void region, with less distortion taking place near the boundaries of the simulation space. The Lennard-Jones potential serves to make the void region larger and more distorted, but at the same time, it also serves to slow down and stop the void growth process by eventually holding each atom in equilibrium after a sufficiently long time.

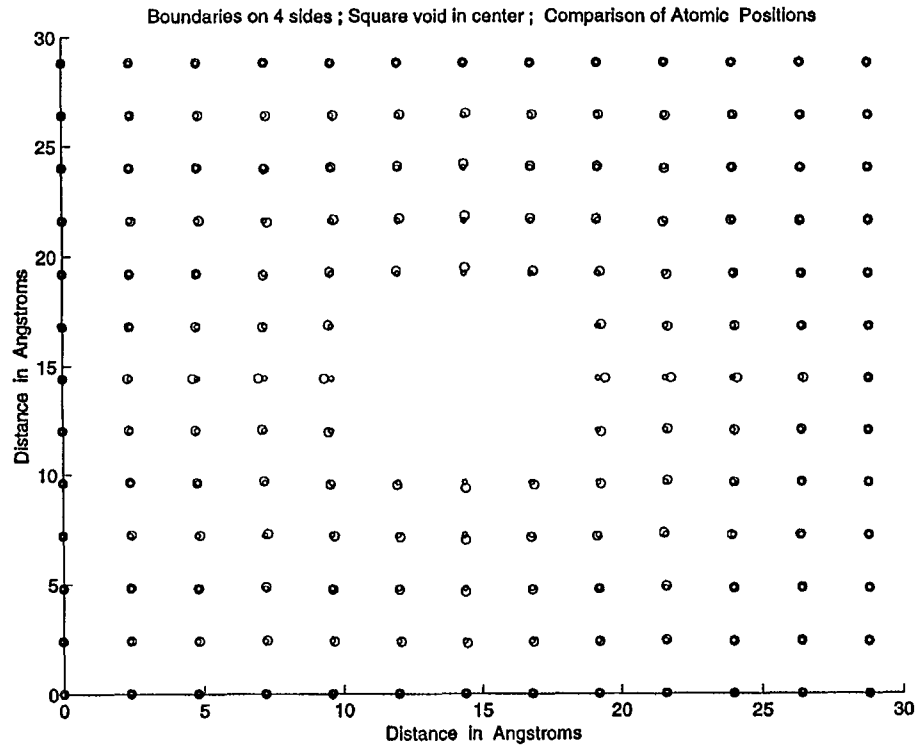

Fig. 4.6 Combined plot of initial and final atomic positions for the simulation region containing a void. As the figure indicates, void growth and distortion are more profound near the vicinity of the void, with the distortion tapering off towards the simulation boundaries.

The next simulations that will be presented in this chapter involve a simulation space that is more realistic. This space will be a square simulation space, just as before. However, only the top and bottom of the simulation space will be bounded. The left and right sides of the space will be unbounded. This matches very closely a slice of a true interconnect. The space is still a 13x13 matrix of atoms for a total of 169 atoms.

Case Two: Lennard-Jones with an Electric Field

This case demonstrates the behavior of the simulation space when there is no electron wind. It is mainly here to illustrate the effect that the electric field has on the simulation space. In reality, there can be no electric field without a corresponding electron wind force. As seen in Fig. 4.7, without an electron wind, the simulation space becomes quite distorted.

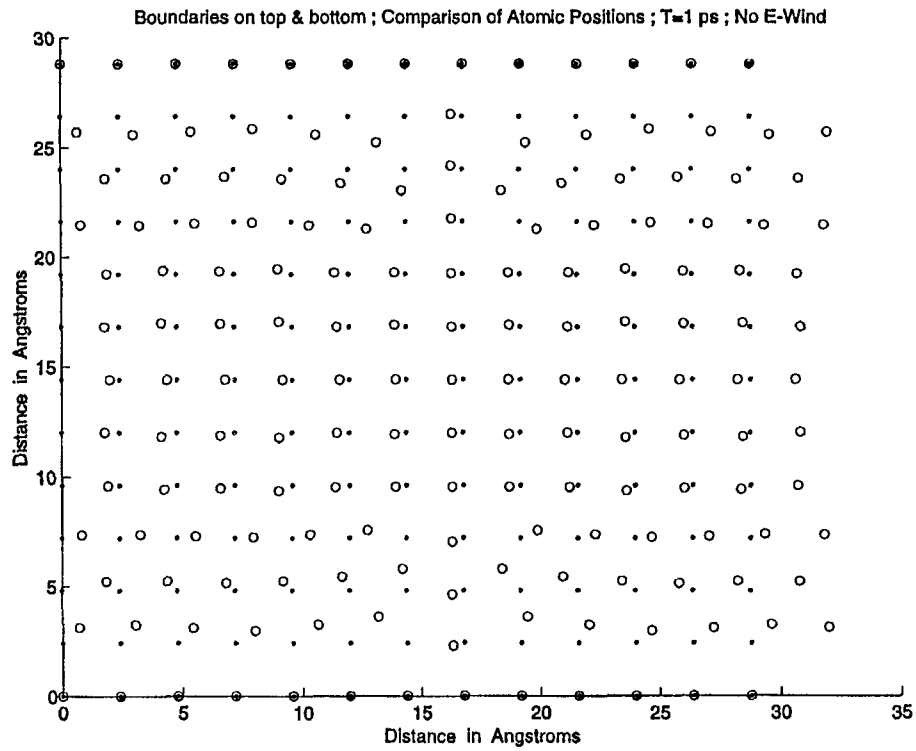

Fig. 4.7 Combined plot of the simulation space when subjected to an electric field, but with no electron wind. The smaller circles are the atoms initial positions, the larger circles are the atoms final positions. Note that the atoms after time T migrate in the direction of the applied electric field.

This figure shows that the atoms will tend to move in the direction of the applied electric field, as they should. This is due to the Coulomb force on the ions. As stated before, the electron wind moves in a direction *opposite* to the electric field, but since there is no electron wind in this case, the atoms are displaced by a large amount parallel to the field direction. When an electron wind is introduced in addition to the electric field and Lennard-Jones potential, the atoms in the simulation space will be shown to actually move in a direction *opposite to the electric field for non-zero values of sigma.* For sigma equal to zero though, the electron wind is no longer random in nature.

Case Three: Lennard-Jones with Electric Field and Electron Wind

In this case, the sigma value for the electron wind model was chosen to equal zero. Hence, the electron wind force exactly counteracts the electric field force. The nearly symmetric plot of Fig. 4.8 was generated as a result. Note that there is no net displacement of the overall simulation space when considered on a macroscopic scale. It is only on a microscopic scale that the individual atomic position changes are realized, particularly for the atoms on the unbounded left and right sides.

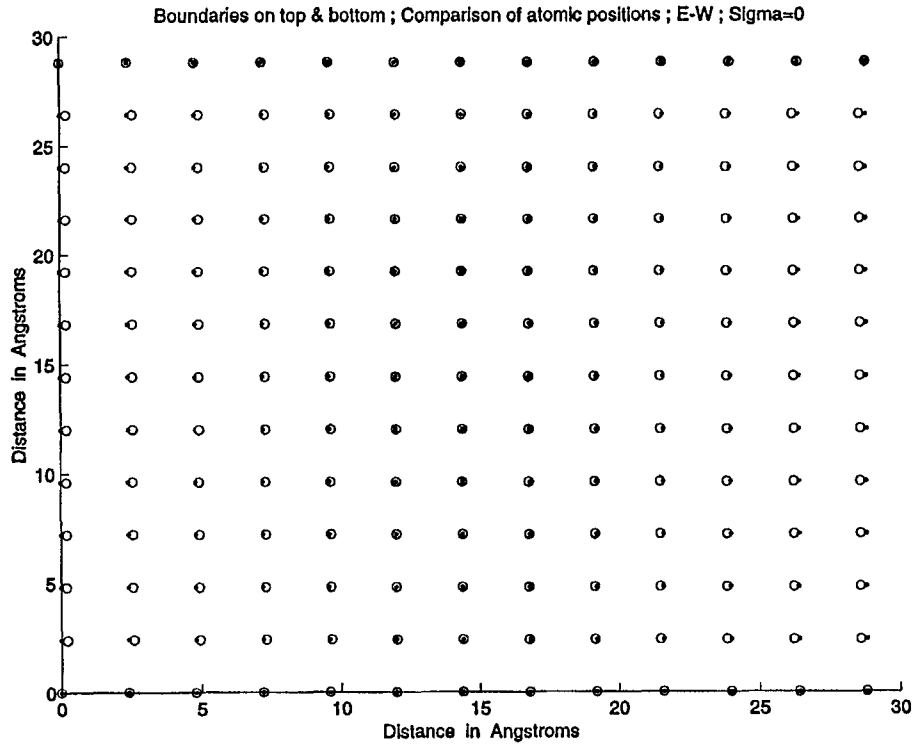

Fig. 4.8 Combined plot of initial and final positions for the atoms in the simulation space. Note that with sigma set to zero, there is no net displacement of the atoms in the simulation space.

This is again due to the Lennard-Jones potential. The atoms on the left and right sides of the simulation space, when viewed from a microscopic perspective, appear to be slightly bent inward or concave. There are no other neighboring atoms in these areas to create a Lennard-Jones potential and hence, the atoms at these two locations are pulled inward by the Lennard-Jones potential created by the interior atoms. On average though, with a sigma of zero, there will be no net displacement of the atoms in the simulation space when viewed on a macroscopic scale.

However, when sigma is changed to non-zero values, Fig. 4.8 changes somewhat indicating a net displacement of the atoms to the left (against the electric field). The

circles represent initial atomic positions and the '+' symbol represents the final atomic positions. This can be seen in Fig. 4.9. In this figure, the electric field is 0.1V/m and sigma is 0.05.

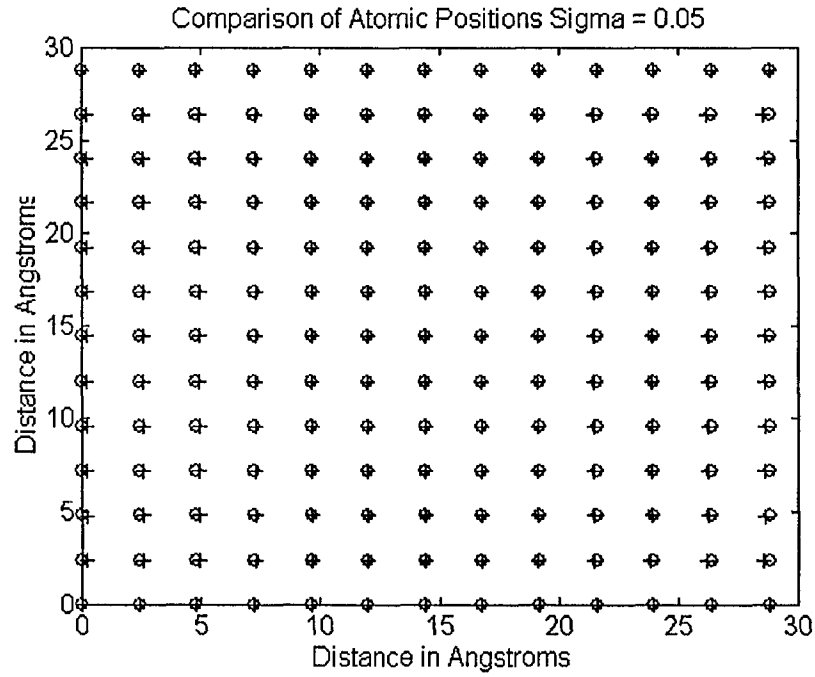

Fig. 4.9 Plot of initial and final atomic positions. "o" = initial atomic positions, "+" = final atomic positions. Some atoms, particularly on the left and right sides, have shifted inwards since there are no boundary conditions there.

It is not completely clear from the figure that there is a net atomic displacement taking place. To show this, the initial and final atomic numerical displacements, which were used to produce the figures, are provided in the following table:

Table 4.1

Data Points of Average Drift Velcoity vs. Sigma

Sigma	Initial Average Atomic Position (Meters)	Final Average Atomic Position (Meters)	Final Average Drift Velocity m/s
0.00	$1.4400000000000 \times 10^{-9}$	$1.4400000000000 \times 10^{-9}$	0.00
0.05	$1.4400000000000 \times 10^{-9}$	$1.4399999999999 \times 10^{-9}$	$-1.0050244442519 \times 10^{-10}$
0.06	$1.4400000000000 \times 10^{-9}$	$1.4399999999999 \times 10^{-9}$	$-1.2242273065785 \times 10^{-10}$
0.07	$1.4400000000000 \times 10^{-9}$	$1.4399999999999 \times 10^{-9}$	$-1.4703135388130 \times 10^{-10}$
0.08	$1.4400000000000 \times 10^{-9}$	$1.4399999999998 \times 10^{-9}$	$-1.7639626562693 \times 10^{-10}$
0.09	$1.4400000000000 \times 10^{-9}$	$1.4399999999998 \times 10^{-9}$	$-1.9728257609390 \times 10^{-10}$
0.1	$1.4400000000000 \times 10^{-9}$	$1.4399999999998 \times 10^{-9}$	$-2.2127081385793 \times 10^{-10}$

In Fig. 4.9, the atoms move slightly under the influence of the now random electron wind force; however this movement is almost imperceptible since the simulation space is symmetric with no voids, hillocks, or grain boundaries. Table 4.1 demonstrates numerically that there is indeed atomic movement taking place when there is a non-zero sigma.

It was stated earlier that the parameter, sigma, used in the present molecular dynamics simulations still needed to be evaluated through comparison with actual data. Variations of sigma for obtaining a range of atomic drift velocities were carried out as a step in this direction. It is also clear from Table 4.1 that the atomic displacement though small, can vary considerably over two orders of magnitude.

4.3 The Role of Sigma in the Simulation Program

Sigma is a very important parameter in our simulation programs since it is the single variable that controls how closely the programs model real-world electromigration behavior. So far, the role of sigma in our simulation programs has been described as a

controlling parameter in how the electron wind is defined. We iteratively ran simulations with varying sigmas and looked at the resulting final drift velocities of the atoms in the simulation space in order to determine a value for sigma that described an electron wind that was realistic. The results can be seen in Fig. 4.10 with the actual data points used shown in Table 4.1. We compared these final drift velocities to those found from other researchers **[34]** and have concluded that a sigma of 0.05 gives an electron wind distribution that helps the program generate appropriate atomic drift velocities. For example, experimental results by Blech **[34]** have yielded velocities of about $1x10^{-10}$ m/s. Therefore, this is a value of sigma that we can trust.

Researchers have discovered that there is a relationship to current density and average drift velocity **[34]**. As the current density is increased, the average drift velocity of the lattice atoms also increases in a linear fashion. This can be seen in Fig. 4.11. This figure, reproduced from a paper by Blech **[34]**, indicates that there is a threshold effect in addition to the linear behavior. For current density below about $1.1x10^5 A/cm^2$, the drift velocity does not change. When the current density is increased beyond $1.1x10^5 A/cm^2$, the threshold point, the drift velocity begins to increase in a linear fashion quite rapidly as indicated by the steep slope.

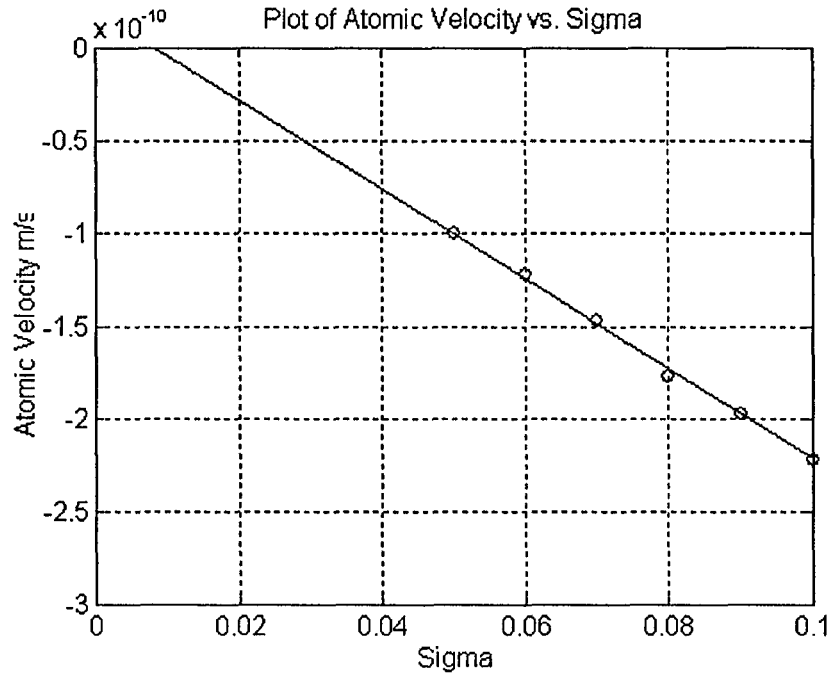

Fig. 4.10 Plot of sigma vs. atomic velocity. As sigma is increased, the drift velocity also increases in a linear fashion. Note the threshold effect occurring for a sigma of about 0.01.

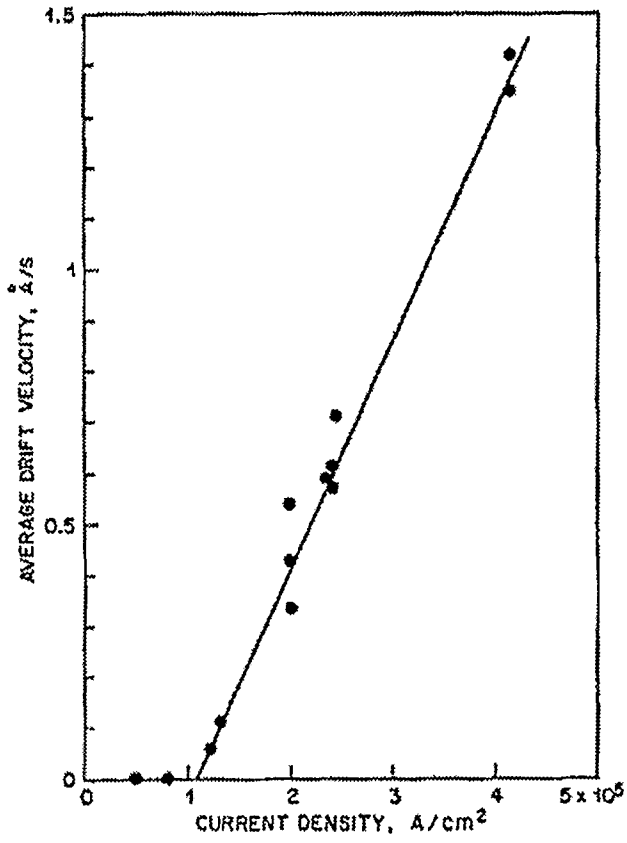

Fig. 4.11 This plot of the average drift velocity vs. current density is indicative of the relationship between these two variables that most researchers have found. Note the threshold point of about $1.1 \times 10^5 A/cm^2$ toward the bottom of the graph and the steep slope of the graph, indicating a fairly rapid increase in drift velocity as the current density is increased beyond this threshold **[34]**.

However, the M.D. simulation programs that we have developed to simulate electromigration do not include current density as input. The programs only deal with the Lennard-Jones potential, electric field, and electron wind. This does not inhibit the program from realistically modeling this phenomenon however. This can be explained by the following reasoning. When other researchers increased the current density in their

experiments and observed net increases in average drift velocities, what was actually taking place was an increase in the internal thermal energy and temperature of the sample. This increase in energy can be described by a Maxwell-Boltzmann distribution as in the following equation:

$$f(E) = K \exp[-\hbar^2(k-k_{dn})^2/2mkT] \quad . \quad (4.1)$$

For comparison from chapter II, the Gaussian distribution for the electron wind can be described by:

$$f(FE) = \frac{1}{\sigma\sqrt{2\pi}} e^{\frac{-(FE-\overline{FE})^2}{2\sigma^2}} \quad . \quad (4.2)$$

Equation (4.1) when plotted has a curve very similar to a Gaussian curve. The mean of this curve would center about k_{dn}, with a σ directly proportional to T. As the equation indicates, as the temperature is increased, the curve flattens out and becomes more broad. This is due to internal electron heating. This type of behavior corresponds to a spread in the Gaussian curve for the electron wind distribution. In this case, with increasing sigma, the electron wind distribution curve flattens out, indicating that the wind force has become more random. For purposes of comparison then, sigma in our program can be thought of as playing the same role as temperature does in traditional experiments.

To explain this relationship further, what is ultimately needed is a rule relating current to sigma. From general definitions of power, two equations can be stated:

$$P = VI \quad , \quad (4.3)$$

and

$$P = (T - T_0)/ R_{th} \quad , \quad (4.4)$$

where P is the power or Joule heating, V is voltage, I is current, R_{th} is the thermal resistance of the material, T is the final temperature, and T_0 is the initial temperature **[35]**.

Equating equations (4.3) and (4.4), gives:

$$I = C(T-T_0) \quad , \qquad (4.5)$$

where I is the current, C is a constant and is equal to $1/VR_{th}$, T_0 is the initial temperature, and T is the final temperature. Solving this equation for T gives:

$$T = I/C + T_0 \quad . \qquad (4.6)$$

Therefore, equation (4.6) predicts a linear relationship between current and temperature. Looking at the Gaussian distribution for the electron wind and the Maxwell-Boltzmann distribution for the energy and comparing the two exponents, it can be reasoned from these two equations (4.1 and 4.2) that sigma is proportional to temperature, as shown in the following equation:

$$\sigma = k_1(T - T_0) \ , \qquad (4.7)$$

where T is the final temperature, K_1 is a constant, and σ is the electron wind variance. Setting equation (4.6) and (4.7) equal to each other, we get:

$$\sigma/K_1 + T_0 = I/C + T_0 \quad . \qquad (4.8)$$

Solving equation (4.8) for I gives the following:

$$I = (C\sigma)/K_1 \qquad , \qquad (4.9)$$

or

$$I = K_2\sigma \qquad , \qquad (4.10)$$

where K_2 is a new constant created to absorb the constants C and K_1 and simplify the equation. As seen in Fig. 4.10 the simulation gave a drift velocity of $1x10^{-10}$m/s for a

sigma of 0.05. Using the plot in Fig. 4.11, this correlates to a current density of about $3.4x10^5 A/cm^2$.

Using the data from Fig. 4.10 and 4.11, sigma can be related to current density. In Fig. 4.11, a current density of about $3.2x10^5 A/cm^2$ corresponds to a velocity of $1.0x10^{-10}$ m/s. From Fig. 4.10, a sigma of 0.05 corresponds to a velocity of $1.0x10^{-10}$m/s. Therefore it can be said that a current density of $3.2x10^5 A/cm^2$ corresponds to a sigma of 0.05 or alternatively, current density is $6.4x10^6\sigma$ or:

$$J = 6.4x10^6\sigma \quad . \qquad (4.11)$$

Comparing this observed result with the analytical result found in equation (4.10), K_3 would be zero and hence, we now have a relation between sigma and current density. Indeed Fig. 4.11 looks very much like Fig. 4.10 including the threshold effects. Both figures indicate that there is a certain sigma (Fig. 4.10, sigma ≈ 0.01) or certain current density (Fig. 4.11, $J \approx 1.1x10^5 A/cm^2$) that must exist before any change in atomic position can be observed. Thus, this further validates the M.D. simulation program in correctly simulating the electromigration phenomenon, and predicts quantities, such as average drift velocity, that are in general agreement with what other researchers have found from laboratory experiments.

4.4 2-D Simulations in the Presence of Imperfections

These simulations were conducted with the same simulation space consisting of 169 atoms. Three cases will be presented, each containing an imperfection. These imperfections consist of an extra half-row of atoms placed in different locations within

the simulation space, each creating a different simulation case and hence different electromigration behavior. These imperfections are known as dislocation boundaries.

Case One: One Half-Plane Dislocation Boundary

This case simulates a conductor line containing a dislocation boundary that extends halfway through its surface. It is created by adding an additional row of atoms that extends one half the way down the simulation space, as shown in Fig. 4.12.

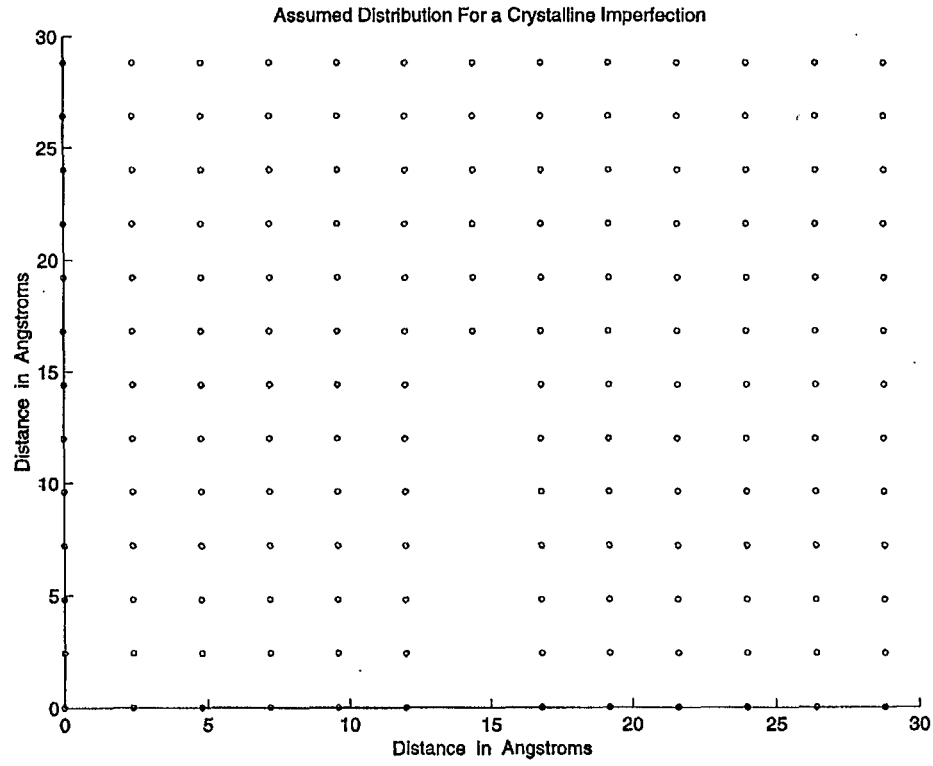

Fig. 4.12 Plot of the simulation space with a one-half plane dislocation. The initial atomic positions are indicated, with a dislocation placed in the middle of the simulation space.

As indicated in Table 4.2, the dislocation raises the final average drift velocity from -1.005×10^{-10} m/s to -1.375×10^{-10} m/s. While this is a notable increase in the velocity, a plot of final positions is not indicated since, when plotted, the differences in position are almost imperceptible. The voided region allows the atoms to move faster through that region since there are no Lennard-Jones forces since inter-atomic distances are high. Enough atoms move faster through this region to raise the total average drift velocity.

Case Two: Two Half-Plane Grain Boundary, Well Separated

This case represents a conductor that contains two dislocation boundaries with each dislocation boundary extending halfway through its surface. The grain boundaries are separated far apart from each other (2.5 Angstroms). There are five columns of atoms separating the two dislocation boundaries as shown in Fig. 4.13.

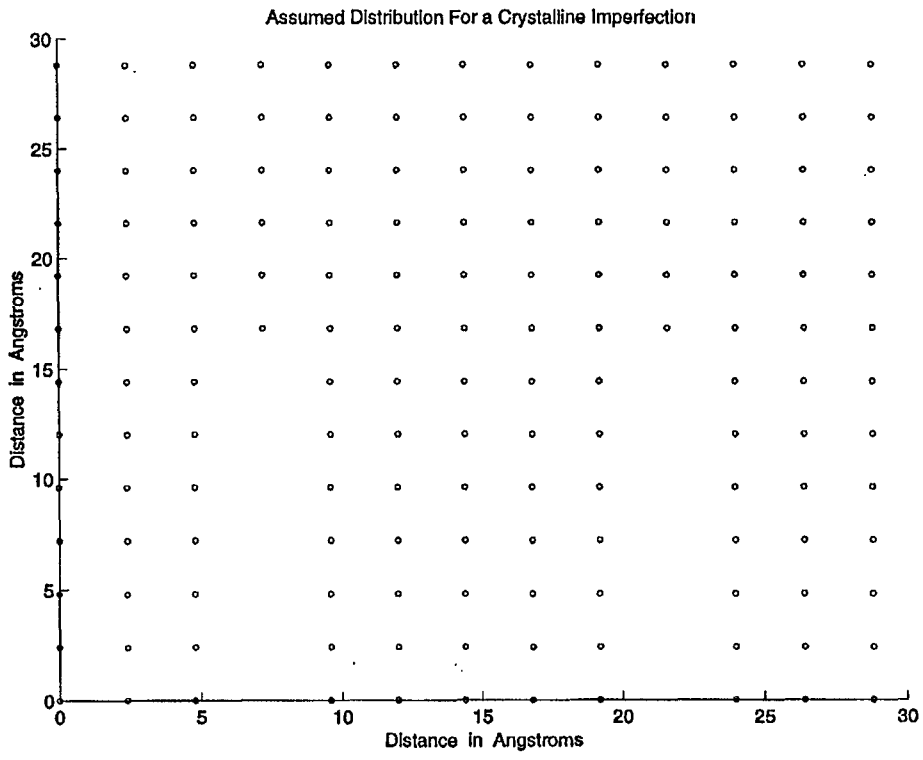

Fig. 4.13 Simulation space containing two dislocation boundaries separated far apart by five columns of atoms. The additional column of atoms slows down the electromigration process, but final average drift velocities are still higher than in case one.

As can be expected, the final average drift velocity, -1.469×10^{-10} m/s, is smaller than in case three, but still larger than in case one. The increased separation distance introduces some additional Lennard-Jones interactions to resist atomic movement as a whole, but there is still considerable atomic movement within each dislocation boundary, enough so that the final average drift velocity is increased.

Case Three: Two Half-Plane Grain Boundary, Close Together

This case represents a conductor that contains two dislocation boundaries that are in close proximity (2.5 Angstroms) to each other. Each dislocation boundary extends halfway through its surface. There is only a single column of atoms separating the two dislocation regions. This simulation space is depicted in Fig. 4.14.

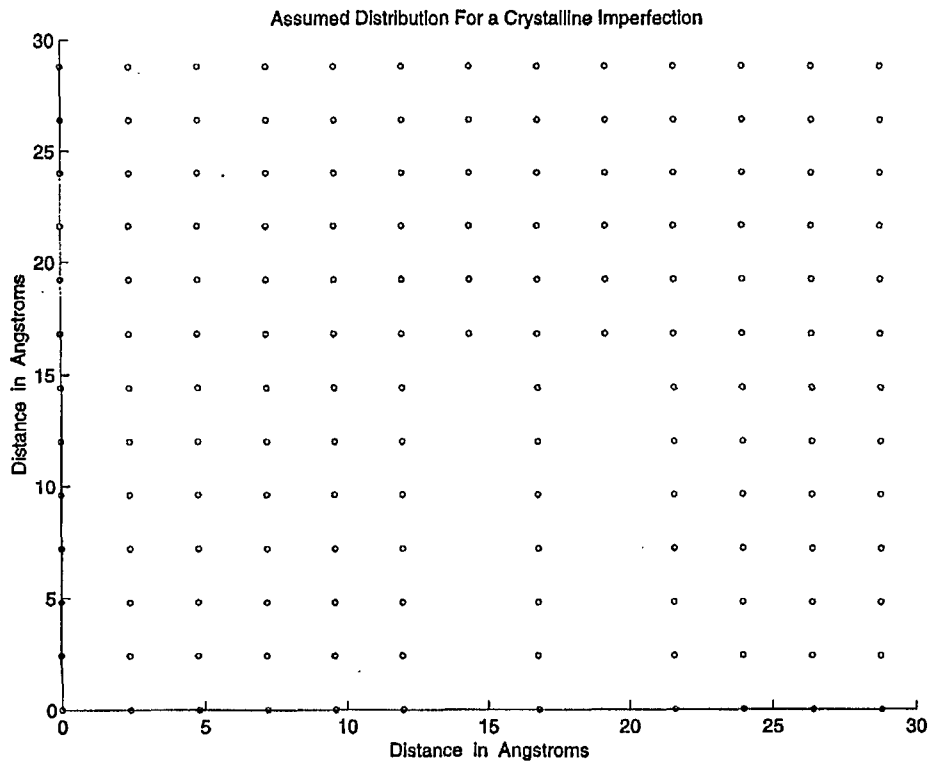

Fig 4.14 Simulation space containing two dislocation boundaries in close proximity to each other. The two regions are separated by only a single column of atoms.

The two dislocations in Fig. 4.14 increase the final average drift velocity even higher, to -3.47×10^{-10} m/s. This represents the highest average drift velocity of all three cases. The close proximity seems to create a voided region that is so large, that the single

column of atoms in the middle are not effective in slowing down incoming and outgoing atoms via a Lennard-Jones interaction. This is reasonable since the Lennard-Jones force is highly dependant on the separation distance and such a large gap of atoms in the simulation space effectively eliminates the Lennard-Jones potential in this region, thereby allowing atoms entering this region to experience less resistance.

Table 4.2 summarizes the results for all three simulation cases with an additional entry for the case of a defect-free simulation space.

Table 4.2

Effects of Dislocation Boundary Type on Drift Velocity

Case	Sigma	Efield V/m	Dislocation Boundary Type	Final Average Drift Velocity m/s	Diffusion Coefficient
One	0.05	0.1	One Half-Plane	-1.375×10^{-10}	-3.558×10^{-11}
Two	0.05	0.1	Two Half-Planes, Well Separated	-1.469×10^{-10}	-3.801×10^{-11}
Three	0.05	0.1	Two Half-Planes, Close Together	-3.47×10^{-10}	-8.979×10^{-11}
N/A	0.05	0.1	No Grain Boundary, Perfect Lattice	-1.005×10^{-10}	-2.600×10^{-11}

CHAPTER V

CONCLUSIONS

Electromigration is a diffusion-based process by which atoms that make up the structure of a conductor are displaced by an electron wind of sufficient magnitude. There are two predominant ways to study this phenomenon numerically. These are macroscopic computer simulations and microscopic computer simulations. Macroscopic models and simulations typically employ bulk material characteristics in their approach. One of the more important bulk material characteristics is the diffusion coefficient. This is a coefficient that describes the rate at which atoms will diffuse into a sample material. Microscopic simulations typically look at the behavior of individual atoms when subjected to various forces such as an electric field and electronic collisions. It is usually assumed in macroscopic simulations that the diffusion coefficient is spatially uniform throughout the entire sample, then various studies are carried out based on this assumption and various quantities are generated such as average drift velocity. The simulations carried out in this thesis made no such assumption. It has been argued here that internal inhomogenities affect electromigration. The simulations employed calculated values of the atomic position and average drift velocity. It is hoped that this approach for determining these quantities more precisely can be used in macroscopic simulations to increase the accuracy of results.

Several steps were taken in an effort to validate the simulation programs to ensure that reasonable results were obtained. This involved simulating simple 1-D and 2-D test cases with only a few atoms and no imperfections. Under these scenarios, comparisons

of data, such as average drift velocity and atomic position, were made with the known results of other researchers **[34]**. The results from these simulations can be summarized as follows:

1) The electron wind moves in a direction that is opposite to the applied electric field serving to counteract some of the deleterious effects of the electric field.
2) The electron wind force is random in nature and can be adequately modeled as a Gaussian distribution with a specific variance.
3) A value of sigma equal to 0.05 models the electron wind most realistically providing accurate results for the average drift velocity.
4) Sigma in our research is correlated to current density in other research. A sigma of 0.05 correlates to a current density of $3.4 \times 10^5 A/cm^2$.
5) In the absence of any defects such as grain boundaries, voids, or hillocks, no net displacement of the atoms is observed.
6) A threshold effect was observed when sigma was plotted against velocity in Fig. 4.11. This is the same threshold effect observed in Fig. 4.10. A minimum value of sigma or current density must be achieved before any electromigration can occur.
7) Atomic displacements occur at different rates based on the proximity of defects and dislocations.

Once these simple test cases were validated to predict the same type of electromigration behavior that has been observed by other researchers **[34]**, the test cases were extended to include various defects such as dislocation boundaries. This provided

insight into how the location and type of dislocation boundary affected the final average drift velocity. From these final simulations, several conclusions can be made:

1) A dislocation boundary has the effect of increasing the drift velocity near the vicinity of the defect, thereby increasing the average drift velocity of the entire simulation space.

2) A dislocation boundary has the effect of decreasing the Lennard-Jones influence of the total force equation by increasing the separation distance of the atoms near the defect.

3) These results agree with what other research has found, that is, defects in a conductor have the affect of increasing the drift velocity leading to electromigration.

5.1 Scope for Future Work

These simulation programs can be used to extend research into the electromigration phenomenon in several ways. One way to extend these simulations to model real-world electromigration behavior would be to take into account 3-D simulation spaces. In doing so, features commonly found in VLSI such as vias and contacts can be taken into account. In addition, study into the effects of not only conductor width, but also conductor thickness can be modeled. In addition, by modifying the parameters, different metals and metal-semiconductor structures can be analyzed. Also, different defects such at triple point junctions and cracks can be modeled.

Intermixing between metallic lines and atoms of the underlying substrate can also be modeled. Finally, by carrying out thermal analysis, effective temperatures and hence sigma, could be computed at high current densities. The temperature dependant thermal conductivity parameter would need to be included for accurate predictions. Once the internal temperature was known, the sigma parameter could be evaluated for this model. The molecular dynamics simulations would then yield details of the electromigration. The occurrence of thermal mean free paths much longer than the length scales of the internal metallic impurity features would allow such an approach. For long time simulations, a coupled molecular dynamics and drift-diffusion scheme could be developed.

It is hoped that the data as well as the simulation techniques used in this thesis can provide a useful contribution to other researchers involved in studying this unusual phenomenon.

REFERENCES

[1]. P. Ho and T. Kwok, Rep. Prog. Phys. **52**, 301 (1989).

[2] P. Ho and D. Gupta, *Diffusion Phenomena in Thin Films and Microelectronic Materials* (Noyes Publications, New Jersey, 1973), p. 398.

[3]. P. Ho, *Proc. 20th IEEE Trans. on Reliability in Physics* (IEEE, New York, 1982), p. 284.

[4]. A. Christou, *Electromigration & Electronic Device Degradation* (John Wiley & Sons, Inc., New York, 1994), pp. 18, 120-122, 174-176.

[5]. G. Bernstein and A. Kriman, *IEEE Encyclopedia* (Wiley, New York, 1999).

[6]. B. Knowlton, J. Clement, and C. Thompson, J. Appl. Phys. **81**, 6073 (1997).

[7]. J. Black, *Proc. 6th IEEE Symp. on Reliability in Physics* (IEEE, New York, 1967), p. 148.

[8]. B. Oliver and D. Bower, *Proc. 8th IEEE Symp. on Reliability in Physics* (IEEE, New York, 1970), p.116.

[9]. A. Learn, Appl. Phys. Lett. **19**, 292 (1971).

[10]. A. Gangulee, J. Appl. Phys. **45**, 3749 (1974).

[11]. B. Agarwala, B. Patnaik, and T. Schnitzel, J. Appl. Phys. **39**, 1487 (1972).

[12]. S. Vaidya, and A. Sinha, *Thin Solid Films* **75**, 253 (1981).

[13]. T. Kwok, *Proc. 4th IEEE VLSI Multilevel Interconnection Conf.* (IEEE, New York, 1987), p. 456.

[14]. B. Agarwala, M. Attardo, and A. Ingraham, J. Appl. Phys. **41**, 3954 (1970).

[15]. G. Scoggan, B. Agarwala, P. Peressini, and A. Brouillard, *Proc. 13th IEEE Symp. on Reliability in Physics* (IEEE, New York, 1978), p. 151.

[16]. S. Vaidya, T. Sheng, and A. Sinha, Appl. Phys. Lett. **36**, 464 (1980).

[17]. K. Eden, W. Roth, and H. Beneking, Microelectronic Eng. **1**, 263 (1983).

[18]. T. Kwok, *Proc. 1st ECS Symp. on ULSI Science and Technology* (The Electrochemical Society, New York, 1987), p. 593.

[19]. H. Shaft, T. Station, J. Mandel, and J. Shott, *IEEE Trans. Electron. Devices* **ED-34**, 673 (1987).

[20]. T. Kwok, *Proc. 26th Symp. on Reliability in Physics* (IEEE, New York, 1988), p. 185.

[21]. P. Ghate, *Proc. 19th IEEE Symp. on Reliability in Physics* (IEEE, New York, 1981), p. 243.

[22]. R. Pasco, and J. Schwarz, Solid State Electronics **26**, 445 (1983).

[23]. B. Root and T. Turner, *Proc. 23rd IEEE Symp. on Reliability in Physics* (IEEE, New York, 1983), p. 100.

[24]. C. Hong and D. Crook, *Proc. 23rd IEEE Symp. on Reliability in Physics* (IEEE, New York, 1983), p. 108.

[25]. A. Diligenti, B. Neri, P. Bagnoli, A. Bersenti, and M. Rizzo, IEEE Electron. Device Lett. **6**, 606 (1985).

[26]. J. Cottle and T. Chen, *Proc. 4th IEEE Conf. VLSI Multilevel Interconnection* (IEEE, New York, 1987), p. 449.

[27]. L. Verlet, Phys. Rev. **159**, 98 (1967).

[28]. E. Kraft, W. Nix, and J. Sanchez Jr., J. Appl. Phys. **76**, 1563 (1994).

[29]. M. Borgesen, M. Korhonen, K. Tu, and C. Li, J. Appl. Phys. **73**, 3790 (1993).

[30]. T. Ohkubo, Y. Hirostsu, and K. Nikawa, Matl. Trans. JIM **37**, 454 (1996).

[31]. W. Eckstein, *Computer Simulation of Ion-Solid Interactions* (Sprinner-Verlag, Berlin, 1991), p. 33.

[32]. D. Harrison Jr., W. Gay, and H. Effron, J. Math Phys. **10**, 1179 (1969).

[33]. G. Cooper and C McGillem, *Probabilistic Methods of Signal and System Analysis* (Saunders College Publishing, TX, 1986), p.65.

[34]. I. Blech, J. Appl. Phys. **47**, 1203 (1976).

[35]. F. Oettinger, D. Blackburn, and S. Rubin, *IEEE Trans. Electron Devices.* **ED-23** 831 (1976).

VITA

JOHN STEPHEN PEAKE
College of Engineering and Technology
Kauffman-Duckworth Hall
Norfolk VA 23529-0236

EDUCATION:

Master of Science Electrical Engineering, December 1998

Bachelor of Science Electrical Engineering, December 1994

Old Dominion University
Norfolk, Virginia

COMPUTER SKILLS:

MIL3 OPNet Network Simulation and Modeling software, Windows NT Server 4.0, Windows 95/98, Windows 3.x, DOS, HP-UNIX, MS Office '97, C, PASCAL, Assembly, Matlab

EXPERIENCE:

Electrical Engineer
NEWPORT NEWS SHIPBUILDING, Newport News VA,
(8/98 – Present)

- Design and implement computer network systems for shipboard use
- Utilize OPNet software to simulate shipboard LANs and WANs to analyze utilization, find bottlenecks, and plan for future capacity
- Prepare, review, and revise routine technical documents, procedures, purchase order requisitions, inspection requirements, work instructions, and drawings as assigned
- Provide engineering on-site problem resolutions to shops and shipboard trades to prevent construction delays
- Ensure that assigned projects are accurate, on time, and within budget

Field Engineer
ELECTRONIC SYSTEMS INC., Virginia Beach VA,
(9/97 – 3/98)

- Perform PC system maintenance, repair, and upgrades for the city of Va. Beach
- Assist in basic network and server troubleshooting for the city of Va. Beach

Electrical Engineer
DYNAMIC ENGINEERING INC., Newport News VA,
(1/97 – 8/97)

- Design, build, and test MIL SPEC electronic systems and circuits at the component level
- Act as system administrator for a networked HP-UNIX based data acquisition system
- Develop instrumentation and control system software using CVI Lab Windows and Microsoft Visual C++
- Direct electronics technicians in the manufacturing of MIL SPEC electronic systems at the component level

Assistant Programmer
COMPTEK FEDERAL SYSTEMS, Langley AFB Hampton VA,
(6/95 - 1/97)

- Provide hardware test support for various government computer systems
- Assist in the development of a LAN from building the PC to creating the network
- Assist in software rehosting and system integration for various government software projects such as the DCT/BCT mobile data terminals
- Assist in the writing/editing of documentation for the DCT/BCT project, as well as Software Quality Control for other government software

ACTIVITIES/ INTERESTS:

- Repairing and building electronic equipment and personal computers
- Computer communications and networking techniques
- Automotive and industrial engine lubrication technology and systems
- Mountain biking (mild competition/endurance)
- Psychology
- Classical Piano